ATTITUDE ESTIMATION PERFORMANCE ENHANCEMENT FOR GOKTURK-2 SATELLITE

A THESIS SUBMITTED TO
THE GRADUATE SCHOOL OF NATURAL AND APPLIED SCIENCES
OF
MIDDLE EAST TECHNICAL UNIVERSITY

BY

ÖZGÜR KAHRAMAN

IN PARTIAL FULFILLMENT OF THE REQUIREMENTS
FOR
THE DEGREE OF DOCTOR OF PHILOSOPHY
IN
GEODETIC AND GEOGRAPHIC INFORMATION TECHNOLOGIES

JULY 2023

Approval of the thesis:

ATTITUDE ESTIMATION ENHANCEMENT FOR GOKTURK-2 SATELLITE

submitted by **ÖZGÜR KAHRAMAN** in partial fulfillment of the requirements for the degree of **Doctor of Philosophy** i**n Geodetic and Geographic Information Technologies, Middle East Technical University** by,

Prof. Dr. Halil Kalıpçılar
Dean, Graduate School of **Natural and Applied Sciences** _____

Prof. Dr. Zuhal Akyürek
Head of the Department, **Geodetic and Geographic Information Technologies, METU** _____

Prof. Dr. Zuhal Akyürek
Supervisor, **Civil Engineering, METU** _____

Assoc. Prof. Dr. Halil Ersin Söken
Co-Supervisor, **Aerospace Engineering, METU** _____

Examining Committee Members:

Prof. Dr. Mehmet Lütfi Süzen
Geology Eng., METU _____

Prof. Dr. Zuhal Akyürek
Civil Eng., METU _____

Prof. Dr. Umut Orguner
Electrical Electronics Eng., METU _____

Prof. Dr. Uğur Murat Leloğlu
Aerospace Eng., THK University _____

Assoc. Prof. Dr. Emre Kıyak
Aviation Electrics and Electronics
Eskişehir Technical University _____

Date: 26.07.2023

I hereby declare that all information in this document has been obtained and presented in accordance with academic rules and ethical conduct. I also declare that, as required by these rules and conduct, I have fully cited and referenced all material and results that are not original to this work.

Name Last name : Özgür Kahraman

Signature :

ABSTRACT

ATTITUDE ESTIMATION PERFORMANCE ENHANCEMENT FOR GOKTURK-2 SATELLITE

Kahraman, Özgür
Doctor of Philosophy, Geodetic and Geographic Information Technologies
Supervisor: Prof. Dr. Zuhal AKYÜREK
Co-Supervisor: Dr. Halil Ersin SÖKEN

July 2023, 122 pages

In terms of Gokturk-2 satellite Attitude and Orbit Control Subsystem- AOCS estimation performance, couple of methods are proposed to increase the onground accuracy. First of all, customized star tracker (STR) delay compensation methods are compared since they are widely used for fine attitude estimation. Due to the processing time for tasks such as star identification, tracking and attitude solution, a STR can provide the attitude quaternion measurements with a time-delay, which may be as high as few 100 milliseconds. This study evaluates different time delay compensation methods to incorporate delayed STR measurements in the Gokturk-2 satellite attitude filter, which is structured as Multiplicative Extended Kalman Filter (MEKF). They are both evaluated using the simulated data generated for an Earth observation satellite and the logged real STR data. The usage of additional gyro data to evaluate the estimation performance of the proposed method is also demonstrated using the real-logged data. The results show that, both demontration results with simulated and real data confirm that one of the proposed methods clearly overcomes the others in terms of attitude estimation accuracy.

Keywords: Gokturk-2, AOCS, Star Tracker Delay.

ÖZ

GÖKTÜRK-2 UYDUSU İÇİN YÖNELİM KESTİRİM PERFORMANSI İYİLEŞTİRMESİ

Kahraman, Özgür
Doktora, Jeodezi ve Coğrafi Bilgi Teknolojileri
Tez Yöneticisi: Prof. Dr. Zuhal AKYÜREK
Ortak Tez Yöneticisi: Dr. Halil Ersin SÖKEN

Temmuz 2023, 122 sayfa

Göktürk-2 uydusunun yönelim ve yörünge kontrol alt sistemi (YYKS) kestirim performansı açısından, yerdeki doğruluğunu arttırmak için birkaç yöntem önerilmektedir. Öncelikle, hassas yönelim kestiriminde geniş olarak kullanılmaları sebebiyle özelleşmiş Yıldızizler gecikme telafi yöntemleri karşılaştırılmaktadır. Yıldız tespiti, takibi ve yönelim çözümü gibi görevlerin işlem süresi nedeniyle, bir Yıldızizler, yönelim kuaterniyon ölçümlerini birkaç 100 milisaniye kadar yüksek olabilecek kadar gecikme ile sağlayabilir. Bu çalışma, Çarpımsal Genişletilmiş Kalman Filtresi (ÇGKF) olarak yapılandırılmış Göktürk-2 uydu yönelim filtresindeki gecikmiş Yıldızizler ölçümlerini birleştirmek için, farklı zaman gecikmesi telafi yöntemlerini değerlendirir. Bu yöntemler, hem bir yer gözlem uydusu için oluşturulmuş benzetim verisi hem de kaydedilmiş gerçek Yıldızizler verisi ile değerlendirilmektedir. Kestirim performansını, önerilen yöntem ile değerlendirmek için ilave dönüölçer verisinin kullanımı gerçek-kayıtlı veri yardımı ile gösterilmiştir. Sonuçlar, benzetim ve gerçek verili gösterim sonuçlarının her ikisinin de, yönelim kestirim doğruluğu açısından, önerilen bir metodun diğer metodlara açıkça üstün gelmesini teyit ettiğini göstermektedir.

Anahtar Kelimeler: Göktürk-2, YYKS, Yıldızizler Gecikmesi

I dedicate to this thesis to all my family members who supported me.

My father Mustafa, my mother Binnur, my brother Oğuz and mother-in-law Meltem.

My wife Duygu, without her support I could never be successful.

My sons, Kerem, Ozan and Eren, I apologize from them for stealing their valuable time.

ACKNOWLEDGMENTS

The author wishes to express his deepest gratitude to his supervisor Prof. Dr. Zuhal Akyürek and co-supervisor Associate Prof. Dr. Halil Ersin Söken for their guidance, advice, criticism, encouragements and insight throughout the research.

The author appreciate his colleagues in TUBITAK UZAY Space Technologies Research Institute for their suggestions and comments.

This study is published under the permission of Republic of Türkiye, Ministry of National Defence, Turkish Air Force Command, E-22081665-152-159/138736.

TABLE OF CONTENTS

ABSTRACT v

ÖZ vi

ACKNOWLEDGMENTS viii

TABLE OF CONTENTS ix

LIST OF TABLES xiii

LIST OF FIGURES xiv

CHAPTERS

1 INTRODUCTION 1

1.1 Gokturk-2 Satellite Overview 1

1.2 AOCS Architecture of Gokturk-2 Satellite 3

1.3 AOCS Estimation Performance and Resultant Geolocation Accuracy 6

2 LITERATURE REVIEW 9

2.1 Spacecraft Attitude Filtering 9

2.2 Incorporating Measurement Delays 11

3 PRELIMINARIES FOR ATTITUDE ESTIMATION 15

3.1 Coordinate systems, reference systems and coordinate frames 15

3.1.1 Space-fixed or celestial reference systems 17

3.1.2 Earth-centered inertial (ECI) and Earth-centered Earth-fixed (ECEF) coordinate frames 17

3.2 Coordinate Systems of Gokturk-2 Satellite 20

3.2.1 Mechanical Reference Frame (MECH) 20

3.2.2 Satellite Body Reference Frame (BODY) 20
3.2.3 Orbital Reference Frame (ORB) 22
3.2.4 Earth Centered Inertial Frame (ECI) 23
3.2.5 Earth Centered Earth Fixed Coordinate Frame (ECEF) 24
3.2.6 Local (Sensor) Coordinate Frames 24
3.3 Attitude Representations 25
3.3.1 Euler Angle Representations 27
3.3.2 Quaternion Representations 28
3.3.3 Direction Cosine (Rotational) matrix to quaternions 29
3.3.4 Quaternion to Direction Cosine matrix transformation 31
3.3.5 Quaternion Product 31
3.4 Spacecraft Dynamics 34
3.5 Spacecraft Kinematics 35
3.6 Attitude Hardware: AOCS equipment of Gokturk-2 satellite 37
3.7 Spacecraft Measurements 50
4 ATTITUDE FILTERING 51
4.1 Kalman Filtering 51
4.2 Multiplicative Extended Kalman Filtering- MEKF for Satellite Attitude Filtering 52
4.3 Dynamics-based and Gyro-based Multiplicative Extended Kalman Filtering 52
4.4 The Dynamics-based Multiplicative Extended Kalman Filter- MEKF 53
4.4.1 Propagation (Prediction) Phase 53
4.4.2 Update (Correction) Phase 55

4.5 Gyro-based Multiplicative Extended Kalman Filter- GBMEKF 57
4.5.1 GBMEKF: Propagation phase 58
4.5.2 GBMEKF: Update phase 62
5 INCORPORATING DELAYED STR MEASUREMENTS IN THE MEKF .65
5.1 Method-1 65
5.2 Method-2 66
5.3 Method-3 66
5.4 Method-4 67
5.5 Method-5 68
5.6 Evaluation and Comparison of Methods for Incorporating Delayed Star Tracker Measurements 69
5.6.1 Estimation Results for the Simulated Data 70
5.6.2 Estimation Results for the True Data 75
5.7 Results and Discussions for Incorporating Delayed STR Measurements in the MEKF 79
6 PERFORMANCE EVALUATION OF GOKTURK-2 SATELLITE AOCS VIA GYRO BASED MEKF 81
6.1 Gyro Noise Analysis 82
6.2 Performance Evaluation of Gokturk-2 Satellite AOCS via Gyro Based MEKF: Results and Discussions 84
7 CONCLUSIONS AND RECOMMENDATIONS 93
REFERENCES 95
APPENDICES
A. Explicit form of the left handed representation of the direction cosine matrix 107

B. Explicit form of the right handed representation of the direction cosine matrix ... 108

C. Possible cases for the left handed notation of quaternion to direction cosine matrix transformation ... 109

D. Possible Cases for the Right Handed Notation of Quaternion to Direction Cosine matrix transformation ... 111

E. Spacecraft Dynamics: Derivation of Satellite's Dynamic Equation via Dyadic Tensor ... 113

CURRICULUM VITAE ... 119

LIST OF TABLES

TABLES

Table 1-1 The Low Earth Orbit- LEO satellite chronology of native Turkish Space Program 3
Table 1-2 Spectral properties of Gokturk-2 Satellite Images [36] 3
Table 3-1 Characteristics of Attitude Representations of Euler Angles Quaternions (Table1.1 of [77]) 26
Table 3-2 AIRBUS Sodern SED 26 Star Tracker Performance Specifications 38
Table 3-3 SGR-10 GPS Receiver Performance Specifications 38
Table 3-4 SSTL Gokturk-2 Gyro Specifications (Expected Values) 40
Table 3-5 SSTL Gokturk-2 Gyro Scale Factor Analysis Results 42
Table 3-6 SATRECI Analog Fine Sensor, FSS-5 Technical Specifications 43
Table 3-7 The Specifications of SATRECI MAG-30 Magnetometers 44
Table 3-8 ZARM TECHNIK Magnetorquer, MT-70 Technical Specifications 45
Table 3-9 TELDIX RSI 15-215/20 Reaction Wheel Specifications 48
Table 5-1 RMSE Results of 100 Monte Carlo Simulation Runs for Zone-4 (arc seconds) 75

LIST OF FIGURES

FIGURES

Figure 1-1 Gokturk-2 AOCS Subsystem Diagram 5
Figure 2-1. Incorporating delayed STR measurements by propagation. 14
Figure 2-2. Incorporating delayed STR measurements by buffering the states and interpolation. 14
Figure 3-1. Hierarchy of reference frames- from space-fixed via earth-fixed to local horizontal (From Figure 2.1 of [71]) 16
Figure 3-2. Process to transform from celestial to terrestrial reference systems (Chart from the IAU Working Group on Nomenclature for Fundamental Astronomy (2006), From Figure 5.1 of [75] 19
Figure 3-3. Satellite Mechanical and Body Reference Frames 21
Figure 3-4. Orbital Reference Frame Definition 22
Figure 3-5. ECI (GCRF) Reference Frame Definition 23
Figure 3-6. ECEF (ITRF) Reference Frame Definition 24
Figure 3-7. AIRBUS SODERN- SED 26 Single Head Star Tracker [85] 37
Figure 3-8. SSTL SGR-10 GPS Receiver and antennas [86] 39
Figure 3-9. SSTL MEMS Gyro Unit [87] 39
Figure 3-10. Gyro-1 Allen Variance Graphic 40
Figure 3-11. Gyro-2 Allen Variance Graphic 41
Figure 3-12. Gyro-3 Allen Variance Graphic 41
Figure 3-13. SATRECI Analog Fine Sensor, FSS-5 43
Figure 3-14. SATRECI Magnetometer, MAG-30 44
Figure 3-15. ZARM TECHNIK Magnetorquer, MT-70 45
Figure 3-16. ZARM TECHNIK Magnetorquer, MT-70 Magnetic Torque – Applied Current Graphic 46
Figure 3-17. TELDIX RSI 15-215/20 Reaction Wheel 47
Figure 3-18. TELDIX RSI 15-215/20 Reaction Wheel- Spinning Axis Definition 47

Figure 3-19. TELDIX RSI 15-215/20 Reaction Wheel- Motor Torque versus Speed 48
Figure 4-1. Small ω approximation errors 61
Figure 5-1. Method 1 Time Chart for STR Measurement Propagation 66
Figure 5-2. Method 2 Time Chart for STR Measurement Propagation 66
Figure 5-3. Method 3 Time Chart for STR Measurement Propagation 67
Figure 5-4. Method 4 Time Chart for STR Measurement Propagation 68
Figure 5-5. Method 5 Time Chart for STR Measurement Propagation 69
Figure 5-6. Spacecraft Maneuver Scheme for Simulation Cases 70
Figure 5-7. Estimation Errors for Simulated Data: Method 3 71
Figure 5-8. Estimation Results for Simulated Data: Method 4 72
Figure 5-9. Estimation Results for Simulated Data: Method 5 73
Figure 5-10. Monte Carlo Simulations Results: RMS Values for Different Methods 74
Figure 5-11. Estimation Results for True Data: Onboard Estimator RPY 76
Figure 5-12. Estimation Results for True Data: Method-4 Estimator RPY 76
Figure 5-13. Estimation Results for True Data: Method-4 Difference of Onboard and Estimated RPY 77
Figure 5-14. Estimation Results for True Data: Method-5 Estimator RPY 78
Figure 5-15. Estimation Results for True Data: Method-5 Estimator RPY 78
Figure 6-1. Allen Variance Graphics of The Gyro Unit obtained from Onboard Data 83
Figure 6-2. Estimation Results for Attitude Angles: Method 5- Onboard Estimator RPY 85
Figure 6-3. Estimation Results for Attitude Angles: Method 5- Estimated RPY 85
Figure 6-4. Estimation Results for Attitude Angles: Method 5- Difference of Onboard and Estimated RPY 86
Figure 6-5. Estimation Results for Attitude Rates (Obtained indirectly from bias values): Method 5- Onboard Filter Estimation- w_{bob} 87

Figure 6-6. Estimation Results for Attitude Rates (Obtained indirectly from bias values): Method 5- Onboard Filter Estimation- Sync w_{bib} 87
Figure 6-7. Estimation Results for Attitude Rates (Obtained indirectly from bias values): Method 5- Filter Estimation- w_{bib} 88
Figure 6-8. Estimation Results for Attitude Rates (Obtained indirectly from bias values): Difference Between Onboard Filter Estimation and Filter Estimation..... 89
Figure 6-9. Attitude Rates obtained from the Gyro Data in Gyro Frame..... 89
Figure 6-10. Attitude Rates obtained from the Gyro Data in Body Frame 90
Figure 6-11. Gyro Biases Estimated via Gyro-based MEKF: Method 5 91
Figure 7-1 Reference Frames for the derivation of spacecraft dynamic equation 113

CHAPTER 1

INTRODUCTION

1.1 Gokturk-2 Satellite Overview

Gokturk-2 satellite, is another milestone in Turkish Space Program, after BILSAT and RASAT satellites. BILSAT satellite was launched in 2003 and during the project period technology transfer program had been executed, [1], [2]. RASAT satellite is manufactured by TÜBİTAK UZAY Space Technologies Research Institute and very important native payloads are developed and qualified [3]. RASAT was launched in 2011 and had been operational until the end of 2022. The images of RASAT satellite has been used in many fields, [4]. The images of the satellite can be acquired from the online portal called GEOPORTAL: TÜBİTAK UZAY Satellite Data Processing and Sharing System (https://gezgin.gov.tr) [5].

Gokturk-2 satellite was launched in 18th of December in 2012 and it is still operational in orbit over 10 years by the time of the current study. The satellite carries various native payloads. Gokturk-2 image processing scheme is given in [6]. The detailed information about the satellite design and the operations can be found in [7]–[9]. On-Board Data Handling (OBDH) subsystem of Gokturk-2 satellite is given in [7]. Power subsystem of Gokturk-2 is given in [8]. The flight operations of the satellite for early years could be seen in [9].

The Gokturk-2 images are widely used in remote sensing area for various applications, [10]–[19]. In the upcoming years, following studies in which Gokturk-2 images are used, have been added to the literature, [20]–[29] and [30]–[35]. In these studies Gokturk-2 images are used for determining roads, classification of agricultural pattern, extracting digital elevation maps, DEM and investigating the accuracy, pan sharpening, band registration and estimating ground sampling distance.

In terms of radiometric calibration of Gokturk-2 images, Topan et. al. [12], Sakarya et. al. [13] and Teke et. al. [36], had studies which evaluate the images. Efendioglu et. al. [19] and Atak et. al. [37], investigated the images for geometric calibration of the Gokturk-2 images.

Küpcü et. al. [10], Ok et. al. [23] and Mutluoğlu et. al. [24] made contribution to the literature in terms of DEM extraction, investigating the accuracy and selection effects on orthorectification success rate. Kocaman et. al. [25] and Ok et. al. [17] studied on 3D images of the Gokturk-2 satellite.

The classification studies with Gokturk-2 images have been performed by Teke et. al. [14], Gurcan et. al. [18] and Bağdatlı et. al. [21]. Bulut et. al. [22] and Göğerçin et. al. [27] used Gokturk-2 satellite images for parameter estimation.

In terms of Pan sharpening, Ozendi et. al. [15], [16], investigated the quality of Gokturk-2 images. Kahraman et. al. [26], made a review of pansharpening algorithms for Gokturk-2 images. Bakioğlu et. al. [30], studied the pan sharpening of Gokturk-2 images via high pass filter.

In relation to discrimination, Kalkan et. al. [11], analyzed vegetation discrimination from Gokturk-2 images. Bugday et. al. [20], determined unofficial forest roads by using Gokturk-2 images. In terms of extraction from the images, Bayram et. al. [28] Batur et. al. [29], Başak et. al. [31], Yesilyurt et. al. [32] and Kaynarca et. al. [34] made contribution to the literature.

The satellite chronology of native Turkish Space Program is given in and the spectral properties of Gokturk-2 satellite is given in Table 1-2.

Table 1-1 The Low Earth Orbit- LEO satellite chronology of native Turkish Space Program

	BILSAT	**RASAT**	**GOKTURK-2**	**GOKTURK-1**	**IMECE**
Launch Date	27.09.2003	17.08.2011	18.12.2012	05.12.2016	15.04.2023
Orbit	686 km	685 km	680 km	686 km	68o km
Mass	129 kg	94 kg	400 kg	1060 kg	700 kg
Resolution	12.6 m PAN 26.7 m MS	7.5 m PAN 15 m MS	2.5 m PAN 5 m MS	0.5 m PAN 2 m MS	0.99 m PAN 3.96 m MS
Swath Width (Nadir)	25 km PAN 55 km MS	30 km	20 km	15 km	17 km

Table 1-2 Spectral properties of Gokturk-2 Satellite Images [36]

Band	Wavelength (nm)	Central Wavelength	FWHM (nm)	E_{SUN}
Blue	0.450 – 0.520	485	74.7	1979
Green	0.520 – 0.600	560	73.5	1857
Red	0.630 – 0.690	660	133.2	1558
NIR	0.760 - 0.900	830	117.1	1056.3
PAN	0.450 – 0.900	675	300	1499

1.2 AOCS Architecture of Gokturk-2 Satellite

The AOCS subsystem is configured in accordance with the project goals. As accurate sensors, star trackers and gyro units are used in AOCS architecture. In terms of star

trackers, instead of multiple optical head units, the single units are used in cold redundant configuration. However, because of the flight software heritage which comes from RASAT satellite, the gyro-less multiplicative extended Kalman Filter is used in AOCS filter and thus gyro units are not considered in nominal operations. Surrey Satellite Technologies Limited, SSTL's GPS receiver, which offers moderate performance is used for orbital information for this purpose.

In terms of coarse attitude estimation modes, three axis magnetometers, magnetorquers and analog fine sunsors are used. These sensor outputs are processed by the Kalman filter in coarse attitude modes.

The actuators of the satellite are 4 reaction wheels which are located in tetrahedral configuration, the magnetorquers and the propulsion system. Four reaction wheels are used to control the satellite in there axes and magnetorquers are used to desaturate the wheels. The chemical propulsion system which uses hydrazine fuel is used for the ability of changing the orbit.

The AOCS architecture of the Gokturk-2 satellite is mainly inherited from RASAT satellite. The details of the commissioning of the satellite, AOCS flight software testing with dynamic attitude simulator environment and defining the attitude performance requirements and budgeting is given in [38]–[40].

The Orbital Dynamics System, ODS software is used in terms of operational settings of Gokturk-2 satellite for precise orbital mechanics analysis, modelling, estimation and control functionalities, [41]. Local Time of the Ascending Node, LTAN target and evolution profiles of the Gokturk-2 satellite are also given in [41].

The details of the AOCS architecture of the Gokturk-2 satellite is given in Figure 1-1.

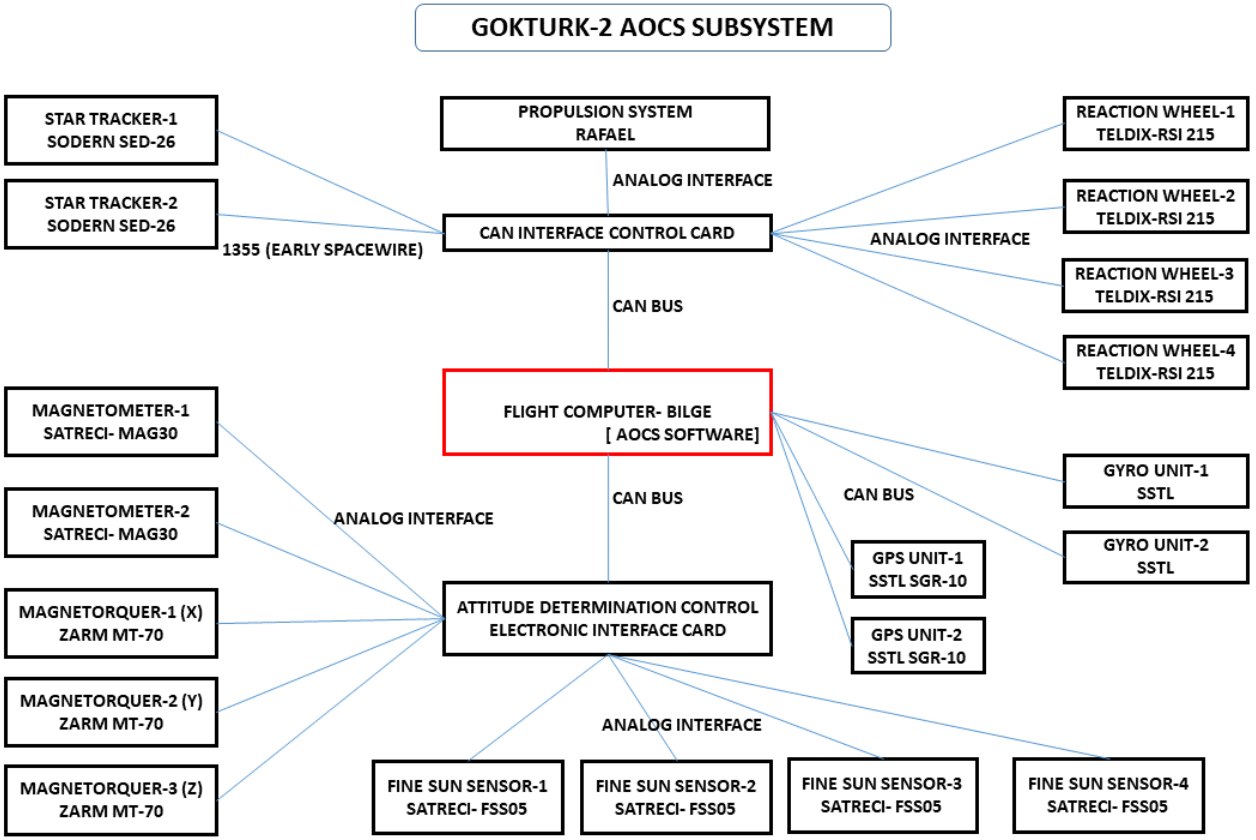

Figure 1-1 Gokturk-2 AOCS Subsystem Diagram

1.3 AOCS Estimation Performance and Resultant Geolocation Accuracy

The attitude estimation requirement of the Gokturk-2 satellite in three-axis is defined as 0.02^0 (3σ). This value states 245 m geometric accuracy onground. The geolocation accuracy depends on both attitude and position errors and these errors are coupled. In terms of attitude hardware performances, the star trackers provide attitude accuracy better than 40 arc seconds (3σ), which corresponds to 135 m error onground. Moreover, GPS module has a 25 m position accuracy (3σ) and the positional error cause nearly 50 m attitude errors relatively. Since the GPS module obtains single frequency solution, the performance evaluation is quite difficult. The star tracker alignment and inertia calibrations are performed onground to increase the resultant filter performance. It is verified that the total error for the attitude estimation is below the requirement level.

It is stated that nominally true or processed attitude and orbit data are used together with the sensor model for georeferencing to indicate the pixel locations, [6]. The geolocation accuracy of the satellite could be improved via ground control points (GCPs) which are the specific points that can be identified on the image and their geographical coordinates are known from on-site Global Positioning System (GPS) measurements. Thus, geolocation accuracy of a remote sensing satellite is defined in two ways: without GCPs and with GCPs. Since the accuracy improvement depends on the number and the distribution of the GCPs, geolocation accuracy with one GCP (specifications are defined) can be used as standard definition.

Gokturk-2 georeferenced image product (2.5 m PAN) has 100 meters or better accuracy (without GCPs), [6]. This accuracy is obtained by on-ground processing of satellite's metadata, which includes attitude and orbit data. The accuracy on the order of the 100 m is analyzed by Teke [6], by using the Landsat 8 panchromatic mosaic images of Turkey which has 12 m CE90 (Circular Error by % 90 range) positional accuracy. The effect of choosing references and digital elevation models for the orthorectification performance is also analyzed by [6].

Geolocation accuracy of the Level-2 (L2) images of Gokturk-2 satellite is analyzed by [37], by using orthophotos acquired from air photographs (30-40 cm resolution) which are included in Geographical Analysis System software which is developed by General Directorate of Mapping (HGK). It is stated that geolocation accuracy of < 10 m (~ with 56 m standard deviation) can be provided in case of using proper ground control points (random points chosen from 30-40 cm resolution orthophotos) and digital terrain elevation data (HGK DTED2) with the assumption of approximate camera model, [37]. As it is emphasized, physical camera model needs to be improved by performing a full calibration campaign so that all camera properties could be represented in the model. A proper test site needs to be determined to achieve this goal, as a good network of GCPs has to be constructed.

Geolocation accuracy that is defined without GCPs, mainly depend on the data acquired from the onboard attitude and orbit sensors. The onboard EKF, filters the outputs of these data and whether this filtered results or the sensor data itself is used in metadata. Thus, attitude and orbit determination performance of the satellite can directly be measured by the geolocation accuracy given without GCPs. However, camera sensor model is also directly affects the geolocation accuracy. In Gokturk-2 satellite, the sensor model information is involved in ground software called Orbital Dynamics System- ODS, which uses georeferencing with backward projection algorithm that depends on line of sight of the pixel position and this algorithm does not use common sensor model parameters namely focal length and principal points.

In terms of Gokturk-2 orbit data, the GPS module is turned on during the imaging interval and the output of its data is filtered by the AOCS filter to obtain position and velocity vectors. If the GPS measurements are not available or the results are not reliable, onboard orbit propagator results are included in the metadata. In Gokturk-2 satellite, single frequency GPS receiver, which has the positional accuracy of <25 meters and velocity accuracy of < 0.25 meters per second is used to obtain orbital information.

In terms of attitude data, operational star tracker's output is filtered by the onboard EKF and resultant quaternions are used in metadata. In operational mode, the attitude data in downloaded metadata is processed by the ground software by polynomial interpolation of 5th order by the ODS software. Since attitude results are obtained in 1 Hz sampling period, polynomial fitting is performed for better geolocation accuracy.

In this thesis, in Chapter 1, the scope of the study is introduced and in Chapter 2, the literature survey has been performed for all regarding chapters. In Chapter 3, necessary foundations for the study is given namely the details of coordinate frames, attitude representations, spacecraft dynamics and kinematics, the details of the attitude hardware equipment, and the measurement models of the sensors. In Chapter 4, academic infrastructure of the Kalman Filtering is given such that basic principles of the Kalman Filtering, equations of the Dynamic-based Multiplicative Extended Kalman Filter and Gyro-based Multiplicative Extended Kalman Filter are given in detail. Incorporating Delayed Star Tracker Measurements in MEKF for Gokturk-2 satellite which is one of the key contributions of the thesis is given in Chapter 5. In this study, 5 different methods are explained in detail and coded in Matlab environment. The original Gokturk-2 satellite data is used for onground post-processing to demonstrate the effects of all the proposed methods. The onboard filter results are compared with the simulation results and the proficiency of the suggested method is demonstrated. The simulation results confirm that, one of the proposed methods clearly overcomes the others in terms of attitude estimation accuracy. In Chapter 6, performance evaluation of Gokturk-2 Satellite Attitude and Orbit Control Subsystem via Gyro Based Multiplicative Extended Kalman Filter is given to evaluate the estimation accuracy. In this study, the attitude estimation accuracy of the filter is assured by using coarse MEMS Gyros. In the last chapter, conclusion and recommendations are summarized and discussed.

CHAPTER 2

LITERATURE REVIEW

2.1 Spacecraft Attitude Filtering

In terms of Gokturk-2 attitude estimation, standard Extended Kalman Filtering, which is almost an industry standard, is implemented onboard. Kalman filtering is one of the major improvements for attitude and orbit determination systems for decades since it has been developed by Rudolph Emil Kalman (1930-2016), [42]. During the years, many versions of Kalman Filters (KF) are developed. Kalman filtering is applied to spacecraft attitude determination systems for various missions. Lefferts et al.'s study, [43] is one of the earliest applications of Kalman filtering which is implemented for spacecraft attitude estimation and common usage of attitude quaternion representations are proposed.

A new approach for nonlinear filtering is firstly proposed by Julier, Uhlmann and Durrant-White in 1995, [44]. Afterwards, in the subsequent studies, it is named as Unscented Kalman Filter, UKF, [45]. The implementation of UKF to the spacecraft attitude estimation is firstly proposed by Crassidis and Markley, [46]. In terms of nonlinear spacecraft attitude estimation methods, a detailed survey research is performed by Crassidis, [47].

The six state EKFs are commonly used in satellite applications. In terms of attitude performance, it depends on the performance needs of the mission and in most cases six state EKFs offer fair performances. However, state augmentation is a must for better attitude performance. The literature should be covered for the comparison of these approaches, [48], [49].

In terms of current studies on attitude estimation, the following literature which is mainly on CubeSats could be focused, [50]–[56]. Here we focus mainly on small

satellites since it is possible to find several publications investigating the actual in-flight results for such missions. The CubeSat concept was first initiated by Stanford University and California Polytechnic State University by including 20 research institutes from all around the world, [57]. Within this progress, new studies came into a live for the attitude estimation of this satellites.

ZDPS-1A pico-satellites are considered as the first 1-10 kg mass range satellites in China's space program. They are slightly heavier than standard CubeSats such that they have the dimension of 15 cm x 15 cm x 15 cm. In this mission, attitude determination and control system- ADCS experiments have been performed to evaluate the correctness and effectiveness of the ADCS via attitude detumbling and stabilizing, [50].

The JAXA's The Small Demonstration Satellite (SDS) program is organized to demonstrate the advanced technologies in-orbit. SDS-4, which is a 50 kg class satellite has been successfully tested for initial acquisition and nominal Sun pointing modes in terms of AOCS, [51].

The Radio Aurora Explorer (RAX) CubeSats are developed for space weather monitoring and commercial-off-the-shelf components such as magnetometers, photodiodes and MEMS gyros, are used in the satellite AOCS configuration. A multiplicative extended Kalman filter is implemented in estimation software and sensor alignment errors are corrected via on-board calibration. It is stated that 0.5^0 (1σ) attitude determination accuracy had been demonstrated by replacing pre-flight calibration with on-orbit calibration which maximized the performance, [52].

ESTCube-1 satellite, which has a mission of centrifugally deploy a tether as a part of the first in-orbit demonstration of electric solar wind technology, owns an attitude determination system- ADS which uses magnetometers, gyro units, sun sensors and unscented Kalman filtering- UKF algorithms. The attitude determination performance have been validated through images taken from on-board camera and on-board ADS via classical attitude determination methods, [53].

Hodoyoshi-3 and 4 satellites are 50 kg class satellites, which were developed by University of Tokyo. It is stated that, in case of any sensor or actuator failure, satellite ADCS survivability has critical role. In terms of lessons learned, it is emphasized that the choice of ADCS modes and defining the mode transitions are very important. Moreover, regarding modes should handle the component failure cases and must be verified by the simulations, [54].

The Seoul National University global navigation satellite system laboratory satellite, SNUGLITE is a two-unit (2U) CubeSat. The core mission objectives are, implementing a methodology of the on-ground processing which includes comparing estimated attitude from the Sun vector, satellite filter and the reference vector obtained from the solar panels, verifying on-board L1/L2C GPS receivers and lastly developing Linear Quadratic Regulator- LQG based EKF algorithms. It is stated that a pointing accuracy of 6.1^0 (RMS) is achieved, [55].

Aalto-1, the Finnish student 3U CubeSat includes payloads such as Aalto Spectral Imager (AaSI), Radiation Monitor (RADMON) and Electrostatic Plasma Brake (EPB). In terms of ADCS in-orbit performance, detumbling of the satellite via B-dot controller has been achieved after solving the magnetorquer driver problem with a firmware update. It is also stated that some other ADCS modes which includes controlled spin up for tether deployment failed, [56].

2.2 Incorporating Measurement Delays

Sensor selection for spacecraft attitude estimation primarily depends on the mission requirements. A variety of sensors can be used. Yet for missions requiring high precision pointing (e.g. for an Earth observation spacecraft) having a star tracker (STR) onboard is inevitable. Then, in most cases the STR is coupled with gyros and a gyro-based attitude filter is used. The filter estimates the attitude and gyro biases, and corrects the gyro readings with the estimated bias terms. If there is no available

gyro then a dynamics-based filter that incorporates also the spacecraft dynamics and estimates the angular velocity terms along with the attitude is used [58].

Irrelevant to the architecture of the attitude filter and type of the used filtering algorithm, if the STR is the primary attitude sensor onboard, STR errors dominate the attitude estimation accuracy. One of these STR errors, which has not been widely discussed in literature is the delay in the measurements. A typical STR provides quaternion measurements at a rate up to a few 10s of hertz [59], [60]. Nonetheless, the delay in the measurements which is simply the time difference in between the timing of the actual star image used for attitude calculation and the timing when these measurements become available to the attitude filter may be as long as few 100 milliseconds. Although this number seems not that much large, when a spacecraft in the middle of an agile maneuver with an angular rate of 1deg/s is considered, 100 millisecond of delay means the satellite has drifted 0.1deg by the time the measurement is processed. In the end, such error, if not accounted for, will cause a serious deterioration in the accuracy of the attitude filter.

In terms of general scope of the incorporating the measurement delay the regarding literature can be evaluated, [61]–[66].

Incorporating infrequent and delayed measurements are presented in [61]. The evaluation methods are classified into two categories such that the first one is fusing the primary measurements when they are arrive and the second one is augmenting the states. It is stated that the results have identical estimation accuracy performances for both methods.

A predictor is proposed to compensate the output measurement delays of an observer via fusing them with the current input measurements, [62]. The predictor architecture is established in a cascade observer-predictor arrangement such that delayed system states are obtained by an observer and predictor compensates for the delay. Similar methodology is extended for attitude estimation problem in the case of sampled and delayed vector measurements, [63]. It is declared that the predictor reconstructs continuous time delay free predictions of the vector measurements.

A Moving Horizon Estimator, MHE, which is a batch estimator is proposed to compensate the time-delayed measurements when dealing with the multi-rate sensor fusion, in [65]. Since the batch estimator has disadvantages in terms of computational load, more efficient implementation which uses linear MHE coping the multi-rate time-delayed measurements have been investigated for fast dynamical systems. It is stated that the performance analysis have been performed and the results indicate that better estimation accuracy is achieved with the proposed implementation for the fast dynamical systems.

A survey study has been performed for incorporating nonuniform and delayed information in state estimation and a novel taxonomy which allows faster selection of the state estimator is proposed in general terms to handle the regarding issue, [64]. The common applications in the literature were summarized and analyzed.

A novel Takagi-Sugeno predictor observer is proposed to handle the constant and known measurement delays in [66]. The observer implemented for wheeled mobile robot for trajectory tracking as the parallel distributed compensation control is used and the Lyapunov stability of the observer is shown.

In few recent studies, methods to incorporate the delayed STR measurements in the attitude filters are discussed. In [67], the measurements are propagated to the filter time (Figure 2-1) and the measurement noise covariance matrix is processed such that the propagation error is included. No discussion related to the filter's optimality and modification of the states, which have been already estimated ($\hat{x}_{k-2}$, $\hat{x}_{k-1}$ in Figure 2-1) is provided. In [68], the last 15 states are buffered and whenever a STR measurement is available, the estimated states are interpolated to the exact timing of the measurements (Figure 2-2). If the whole trajectory of states is recalculated until the current step, this method, which is called filter recalculation method [69], provides optimal estimates for the whole estimation history. Yet, due to the buffered states it is computationally expensive. Last, in [69] the filter recalculation method and Larsen's method [70] are compared for a navigation filter for autonomous space rendezvous.

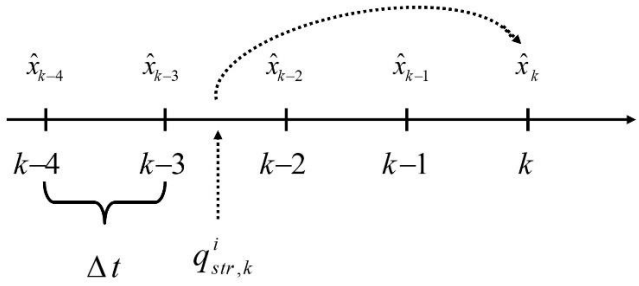

Figure 2-1. Incorporating delayed STR measurements by propagation.

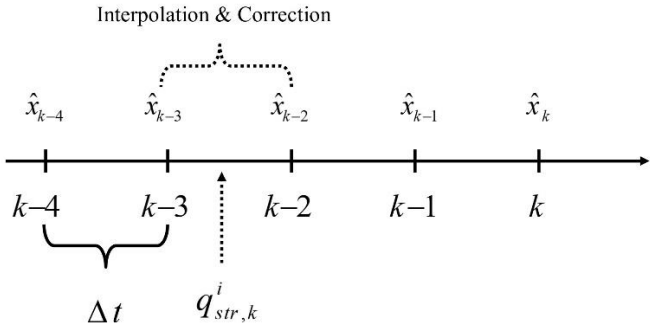

Figure 2-2. Incorporating delayed STR measurements by buffering the states and interpolation.

CHAPTER 3

PRELIMINARIES FOR ATTITUDE ESTIMATION

In this chapter, preliminary subjects are explained in detail to construct a baseline for the current study related with Gokturk-2 satellite.

3.1 Coordinate systems, reference systems and coordinate frames

The reference systems can be defined by distinguishing the three concepts first: coordinate system, reference system and reference frame [71].

Rummel et. al. [71], state that, coordinate system in three dimensions can be formed by its origin which has 3 elements, orientation of axes which has 3 elements and the scale, via using the orthonormal base vectors. The transformation of coordinates for a two coordinate frames consist of a shift of origin, and rotation of the base vectors. However, a reference system involves a descriptive coordinate system, model parameters and specified constants. Lastly, a reference frame involves all required parts to materialize the reference system in real world, such as catalogue of celestial objects for celestial frames and coordinates of terrestrial points for terrestrial frames.

When referring to Feissel, Vallado et. al. [72], explain that a frame is defined in a specific time and realized by observations, [73], [74]. According to Vallado et. al., a Cartesian coordinate system can be specified by its origin, fundamental plane and preferred direction and it is also necessary to define the sense or positive direction which shows whether the system is right handed or left handed [72]. Vallado et. al. [72], state that “system” and “frame” can be used instead of each other and explains that in fact there is a difference between them, thus in the above definition “frame” has to be used.

The hierarchy of the reference systems can be defined in three levels: space fixed or celestial reference systems, Earth fixed or terrestrial reference systems and local horizontal or topocentric systems and the relationship between these frames can be seen in Figure 3-1.

The conventional reference systems, which involve International Celestial Reference System and International Terrestrial Reference Frame, are realized by International Earth Rotation Systems Service (IERS), a service belongs to the International Association of Geodesy (IAG) and of the International Astronomical Union. The models, parameters and procedures related with the reference systems are given in IERS Conventions document (Technical document 36) [71], [75].

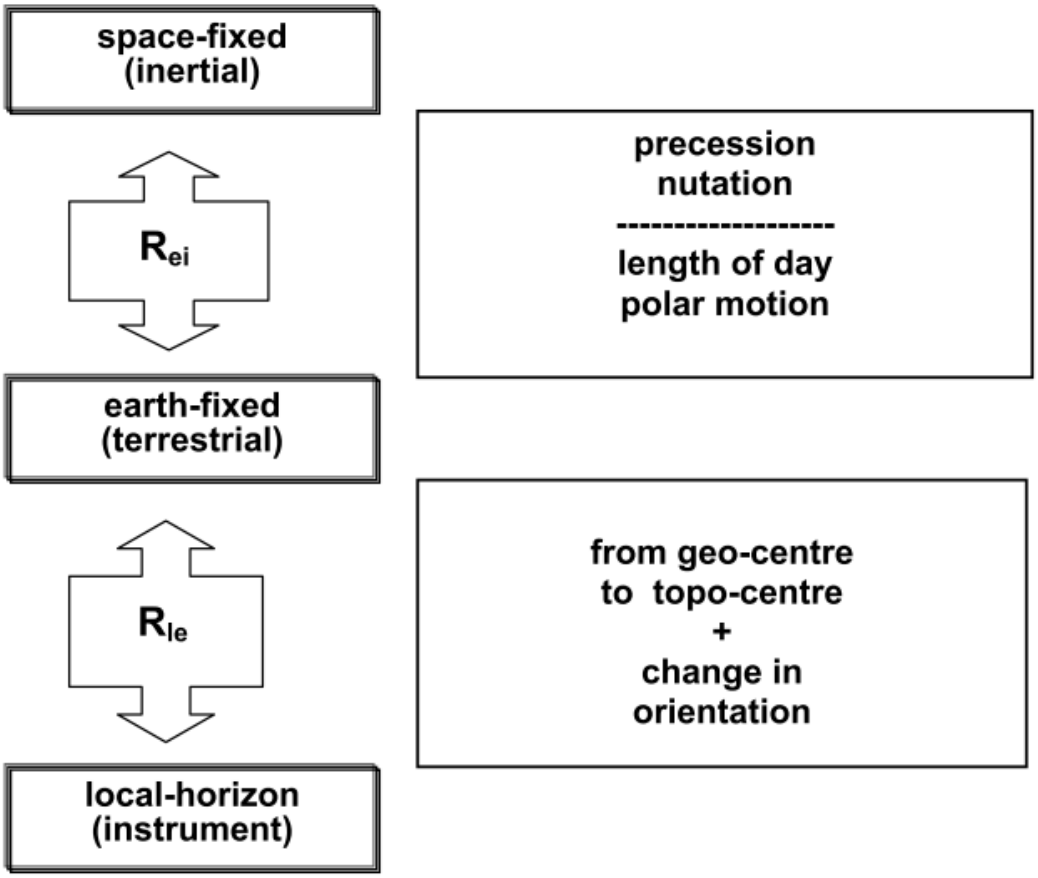

Figure 3-1. Hierarchy of reference frames- from space-fixed via earth-fixed to local horizontal (From Figure 2.1 of [71])

3.1.1 Space-fixed or celestial reference systems

Kaplan [76] states that, Celestial Reference Systems can be separated into two categories namely, barycentric and geocentric, [76]. Barycentric celestial reference system (BCRS) is used for astrometric observations. It is used for the objects located outside the gravitational vicinity of Earth. The center or the origin of the coordinate frame is the center of the Solar System called barycenter.

However, geocentric celestial reference system (GCRS) is used to specify the location and motions of near-Earth objects. The origin of the Geocentric Reference Frame, GCRF is Earth. GCRF is an Earth-centered inertial reference frame. It is stated that ICRS is a barycentric system, [75]. Their origin and the axes directions are the same and the only difference is that ICRS does not rotate with respect to the stars and the galaxies.

ICRF is realized with the use of extra-galactic radio source, mostly quasars, via Very Long Baseline Interferometry, VLBI with the accuracy of 1 miliarcsecond or better.

In Gokturk-2 satellite, the attitude of the satellite is obtained from the star tracker units. Those equipment have star catalogs inside their memory units and those catalogs are defined with respect to GCRF.

3.1.2 Earth-centered inertial (ECI) and Earth-centered Earth-fixed (ECEF) coordinate frames

The reference systems could also be classified according to their motions being inertial (non-rotating and non-accelerating) or non-inertial (rotating or accelerating). According to this classification, ECI (Earth Centered Inertial) and ECEF (Earth Centered Earth Fixed) frames are defined.

ECI frame is defined as non-accelerating reference frame. The origin is geocentric, the Z axis is towards the Geographic North Pole and the X axis is towards the Vernal Equinox. Soken et. al. [77], imply that there are different kinds of ECI frames, which

vary according to the precession and nutation of Earth, the vernal Equinox, the equatorial plane of Earth and the ecliptic with respect to time. It is dependent on the definition of these parameters, whether they are the mean or true values at specific epoch. The examples of the different ECI frames are given below:

- Geocentric celestial reference frame (GCRF), is defined as the Earth-centered version of the ICRF.
- J2000 frame, is defined in Earth's mean equator and mean equinox (that is why it is also called MEME frame) at 12:00 Terrestrial Time on January 1, 2000. In Gokturk-2 satellite, the star tracker measurements are defined in J2000 frame.
- MOD, a mean of date, is defined with the mean equator and equinox for particular date. By considering the precession the coordinate transformation between J2000 and MOD frame can be performed.
- TOD, true of data, is an intermediate coordinate frame. The coordinate transformation can be performed between MOD to TOD frames via the nutation information.
- TEME, true equator mean equinox frame, is used in NORAD'S two-line element set, however it is stated that it does not use the conventional mean equinox.

In terms of ECEF frame, International Terrestrial Reference Frame- ITRF is used in Gokturk-2 satellite. The coordinate transformation from ITRF to Terrestrial Intermediate Reference Frame TIRF is performed by using polar motion. Moreover coordinate transformation from TIRF to TEME is performed via Greenwich Mean Sidereal Time GMST.

The detailed transformation process between ICRS and the ITRS systems are defined in the Figure 3-2. The general definitions of the coordinate systems used for Satellite Geodesy can be found in the literature [72]–[78].

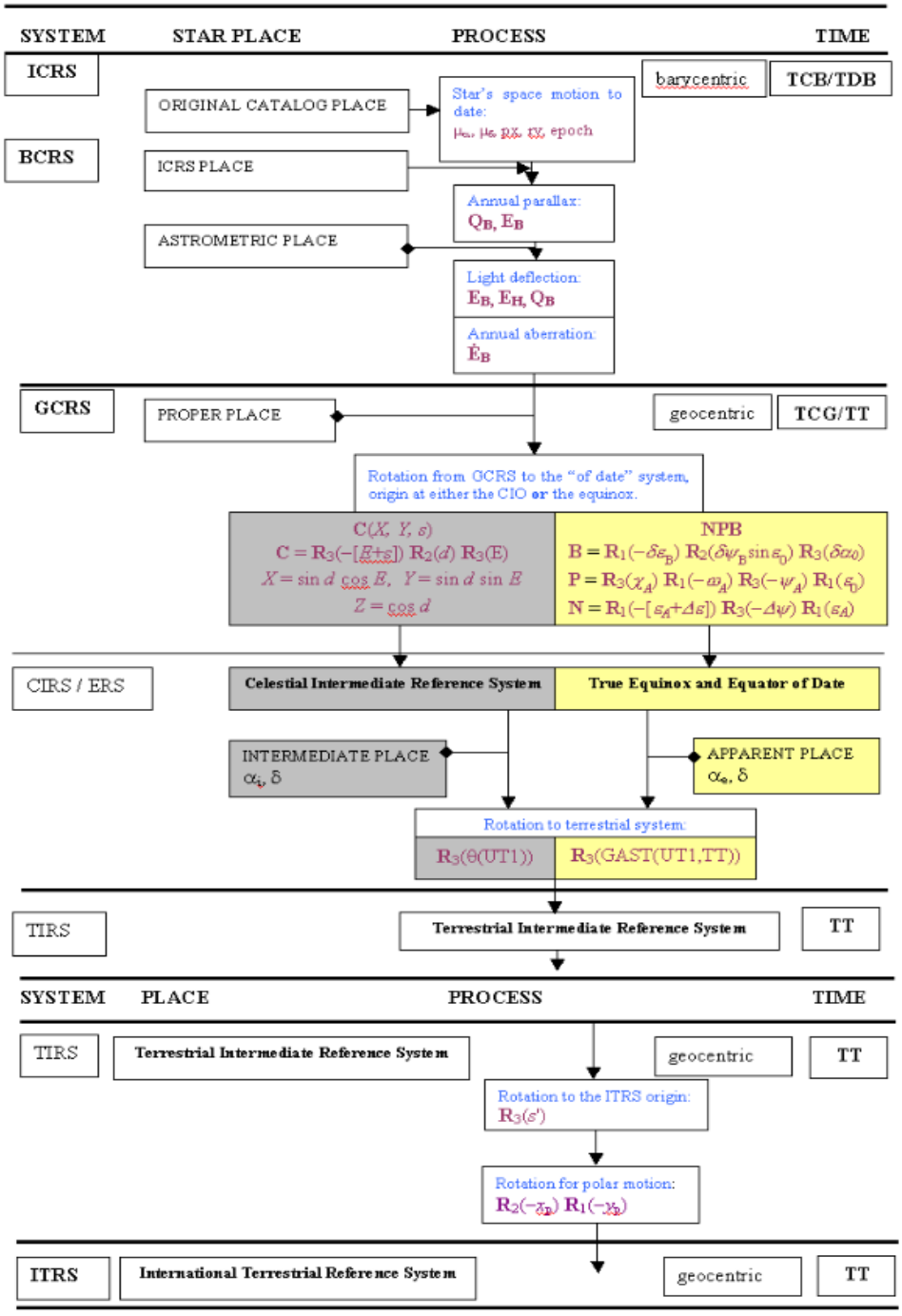

Figure 3-2. Process to transform from celestial to terrestrial reference systems (Chart from the IAU Working Group on Nomenclature for Fundamental Astronomy (2006), From Figure 5.1 of [75]

3.2 Coordinate Systems of Gokturk-2 Satellite

In this chapter, the coordinate frame definitions for Gokturk-2 satellite which orbits in Sun Synchronous Low Earth Orbit is explained.

3.2.1 Mechanical Reference Frame (MECH)

The axes of Gokturk-2 satellite mechanical reference frame are defined such that:

+ Z axis: Coincides with payload's main direction. The interface between launch vehicle is on the –Z surface. It is the normal vector of the Earth sided surface during the nominal operations.

+ X axis: Defines the flight direction.

+ Y axis: Defined according to Right Hand Rule via Z and X axes.

Origin: The midpoint of the separation ring, obtained from the mechanical measurements.

The satellite mass distribution, inertia values are measured and Center of Gravity is defined with respect to the mechanical reference frame.

3.2.2 Satellite Body Reference Frame (BODY)

+ Z axis: Same as the Mechanical Reference Frame

+ X axis: Same as the Mechanical Reference Frame

+ Y axis: Same as the Mechanical Reference Frame

Origin: The origin is defined as the center of gravity of the satellite.

The Body Reference Frame is the main reference frame for the attitude representation of the satellite. The attitude of the satellite is defined as the rotation

of orbital frame with respect to the satellite body frame. The roll, pitch and yaw angles are defined with respect to this coordinate reference frame. The mechanical and body frame definitions are given in Figure 3-3.

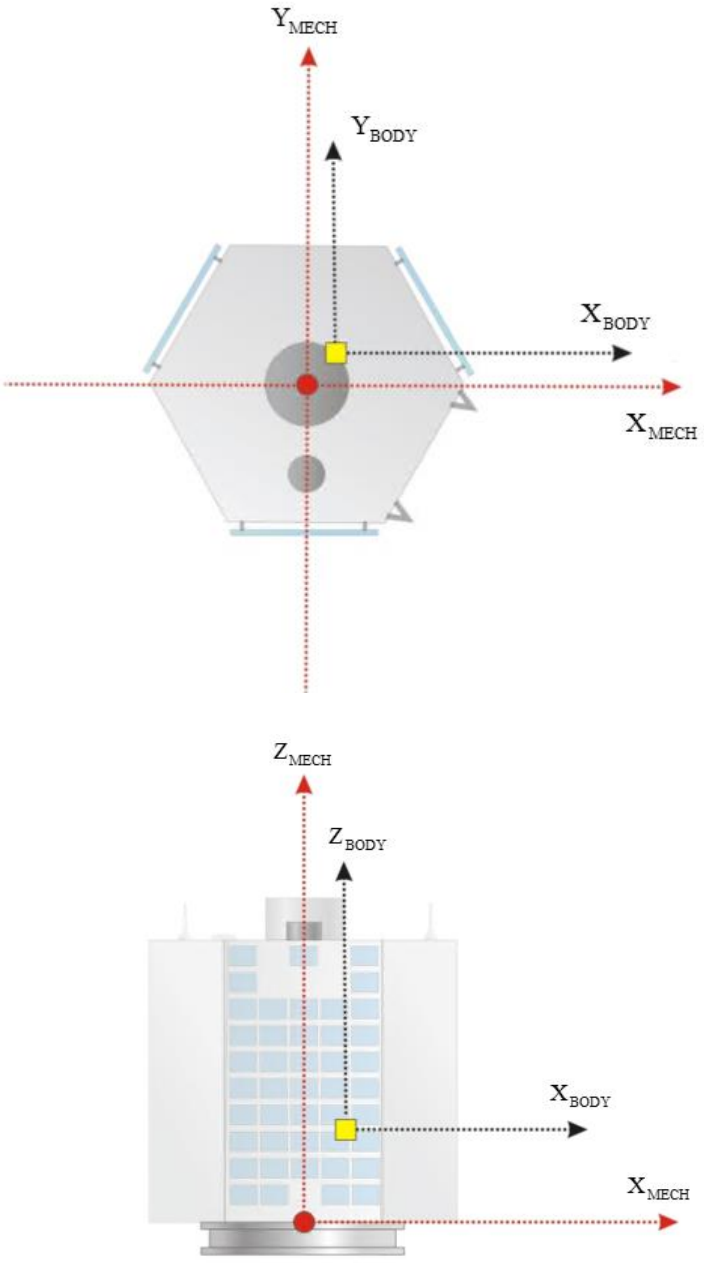

Figure 3-3. Satellite Mechanical and Body Reference Frames

3.2.3 Orbital Reference Frame (ORB)

+ Z axis: From Center of Gravity, COG to Earth's center.

+ Y axis: The opposite of the normal vector of the orbital plane.

+ X axis: Defined according to Right Hand Rule via Z and X axes.

Origin: The origin is defined as the center of gravity of the satellite.

The Orbital Reference Frame is used to define the attitude of the satellite with respect to satellite's body frame as stated above. The coordinate transformation from orbital body frame is performed via "213" order. Orbital reference frame definition is given in Figure 3-4.

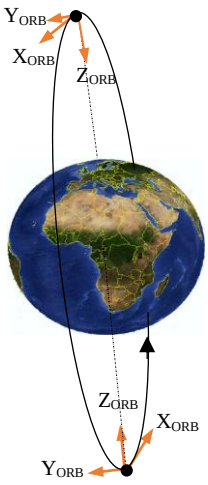

Figure 3-4. Orbital Reference Frame Definition

3.2.4 Earth Centered Inertial Frame (ECI)

In Gokturk-2 satellite, in terms of ECI frame, J2000 frame is used. As stated before, the star tracker measurements obtained from the star trackers are defined with respect to J2000 frame. It is also assumed that the difference between GCRF and J2000 is negligible. Thus GCRF term is used for consistency.

+ Z axis: Approximately Normal to Equatorial Plane, from approximately Earth Center to North Pole.

+ Y axis: Defined according to Right Hand Rule via Z and X axes.

+ X axis: Approximately in the direction of the Vernal Equinox inside the equatorial plane

Origin: The origin is defined as the Earth Center and it is the same point as the ITRF center.

The ECI reference frame definition is given in Figure 3-5.

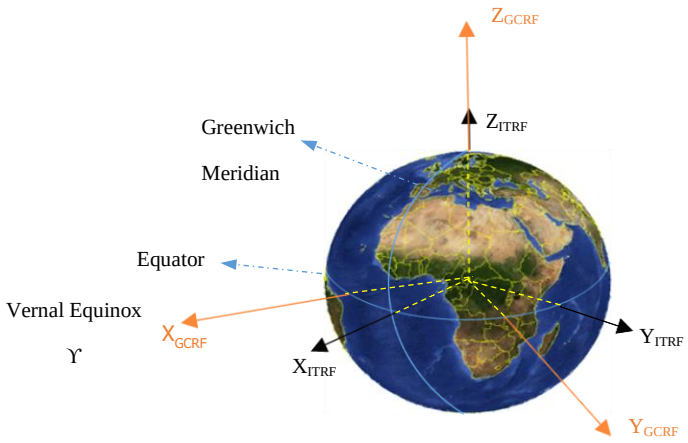

Figure 3-5. ECI (GCRF) Reference Frame Definition

3.2.5 Earth Centered Earth Fixed Coordinate Frame (ECEF)

In Gokturk-2 satellite ITRF is used as ECEF.

+ Z axis: Normal to Equatorial Plane, from Earth Center to North Pole.

+ Y axis: Defined according to Right Hand Rule via Z and X axes.

+ X axis: From Earth Center to 0 degree Latitude and 0 degree Longitude Point

Origin: The origin is defined as the Earth Center and it is the same point as the GCRF center.

The definition of ECEF is given in Figure 3-6.

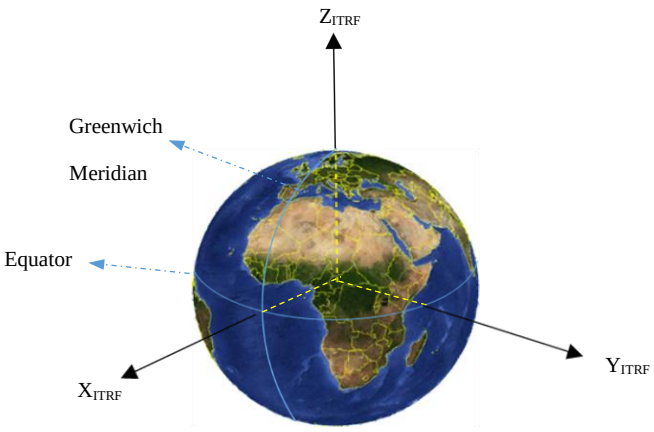

Figure 3-6. ECEF (ITRF) Reference Frame Definition

3.2.6 Local (Sensor) Coordinate Frames

In interface control documents of each sensors, the coordinate frames are defined specifically. The proper coordinate transformations are performed to obtain the measurements in spacecraft's body frame.

3.3 Attitude Representations

The attitude of the satellite can be represented in various ways. Euler axis / angles representation, rotation vector representation, quaternion representation, Gibbs vector representation, Rodrigues parameter representation, modified Rodrigues representation and Euler angle representations are the most common attitude representations, [77], [78]. A survey of attitude representation is also performed by Shuster, [79].

In Gokturk-2 satellite, quaternion representations are used inside the Kalman Filtering Algorithms and Euler Angle representation is used for monitoring the satellite attitude and mission planning.

Soken et. al., state that the choice of the representation depends on estimation algorithm, type and mission of the spacecraft, selection of the attitude reference frame and one of these techniques may be more convenient than others, [77]. By referring Wertz and Bak, [80], [81], Soken et. al., describe the comparison of the common 4 attitude representation methods: Euler Angles, quaternions, Gibbs Vector and modified Rodrigues Parameters, given in Table 3-1.

Table 3-1 Characteristics of Attitude Representations of Euler Angles Quaternions (Table1.1 of [77])

Representation	**Number of parameters**	**Advantages**	**Disadvantages**
Euler Angles	3	• No redundant parameters. • Clear physical interpretation • Minimal set for attitude representation.	• Trigonometric functions in both rotation matrix and kinematic relations. • Singular for specific rotations. • No convenient product rule.
Quaternions	4	• Convenient product rule. • Simple kinematic relation. • No trigonometric functions. • No singularities	• For parameters do not have intuitive physical meaning. • One redundant parameter.
Gibbs Vector	3	• No redundant parameters. • There is no sign ambiguity in the definition. • The components are independent parameters.	• It becomes infinite when the rotation angle is an odd multiple of 180°. • No clear physical interpretation.
Modified Rodrigues Parameters	3	• No redundant parameters. • The singularity is never encountered in practice	• Singular at 2π

3.3.1 Euler Angle Representations

The Euler angle representation express a coordinate transformation via consecutive rotations about 3 different axes, which have been performed by direction cosine matrices, that are formed by Euler angles, [77], [78].

In Gokturk-2 satellite, Euler angles have not been implemented in dynamic equations because of their singular nature, instead they are used in mission planning phase. In the AOCS software, the Euler sequence of 2-1-3 is implemented. This sequence is performed firstly by a rotation around pitch angle axis (θ), and then a second rotation around roll angle axis (ϕ) and a third rotation around yaw angle axis (ψ). The Euler sequence of 2-1-3 is preferred in LEO satellites, however in GEO satellites 3-2-1 sequence is common, [82]. The 2-1-3 Euler sequence physically originates from the structure of the satellite dynamics. Pitch angle axis is orthogonal to the orbital plane and the rotation around it corresponds to azimuth changes. Moreover the rotation around the roll angle axis corresponds to elevation changes. Those changes define satellite's swath width, [82].

The rotation matrices for each rotation can be defined such that:

$$R_x = \begin{bmatrix} 1 & 0 & 0 \\ 0 & \cos\varphi & \sin\varphi \\ 0 & -\sin\varphi & \cos\varphi \end{bmatrix} \tag{3.1}$$

$$R_y = \begin{bmatrix} \cos\theta & 0 & -\sin\theta \\ 0 & 1 & 0 \\ \sin\theta & 0 & \cos\theta \end{bmatrix} \tag{3.2}$$

$$R_z = \begin{bmatrix} \cos\psi & \sin\psi & 0 \\ -\sin\psi & \cos\psi & 0 \\ 0 & 0 & 1 \end{bmatrix} \tag{3.3}$$

The corresponding rotation matrix is calculated by multiplying the above matrices, given in Equation (3.4).

$$A_{213} = R_Z \cdot R_X \cdot R_Y \tag{3.4}$$

If the rotation matrices are written explicitly:

$$A_{213} = \begin{bmatrix} \cos\psi & \sin\psi & 0 \\ -\sin\psi & \cos\psi & 0 \\ 0 & 0 & 1 \end{bmatrix} \cdot \begin{bmatrix} 1 & 0 & 0 \\ 0 & \cos\varphi & \sin\varphi \\ & -\sin\varphi & \cos\varphi \end{bmatrix} \cdot \begin{bmatrix} \cos\theta & 0 & -\sin\theta \\ 0 & 1 & 0 \\ \sin\theta & 0 & \cos\theta \end{bmatrix} \tag{3.5}$$

$$A_{213} = \begin{bmatrix} \cos\psi\cos\theta + \sin\psi\sin\varphi\sin\theta & \sin\psi\cos\varphi & -\cos\psi\sin\theta + \sin\psi\sin\varphi\cos\theta \\ -\sin\psi\cos\theta + \cos\psi\sin\varphi\sin\theta & \cos\psi\cos\varphi & \sin\psi\sin\theta + \cos\psi\sin\varphi\cos\theta \\ \sin\theta\cos\varphi & -\sin\varphi & \cos\theta\cos\varphi \end{bmatrix} \tag{3.6}$$

3.3.2 Quaternion Representations

The quaternions are first introduced by Hamilton in 1844, [83]. Crassidis et. al., describe that the notation used in the common literature is different than the Hamilton's notation, [78]. It is also stated that the notation is compliant with the Jet Propulsion Laboratory- JPL Conventions, [84]. The basic notation for a quaternion can be defined such that it has three vector parts and a scalar part. The attitude representation by a quaternion $\mathbf{q}$ indicates a single rotation by angle Φ from one coordinate frame to another. The Euler symmetric parameters, also called quaternion components, are defined in Equation (3.7), [80]:

$$\boldsymbol{q} \equiv \begin{bmatrix} q_1 \\ q_2 \\ q_3 \\ q_4 \end{bmatrix} \tag{3.7}$$

$$q_1 = e_1 \sin\frac{\Phi}{2} \tag{3.8}$$

$$q_2 = e_2 \sin\frac{\Phi}{2} \tag{3.9}$$

$$q_3 = e_3 \sin\frac{\Phi}{2} \tag{3.10}$$

$$q_4 = \cos\frac{\Phi}{2} \tag{3.11}$$

The mathematical properties of quaternions provide flexibility in terms of defining equations more effectively, [84].

In Gokturk-2 satellite, the rotations are defined by quaternions which satisfy the unity constraint. The four quaternion parameters are not independent such that whole quaternion contains 3 independent angle data and it satisfies the following constraint.

$$|\boldsymbol{q}| = \sqrt{\boldsymbol{q}^T\boldsymbol{q}} = \sqrt{|\mathbf{q}|^2 + q_4^2} = 1 \tag{3.12}$$

Quaternions are defined either in right handed or left handed notation. In Wertz [80], quaternions are defined as the following formulation of Hamilton and Whittaker which corresponds to the right handed notation.

$$\boldsymbol{q} \equiv q_1 i + q_2 j + q_3 k + q_4$$

$$\begin{aligned} ij &= -ji = k \\ jk &= -kj = i \\ ki &= -ik = j \\ i^2 &= j^2 = k^2 = -1 \end{aligned} \tag{3.13}$$

3.3.3 Direction Cosine (Rotational) matrix to quaternions

The direction cosine matrix can be expressed in different ways with respect to the notation of the quaternions. In Wertz, [80] Chapter 12, the left handed version of the direction cosine matrix expressed in terms of the quaternions are given. It should be noted that in that reference regarding appendix section is referenced for the quaternions however in that section right handed quaternion notation is given.

The formula for the left handed representation of the direction cosine matrix is presented in Equation (3.14).

$$A(\boldsymbol{q}) = (q_4^2 - \boldsymbol{q}^2) I_{3x3} + 2\boldsymbol{q}\boldsymbol{q}^T - 2q_4 Q \tag{3.14}$$

where Q is defined as follows:

$$Q \equiv \begin{bmatrix} 0 & -q_3 & q_2 \\ q_3 & 0 & -q_1 \\ -q_2 & q_1 & 0 \end{bmatrix}$$

Trawny [84] gives an alternative formula which gives the same result in Equation (3.14).

$$A(\boldsymbol{q}) = (2q_4^2 - 1) I_{3x3} + 2\boldsymbol{q}\boldsymbol{q}^T - 2q_4 Q \tag{3.15}$$

The explicit form of Equation (3.14) is given in Appendix A.

The formula for the <u>right handed</u> representation of the direction cosine matrix is presented in Equation (3.16). It is the transpose of the left handed $A(\boldsymbol{q})$ matrix.

$$A(\boldsymbol{q}) = (q_4^2 - \boldsymbol{q}^2) I_{3x3} + 2\boldsymbol{q}\boldsymbol{q}^T + 2q_4 Q$$

$$Q \equiv \begin{bmatrix} 0 & -q_3 & q_2 \\ q_3 & 0 & -q_1 \\ -q_2 & q_1 & 0 \end{bmatrix} \tag{3.16}$$

The explicit form of Equation (3.16) is given in Appendix B .

3.3.4 Quaternion to Direction Cosine matrix transformation

3.3.4.1 Left Handed Notation

$$A(\boldsymbol{q}) = \begin{bmatrix} q_1^2 - q_2^2 - q_3^2 + q_4^2 & 2q_1q_2 + 2q_4q_3 & 2q_1q_3 - 2q_4q_2 \\ 2q_2q_1 - 2q_4q_3 & -q_1^2 + q_2^2 - q_3^2 + q_4^2 & 2q_2q_3 + 2q_4q_1 \\ 2q_3q_1 + 2q_4q_2 & 2q_3q_2 - 2q_4q_1 & -q_1^2 - q_2^2 + q_3^2 + q_4^2 \end{bmatrix} \tag{3.17}$$

$$\begin{aligned} q_1 &= \pm\frac{1}{2}\left(1 + A_{11} - A_{22} - A_{33}\right)^{1/2} = \pm\frac{1}{2}\left(1 + 2A_{11} - trace(A)\right)^{1/2} \\ q_2 &= \pm\frac{1}{2}\left(1 - A_{11} + A_{22} - A_{33}\right)^{1/2} = \pm\frac{1}{2}\left(1 + 2A_{22} - trace(A)\right)^{1/2} \\ q_3 &= \pm\frac{1}{2}\left(1 - A_{11} - A_{22} + A_{33}\right)^{1/2} = \pm\frac{1}{2}\left(1 + 2A_{33} - trace(A)\right)^{1/2} \\ q_4 &= \pm\frac{1}{2}\left(1 + A_{11} + A_{22} + A_{33}\right)^{1/2} = \pm\frac{1}{2}\left(1 + trace(A)\right)^{1/2} \end{aligned} \tag{3.18}$$

There are 4 possible cases for the transformation. Trawny [84] states that, the largest pivotal element should be used for maximum numerical accuracy and the maximum of $\left(|q_1|,|q_2|,|q_3|,|q_4|\right)$ corresponds to the most positive $\left(A_{11}, A_{22}, A_{33}, trace(A)\right)$.

The explicit forms of these 4 cases are given in Appendix C.

3.3.4.2 Right Handed Notation

$$A(\boldsymbol{q}) = \begin{bmatrix} q_1^2 - q_2^2 - q_3^2 + q_4^2 & 2q_1q_2 - 2q_3q_4 & 2q_1q_3 + 2q_2q_4 \\ 2q_1q_2 + 2q_3q_4 & -q_1^2 + q_2^2 - q_3^2 + q_4^2 & 2q_2q_3 - 2q_1q_4 \\ 2q_1q_3 - 2q_2q_4 & 2q_2q_3 + 2q_1q_4 & -q_1^2 - q_2^2 + q_3^2 + q_4^2 \end{bmatrix} \tag{3.19}$$

Similar to the left handed notation, the explicit forms of 4 possible transformation cases are given in Appendix D.

3.3.5 Quaternion Product

The quaternion product operation can be performed as in Equation (3.20).

$$
\begin{aligned}
\bar{\boldsymbol{q}} \times \bar{\boldsymbol{p}} &= \left(q_1\hat{i} + q_2\hat{j} + q_3\hat{k} + q_4\right)\left(p_1\hat{i} + p_2\hat{j} + p_3\hat{k} + p_4\right) \\
&= q_1p_1(\hat{i}^2) + q_1p_2(\hat{i}\,\hat{j}) + q_1p_3(\hat{i}\,\hat{k}) + q_1p_4(\hat{i}) \\
&+ q_2p_1(\hat{j}\,\hat{i}) + q_2p_2(\hat{j}^2) + q_2p_3(\hat{j}\,\hat{k}) + q_2p_4(\hat{j}) \\
&+ q_3p_1(\hat{k}\,\hat{i}) + q_3p_2(\hat{k}\,\hat{j}) + q_3p_3(\hat{k}^2) + q_3p_4(\hat{k}) \\
&+ q_4p_1(\hat{i}) + q_4p_2(\hat{j}) + q_4p_3(\hat{k}) + q_4p_4
\end{aligned} \tag{3.20}
$$

3.3.5.1 Right handed (Hamiltonian) notation

The right handed (Hamiltonian) notation is given from Equation (3.21) to Equation (3.23).

$$
\begin{aligned}
i^2 = j^2 = k^2 &= -1 \\
ij = -ji &= k \\
jk = -kj &= i \\
ki = -ik &= j
\end{aligned} \tag{3.21}
$$

Equation (3.20) can be rearranged by using right handed notation given in Equation (3.21).

$$
\begin{aligned}
\bar{\boldsymbol{q}} \times \bar{\boldsymbol{p}} &= \left(q_1\hat{i} + q_2\hat{j} + q_3\hat{k} + q_4\right)\left(p_1\hat{i} + p_2\hat{j} + p_3\hat{k} + p_4\right) \\
&= -q_1p_1 + q_1p_2(\hat{k}) - q_1p_3(\hat{j}) + q_1p_4(\hat{i}) \\
&- q_2p_1(\hat{k}) - q_2p_2 + q_2p_3(\hat{i}) + q_2p_4(\hat{j}) \\
&+ q_3p_1(\hat{j}) - q_3p_2(\hat{i}) - q_3p_3 + q_3p_4(\hat{k}) \\
&+ q_4p_1(\hat{i}) + q_4p_2(\hat{j}) + q_4p_3(\hat{k}) + q_4p_4 \\
&= \left(q_4p_1 - q_3p_2 + q_2p_3 + q_1p_4\right)\hat{i} \\
&+ \left(q_3p_1 + q_4p_2 - q_1p_3 + q_2p_4\right)\hat{j} \\
&+ \left(q_2p_1 + q_1p_2 + q_4p_3 + q_3p_4\right)\hat{k} \\
&+ \left(-q_1p_1 - q_2p_1 - q_3p_3 + q_4p_4\right)
\end{aligned} \tag{3.22}
$$

Equation (3.22) can be represented in matrix form as in Equation (3.23):

$$\bar{\boldsymbol{q}} \times \bar{\boldsymbol{p}} = A(\bar{\boldsymbol{q}}) \cdot \bar{\boldsymbol{p}} = \begin{bmatrix} q_4 & -q_3 & q_2 & q_1 \\ q_3 & q_4 & -q_1 & q_2 \\ -q_2 & q_1 & q_4 & q_3 \\ -q_1 & -q_2 & -q_3 & q_4 \end{bmatrix} \cdot \begin{bmatrix} p_1 \\ p_2 \\ p_3 \\ p_4 \end{bmatrix} \tag{3.23}$$

3.3.5.2 Left handed notation

Similar to the right handed notation, the left handed notation is given from Equation (3.24) to Equation (3.27).

$$\begin{aligned} i^2 = j^2 = k^2 = -1 \\ ij = -ji = -k \\ jk = -kj = -i \\ ki = -ik = -j \end{aligned} \tag{3.24}$$

Equation (3.20) can be rearranged by using left handed notation given in Equation (3.24).

$$\begin{aligned} \bar{\boldsymbol{q}} \times \bar{\boldsymbol{p}} &= \left(q_1\hat{i} + q_2\hat{j} + q_3\hat{k} + q_4\right)\left(p_1\hat{i} + p_2\hat{j} + p_3\hat{k} + p_4\right) \\ &= -q_1p_1 - q_1p_2(\hat{k}) + q_1p_3(\hat{j}) + q_1p_4(\hat{i}) \\ &+ q_2p_1(\hat{k}) - q_2p_2 - q_2p_3(\hat{i}) + q_2p_4(\hat{j}) \\ &- q_3p_1(\hat{j}) + q_3p_2(\hat{i}) - q_3p_3 + q_3p_4(\hat{k}) \\ &+ q_4p_1(\hat{i}) + q_4p_2(\hat{j}) + q_4p_3(\hat{k}) + q_4p_4 \end{aligned} \tag{3.25}$$

$$\begin{aligned} &= \left(+q_4p_1 + q_3p_2 - q_2p_3 + q_1p_4\right)\hat{i} \\ &+ \left(-q_3p_1 + q_4p_2 + q_1p_3 + q_2p_4\right)\hat{j} \\ &+ \left(+q_2p_1 - q_1p_2 + q_4p_3 + q_3p_4\right)\hat{k} \\ &+ \left(-q_1p_1 - q_2p_1 - q_3p_3 + q_4p_4\right) \end{aligned}$$

Equation (3.25) can be represented in matrix form as follows for left handed notation:

$$\bar{\boldsymbol{q}} \times \bar{\boldsymbol{p}} = A(\bar{\boldsymbol{q}}) \cdot \bar{\boldsymbol{p}} = \begin{bmatrix} q_4 & q_3 & -q_2 & q_1 \\ -q_3 & q_4 & q_1 & q_2 \\ q_2 & -q_1 & q_4 & q_3 \\ -q_1 & -q_2 & -q_3 & q_4 \end{bmatrix} \cdot \begin{bmatrix} p_1 \\ p_2 \\ p_3 \\ p_4 \end{bmatrix} \tag{3.26}$$

$$\bar{\boldsymbol{q}} \times \bar{\boldsymbol{p}} = A(\bar{\boldsymbol{q}}) \cdot \bar{\boldsymbol{p}} = \begin{bmatrix} q_4 & -q_3 & q_2 & q_1 \\ q_3 & q_4 & -q_1 & q_2 \\ -q_2 & q_1 & q_4 & q_3 \\ -q_1 & -q_2 & -q_3 & q_4 \end{bmatrix} \cdot \begin{bmatrix} p_1 \\ p_2 \\ p_3 \\ p_4 \end{bmatrix} \tag{3.27}$$

3.4 Spacecraft Dynamics

The satellite attitude dynamics defines the time derivative of the attitude angles, namely angular velocities with governing physical quantities. The satellite attitude dynamics equation is obtained from the rotational mechanics via the preservation of the angular momentum which is given in Equation (3.28) and Equation (3.29), [77], [80].

$$\frac{\mathrm{d}\mathbf{L}}{\mathrm{dt}} = \mathbf{N} - \boldsymbol{\omega}_{\mathrm{bi}}^{\mathrm{b}} \times \mathbf{L} = J \frac{\mathrm{d}\boldsymbol{\omega}_{\mathrm{bi}}^{\mathrm{b}}}{\mathrm{dt}} \tag{3.28}$$

$$\mathbf{L} = J \boldsymbol{\omega}_{\mathrm{bi}}^{\mathrm{b}} \tag{3.29}$$

L is the total angular momentum acting on the satellite, J is the satellite's inertia matrix which defines the distribution of the satellite mass, $\boldsymbol{\omega}_{\mathrm{bi}}^{\mathrm{b}}$ is the angular velocity vector, which defines the body rates with respect to the inertial frame and defined in body frame. The resultant equation for satellite dynamics is obtained via Equation (3.28) and Equation (3.29), and derived in terms of the rate of change of vectors in rotating frames, [80].

Equation (3.30) gives the fundamental form of the satellite dynamic equation.

$$\frac{\mathrm{d}\boldsymbol{\omega}_{\mathrm{bi}}^{\mathrm{b}}}{\mathrm{dt}} = J^{-1}\left[\mathbf{N} - \boldsymbol{\omega}_{\mathrm{bi}}^{\mathrm{b}} \times \left(J\boldsymbol{\omega}_{\mathrm{bi}}^{\mathrm{b}}\right)\right] \tag{3.30}$$

N is the sum of disturbance torques vector which is total disturbance torques acting on the satellite, namely gravity gradient torque, aerodynamic torque, solar pressure disturbance torque and residual magnetic torque. The derivation of the satellite dynamic equation via dyadic notation is not common in the literature and the details are given in Appendix section. The modified version of Equation (3.30) in which the reaction wheel terms are added is given in the next section, in Equation (4.5).

3.5 Spacecraft Kinematics

In Gokturk-2 satellite, the quaternions are used to represent the attitude states, namely Roll, Pitch and Yaw angles. The kinematic equations of motion in quaternions, or alternatively propagation of quaternions by time is performed by using Equation (3.39). The derivation of this equation can be found in [77], [78], [80].

The quaternion multiplication in matrix notation can be defined as in Equation (3.31) by using the property of time dependence of the quaternion multiplication:

$$\begin{bmatrix} q_1^{\mathrm{II}} \\ q_2^{\mathrm{II}} \\ q_3^{\mathrm{II}} \\ q_4^{\mathrm{II}} \end{bmatrix} = \begin{bmatrix} q_4^{\mathrm{I}} & q_3^{\mathrm{I}} & -q_2^{\mathrm{I}} & q_1^{\mathrm{I}} \\ -q_3^{\mathrm{I}} & q_4^{\mathrm{I}} & q_1^{\mathrm{I}} & q_2^{\mathrm{I}} \\ q_2^{\mathrm{I}} & -q_1^{\mathrm{I}} & q_4^{\mathrm{I}} & q_3^{\mathrm{I}} \\ -q_1^{\mathrm{I}} & -q_2^{\mathrm{I}} & -q_3^{\mathrm{I}} & q_4^{\mathrm{I}} \end{bmatrix} \begin{bmatrix} q_1 \\ q_2 \\ q_3 \\ q_4 \end{bmatrix} \tag{3.31}$$

By assuming $\mathbf{q}$ corresponds to attitude of the satellite with respect to the reference system at time t and $\mathbf{q}^{\mathrm{II}}$ corresponds to the attitude of the body with respect to reference system at time $\mathrm{t}+\Delta\mathrm{t}$, $\mathbf{q}^{\mathrm{I}}$ which is the representation of position at $\mathrm{t}+\Delta\mathrm{t}$ can be defined as:

$$q_1^I \equiv e_1 \sin\frac{\Delta\Phi}{2}, \tag{3.32}$$

$$q_2^I \equiv e_2 \sin\frac{\Delta\Phi}{2}, \tag{3.33}$$

$$q_3^I \equiv e_3 \sin\frac{\Delta\Phi}{2}, \tag{3.34}$$

$$q_4^I \equiv e_4 \cos\frac{\Delta\Phi}{2}, \tag{3.35}$$

where e_1, e_2 and e_3 are the components of the rotation axis unit vector along 1, 2 and 3 triad at time t, and $\Delta\Phi$ is the rotation in time Δt. According to above definitions, after the proper multiplication the following equation is obtained.

$$\mathbf{q}(t+\Delta t) \approx \left\{ \cos\frac{\Delta\Phi}{2} I + sin\frac{\Delta\Phi}{2} \begin{bmatrix} 0 & e_3 & -e_2 & e_1 \\ -e_3 & 0 & e_1 & e_2 \\ e_2 & -e_1 & 0 & e_3 \\ -e_1 & -e_2 & -e_3 & 0 \end{bmatrix} \right\} \mathbf{q}(t) \tag{3.36}$$

I is the identity matrix of 4x4. If small angle assumption which results as follows is made:

$$\cos\frac{\Delta\Phi}{2} \approx 1 \tag{3.37}$$

$$\sin\frac{\Delta\Phi}{2} \approx \frac{1}{2}\omega\Delta t \tag{3.38}$$

$$\mathbf{q}(t+\Delta t) \approx \left\{ I + \frac{1}{2} \begin{bmatrix} 0 & \omega_3 & -\omega_2 & \omega_1 \\ -\omega_3 & 0 & \omega_1 & \omega_2 \\ \omega_2 & -\omega_1 & 0 & \omega_3 \\ -\omega_1 & -\omega_2 & -\omega_3 & 0 \end{bmatrix} \Delta t \right\} \mathbf{q}(t) \tag{3.39}$$

By defining the skew-symmetric matrix as follows,

$$\Omega(\omega) = \begin{bmatrix} 0 & \omega_3 & -\omega_2 & \omega_1 \\ -\omega_3 & 0 & \omega_1 & \omega_2 \\ \omega_2 & -\omega_1 & 0 & \omega_3 \\ -\omega_1 & -\omega_2 & -\omega_3 & 0 \end{bmatrix} \tag{3.40}$$

The Equation (3.39) becomes,

$$\mathbf{q}(t+\Delta t) \approx \left\{ I + \frac{1}{2}\Omega(\omega)\Delta t \right\} \mathbf{q}(t) \tag{3.41}$$

The derivation is finalized as follows:

$$\frac{d\mathbf{q}(t)}{dt} \cong \frac{\mathbf{q}(t+\Delta t) - \mathbf{q}(t)}{\Delta t} = \frac{1}{2}\Omega(\omega)\mathbf{q}(t) \tag{3.42}$$

3.6 Attitude Hardware: AOCS equipment of Gokturk-2 satellite

3.6.1.1 Star Trackers

Two AIRBUS Sodern SED 26 star tracker units are used in cold redundant configuration for the satellite, (Figure 3-7). Since the satellite image resolution is 2.5 meters in PAN band, moderate performance star trackers have been chosen instead of multiple head star tracker units.

Figure 3-7. AIRBUS SODERN- SED 26 Single Head Star Tracker [85]

The performance specifications of the star trackers are given as follows in Table 3-2:

Table 3-2 AIRBUS Sodern SED 26 Star Tracker Performance Specifications

EOL performances (X-Y axes / Z axis)	Nominal accuracy	Degraded accuracy	Degraded accuracy	Unit	Statistical distribution
Rate	0.5	5	10	deg/s	-
Acceleration	< 0.025	<1	<10	deg/s²	-
Bias	11 / 11	11 / 11	11/11	arc second	-
Low Frequency Errors	11 / 28	Maximal degradation 50%	Maximal degradation 100%	arc second	3 sigma
High Frequency Errors (NEA)	11 / 71	Maximal degradation 200%	Maximal degradation 400%	arc second	3 sigma
Attitude determination accuracy	19 / 77	Maximal degradation 100% /200%	Maximal degradation 100% /400%	arc second	Root Sum Square

3.6.1.2 GPS Receivers

SSTL SGR-10 GPS receivers which is shown in Figure 3-8, provide orbital information for the satellite. The performance specifications of the GPS receivers are given in Table 3-3.

Table 3-3 SGR-10 GPS Receiver Performance Specifications

Position Accuracy	~10-20 meter
Velocity Accuracy	~0.15 m/s – 0.25 m/s
Time Accuracy	0.5 µs
Data Coordinate System	WGS84
Cold Start Duration	200 – 300 s
Warm Start Duration	50 – 90 s

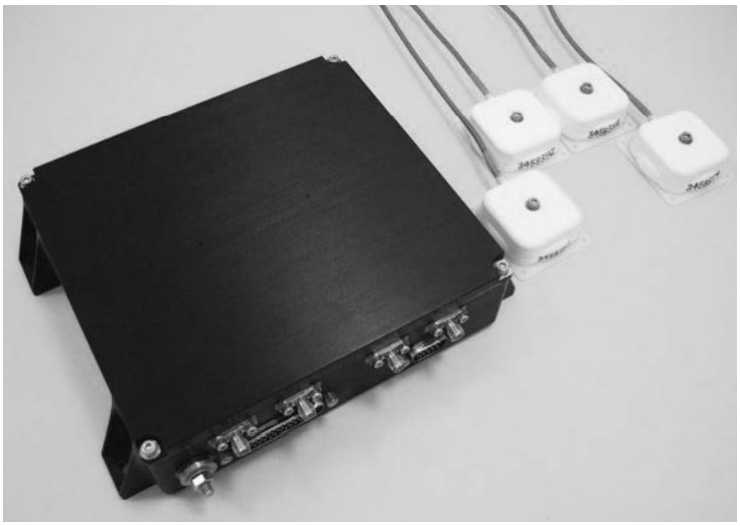

Figure 3-8. SSTL SGR-10 GPS Receiver and antennas [86]

3.6.1.3 Gyro Unit

SSTL MEMS Gyro Unit which is shown in Figure 3-9, used as a gyroscope unit in AOCS architecture. The performance specifications are given in Table 3-4.

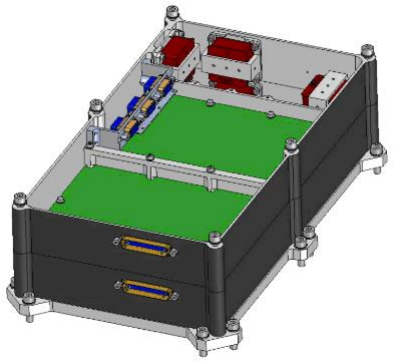

Figure 3-9. SSTL MEMS Gyro Unit [87]

Table 3-4 SSTL Gokturk-2 Gyro Specifications (Expected Values)

Nominal Bias	0.5 deg / sec
Bias Instability	20 deg / hour over 1 hour
Bias Drift	< 0.005 deg/s/s (Start) <0.001 deg/s/s (After 60 second) Negligible (After 600 second)
Angular Random Walk	< 1.2 deg /sqrt-hour
Bandwidth	10 Hz
Resolution	1 / 197 deg/s

The details of the Allen Variance Graphics are given in Figure 3-10, Figure 3-11, and Figure 3-12. The Gyro Scale Factor Analysis Results are given in Table 3-5. These specifications can be used for curve fitting purposes to estimate the gyro scale factor with respect to temperature changes.

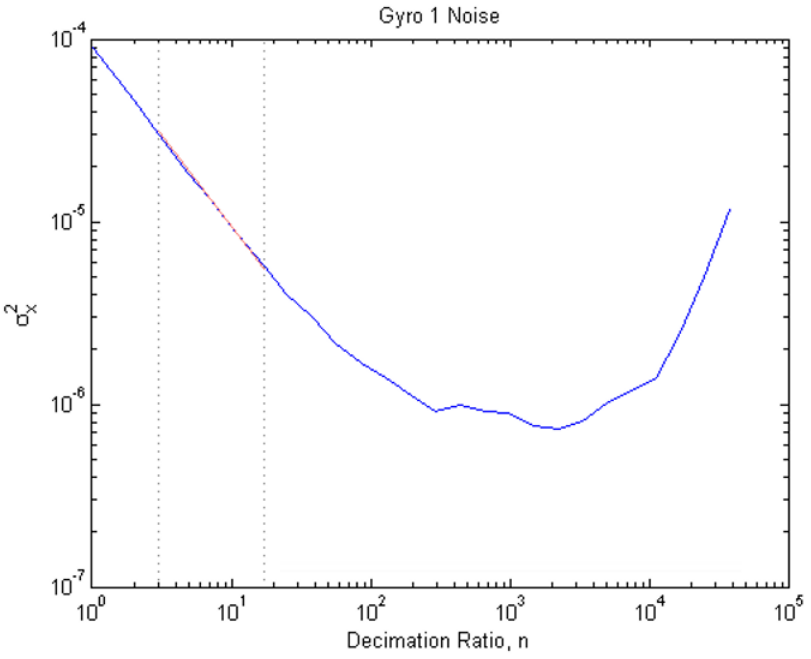

Figure 3-10. Gyro-1 Allen Variance Graphic

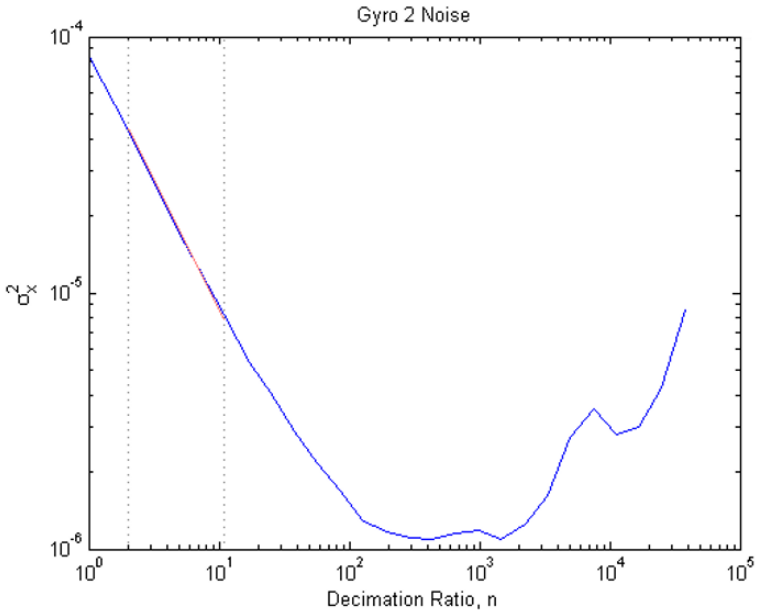

Figure 3-11. Gyro-2 Allen Variance Graphic

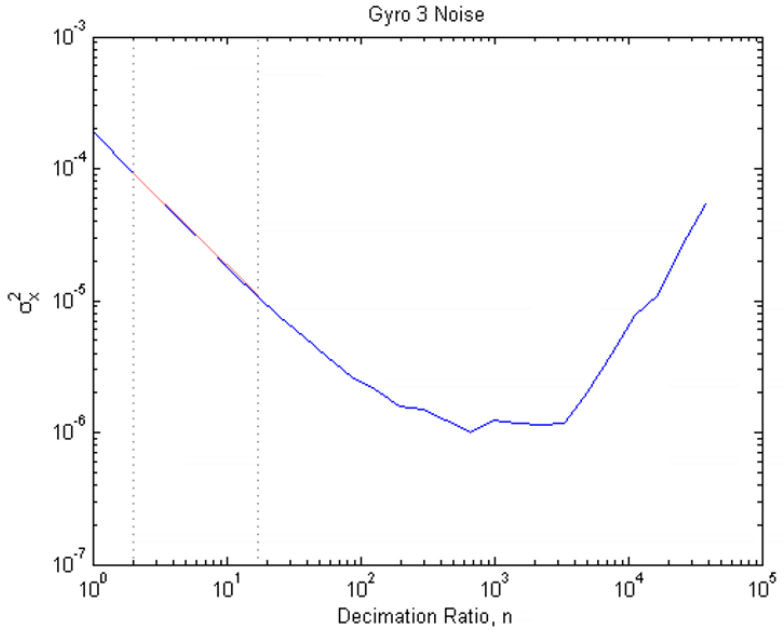

Figure 3-12. Gyro-3 Allen Variance Graphic

Table 3-5 SSTL Gokturk-2 Gyro Scale Factor Analysis Results

Parameter	**Interval**	**Unit**	**X0**	**Y0**	**Z0**	**X1**	**X2**	**X3**
Rate Scale Factor	197±5	Bit / (0/s)	193.933	196.924	196.710	198.084	196.239	198.810
Resolution	<20	0/hour	18.563	18.281	18.301	18.174	18.345	18.108
Scale Factor Linearity	Max ±1	Percent over interval	0.2326	0.2439	0.1025	0.198	0.2529	0.3492
Scale Factor Temperature Dependency	Max ±1	Percent over interval	0.6569	0.6668	0.212	0.8314	0.7508	0.528
Nominal Rate Bias		Bits	-32.431	-1.276	-20.528	-22.87	-26.659	-53.138
@ 20^{0}C	Max ±0.5	^{0}/s	-0.1672	-0.0065	-0.1044	-0.1155	-0.1359	-0.2673
Angular Rate Range	<-9.0	^{0}/s	10.388	10.3884	10.3018	10.2185	10.2953	10.0290
@ 20^{0}C	>-9.0	^{0}/s	-9.9777	-10.047	-9.8673	-9.8341	-9.9760	-9.5308
Angular Rate Range over Full Temperature	>8.0	^{0}/s	9.9726	10.0417	9.8622	9.8291	9.9709	9.5258

3.6.1.4 Sun Sensors

The Korean SATRECI Sun sensors which provides Sun Angle directions are used in Gokturk-2 satellite, Figure 3-13. The analog sensor inputs are processed in coarse attitude estimation mode and the specifications are given in Table 3-6.

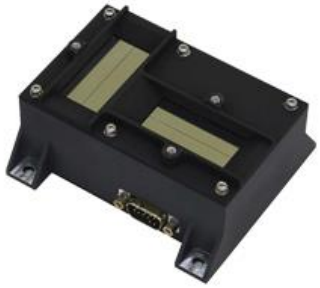

Figure 3-13. SATRECI Analog Fine Sensor, FSS-5

Table 3-6 SATRECI Analog Fine Sensor, FSS-5 Technical Specifications

Measurement Range	$\pm 60^0$ (2 axis)
Accuracy	0.5^0
Noise Characteristics	Albedo < 0.05^0 (3σ)

3.6.1.5 Magnetometers

In Gokturk-2 satellite, 2 redundant 3-axis magnetometers which are manufactured by SATRECI Company, are used, Figure 3-14. The technical specifications are given in Table 3-7.

Figure 3-14. SATRECI Magnetometer, MAG-30

The magnetometer are analog devices and the equipment have an interface to ADCS Electronic Interface Card. The Onboard computer, gets the data through this interface card unit.

Table 3-7 The Specifications of SATRECI MAG-30 Magnetometers

Measurement Range	± 60 µT
Resolution	< 30 nT
Linearity	0.1 % error
Bias	0.1 µT
Bias Drift	0.5 nT
Power Consumption	0.24 W

3.6.1.6 Magnetorquers

Figure 3-15. ZARM TECHNIK Magnetorquer, MT-70

There are 3 magnetorquer equipment in Gokturk-2 satellite manufactured by ZARM TECHNIK, Figure 3-15. Magnetorquers are used in coarse attitude mode to control the spin rate of the satellite. They are also used to desaturate the momentum of the reaction wheels during the nominal mode. The specifications of the magnetorquers are given in Table 3-8.

Table 3-8 ZARM TECHNIK Magnetorquer, MT-70 Technical Specifications

Maximum Magnetic Dipole Moment	70 Am^2 (maximum linear current)
Maximum Residual Magnetic Field	< % 0.3

The relationship between Magnetic Torque and the applied current is given in Figure 3-16.

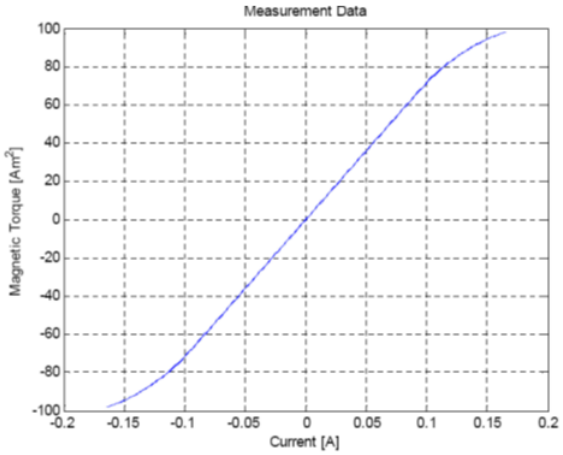

Figure 3-16. ZARM TECHNIK Magnetorquer, MT-70 Magnetic Torque – Applied Current Graphic

Magnetorquers are also analog devices and control torques generated by AOCS software are sent through the ADCS Electronic Interface Card.

3.6.1.7 Reaction Wheels

Collins Aerospace (Former Rockwell Collins) Teldix RSI 15-215/20 model, 4 reaction wheels are used to control the satellites in three axes, Figure 3-17. Reaction wheels are located in tetrahedral configuration in the satellite. The reason for that is to assure the redundancy in case of one unit failure and maximize the torque in any axis, in terms of agility of the spacecraft. The axis definitions are given in Figure 3-18. The specifications of the wheels and the torque-speed characteristics can be found in Table 3-9 and Figure 3-19.

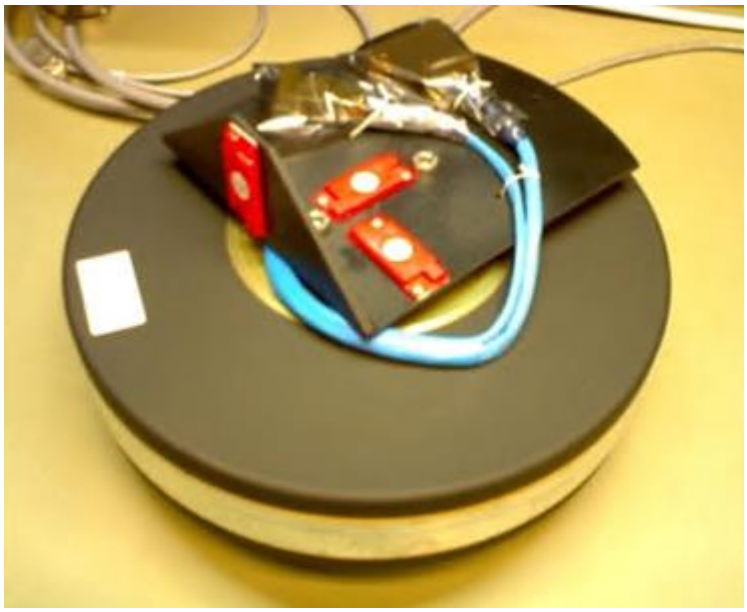

Figure 3-17. TELDIX RSI 15-215/20 Reaction Wheel

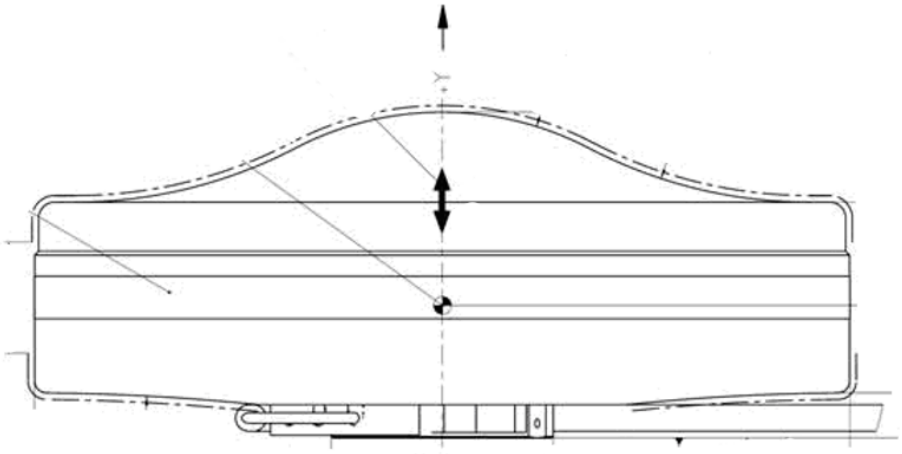

Figure 3-18. TELDIX RSI 15-215/20 Reaction Wheel- Spinning Axis Definition

Table 3-9 TELDIX RSI 15-215/20 Reaction Wheel Specifications

Motor Scale Factor	0.141 Nm/A
Operational Speed Range	±2500 rpm
Safe Speed	8000 rpm
Speed range with full torque capability	± 2000 rpm
Nominal Motor Torque	±0.235 Nm
Loss Torque @1800 rpm	< 0.003 Nm
Rotating Mass Inertia	703.7 ± 6.96 kg.cm^2
Motor Rotor Inertia	12.5 ±0.20 kg.cm^2
Ball Bearing Inertia	716.2 ± 7.16 kg.cm^2

The Motor torque versus speed characteristics is given in Figure 3-19.

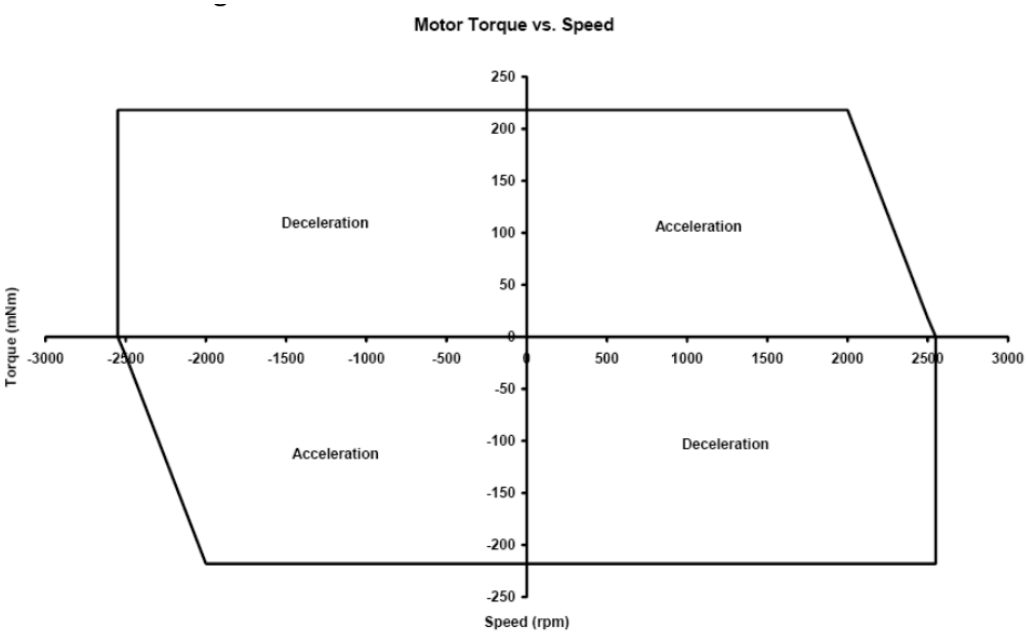

Figure 3-19. TELDIX RSI 15-215/20 Reaction Wheel- Motor Torque versus Speed

3.6.1.8 Propulsion System

The chemical propulsion system is used to control the orbit of the Gokturk-2 satellite. The control commands generated by OBC are sent through CAN interface card to the valves and telemetry data is provided by the same interface unit. The system has 1 N torque capacity.

3.6.1.9 CAN Interface Card Unit

CAN interface card unit- CAK is used to communicate with the equipment that do not have CAN interface such as star trackers and reaction wheels. The unit has also used to control propulsion system, multiplexing the GNSS receiver's synchronization signal (PPS), reading the thermistor data and control the pyro units.

CAN interface card functionalities are given as follows:

- Multiplexing the Pulse Per Second- PPS signal generated by the GPS receiver for the following equipment: SSDR, Gyro Unit, OBC386, BILGE 32G.
- Digital to Analog Conversions, Analog to Digital Conversions, signal amplifications for Reaction Wheels, Propulsion System, Star Tracker, IKS Thermistors, Battery Thermistors, Solar Panel Array Mechanisms, Pyro Units
- Communication with the Flight Computer- OBC 386.

3.6.1.10 ADCS Electronic Interface Card

ADCS Electronic Interface Card is designed to connect the analog coarse sensors namely, magnetometers, magnetorquers and sun sensors to the CAN Data Bus. Magnetorquers are driven by this card in terms of pulse width modulation capability.

3.7 Spacecraft Measurements

The star tracker and the gyro measurements can be used in AOCS high accuracy mode. As it stated before, dynamics-based MEKF is used in Gokturk-2 satellite onboard configuration. However, gyro measurements can be used for the proposed gyro-based filter.

The Star tracker measurements are quaternion outputs. They are processed by the CAN Interface card and broadcasted to the Onboard Computer- OBC. Each measurements have their time tag, thus the delay can be processed by the algorithm. The star tracker unit provides quaternions in 1 Hz sampling interval, and the same interval is also used for Gokturk-2 AOCS architect.

The star tracker unit include a star catalog in itself. In lost in space mode, the stars in field of view are processed by the equipment and the locations of the stars are compared with the taken image. Finally the initial attitude is obtained. Afterwards the equipment starts to work in tracking mode and provides quaternions at 1 Hz in this nominal mode.

Gyro unit can also provide measurements in 1 Hz sampling interval. The equipment provides attitude rates directly. The bias values are estimated via the filter and the resultant attitude rates are obtained from this process.

CHAPTER 4

ATTITUDE FILTERING

4.1 Kalman Filtering

Kalman filtering is firstly proposed by Rudolph Emil Kalman (1930-2016), in 1960, [42]. In the following years many versions of Kalman Filters are developed. Crassidis [88], performed a detailed survey related with this issue. Kalman filtering is implemented for spacecraft attitude determination systems for different satellite missions. Lefferts et al.'s study [43] can be focused such that, it is one of the earliest applications of Kalman filtering which is implemented for spacecraft attitude estimation. In regarding study, common usage of attitude quaternion representations are proposed.

In most applications Extended Kalman Filters (EKFs) are still commonly used because of its computational advantage and easy tuning capabilities. Discrete time EKFs are used in airplanes, Unmanned Air Vehicles- UAVs, satellites and in all applications where estimation is performed in real time. The stochastic stability of the discrete time EKF is investigated by [89], and it is stated that estimation error is bounded with the assumptions of small initial estimation error and small disturbance noise. The standard Kalman filter works with linear functions under the assumption of Gaussian distribution. The Extended Kalman Filter uses nonlinear process in propagation phase.

The attitude of the satellite can be represented in quaternion forms to avoid the singularities. The attitude of the Gokturk-2 satellite is defined as the rotation of satellite's body frame with respect to orbital frame.

4.2 Multiplicative Extended Kalman Filtering- MEKF for Satellite Attitude Filtering

There are several filtering methods in the literature which the quaternions are involved, such as quasi-measurement method, norm-constrained Kalman Filtering, Unscented Kalman Filtering and Multiplicative Extended Kalman Filtering, [77]. In Gokturk-2 satellite MEKF is used because of its simplicity and relatively low computational load. The details of the MEKF implementation is given in Section 4.4.2.

4.3 Dynamics-based and Gyro-based Multiplicative Extended Kalman Filtering

The angular rates can be obtained either from satellite dynamic equation or indirectly from gyro units. Markley and Crassidis state that precise angular rate information is required for precise pointing and attitude maneuvering and furthermore add that it is also required for filtering noisy attitude sensor data, [78]. Thus in gyro-less, dynamic-based filters angular rates are directly the part of the states, however in gyro-stellar or gyro-based filters, the bias value of the gyros are estimated and used as a state. The angular velocities are calculated according to the gyro measurement outputs and the estimated bias values.

In Gokturk satellite, although there is a MEMS gyro unit in the satellite, dynamics-based MEKF is used for operational reasons. In terms of performance improvement, gyro-based MEKF is proposed to be used. The details of these filters are given in the next sections. These two approaches for attitude filtering are compared with each other in [77], [90] and the advantages of gyro-based filtering over dynamic-based filtering is stated as follows by referring [91] :

- Low computational load
- Lack of need of the satellite inertia accurately.

- Lack of need for the realistic modelling of the disturbance torques.

The disadvantage of the gyro-based filter can be defined such that in case of gyro unit failures the propagation phase will be invalid. Using gyro-based filter over a dynamic-based filter is also not advantageous in case the accuracy of the gyro units in terms of angular random noise and variation of bias, is worse than the accuracy of the dynamic model. In Gokturk Satellite, since the low accuracy level MEMS gyros are used, it is assumed that the performance will be lower than the dynamic model and thus dynamic-based filtering has been preferred. However in this study, it is claimed that Gyro units could be used to obtain the same level attitude accuracy in spite of its accuracy level.

4.4 The Dynamics-based Multiplicative Extended Kalman Filter- MEKF

When there is no gyro onboard the spacecraft, the filter must estimate the attitude and the rates by using the dynamics equation along with the kinematics. In this case, if the attitude is represented in quaternions in the attitude filter, the global state vector to be estimated is

$$\mathbf{x} = \begin{bmatrix} \boldsymbol{q}^{\mathbf{T}} & \boldsymbol{\omega}^{\mathbf{T}} \end{bmatrix}^{T} \tag{4.1}$$

4.4.1 Propagation (Prediction) Phase

State Propagation. Trawny [84] defines that integrating quaternion is equivalent to solving a specific differential equation. Quaternions are propagated through following kinematic equation:

$$\dot{\boldsymbol{q}} = \frac{1}{2}\Omega(\boldsymbol{\omega})\boldsymbol{q} \tag{4.2}$$

where $\Omega(\boldsymbol{\omega})$ is a skew-symmetric matrix of angular velocity $\boldsymbol{\omega} = \begin{bmatrix} \omega_1 & \omega_2 & \omega_3 \end{bmatrix}^{T}$ and it is given in matrix form as follows:

$$\Omega(\boldsymbol{\omega}) = \begin{bmatrix} 0 & \omega_3 & -\omega_2 & \omega_1 \\ \omega_3 & 0 & \omega_1 & \omega_2 \\ \omega_2 & -\omega_1 & 0 & \omega_3 \\ -\omega_1 & -\omega_2 & -\omega_3 & 0 \end{bmatrix} \tag{4.3}$$

Quaternions could also be propagated through discrete analytical solution of the kinematic equation [92]:

$$\boldsymbol{q}_{k/k-1} = \left[\frac{\boldsymbol{\omega}_{k-1}{}^{\mathrm{T}}}{\|\boldsymbol{\omega}_{k-1}\|} \sin\left(\frac{\|\boldsymbol{\omega}_{k-1}\|\Delta t}{2} \right) \quad \cos\left(\frac{\|\boldsymbol{\omega}_{k-1}\|\Delta t}{2} \right) \right]^{\mathrm{T}} \otimes \boldsymbol{q}_{k-1} \tag{4.4}$$

Here Δt is the sampling time step and $\otimes$ defines the quaternion multiplication.

The angular velocity vector, $\boldsymbol{\omega}_{bi}^{b}$, which is defining the body rates with respect to the inertial frame and defined in body frame, is propagated through satellite's dynamic equation:

$$\frac{d\boldsymbol{\omega}_{bi}^{b}}{dt} = J^{-1}\left[\boldsymbol{T}^{b} - \left(\frac{d\boldsymbol{h}_{wheel}^{b}}{dt} \right)^{b} - \left\{ \boldsymbol{\omega}_{bi}^{b} \times \left(J\boldsymbol{\omega}_{bi}^{b} + \boldsymbol{h}_{wheel}^{b} \right) \right\} \right] \tag{4.5}$$

Here J is the satellite tensor of inertia, $\boldsymbol{h}_{wheel}^{b}$ is the reaction wheel's angular momentum vector represented in satellite body frame, $\boldsymbol{T}^{b}$ is the total disturbance torque acting on the satellite and $\left(\frac{d\vec{\boldsymbol{h}}_{wheel}^{b}}{dt} \right)^{b}$ is the reaction wheel's torque vector represented in satellite body frame.

State Covariance Matrix Propagation. The standard propagation equation of the covariance matrix can be given as:

$$P_{k/k-1} = \Phi_k \cdot P_{k-1/k-1} \cdot \Phi_k{}^{T} + Q_k \tag{4.6}$$

where $P_{k/k-1}$ is the propagated covariance matrix of the states, Q_k is the process noise covariance matrix and Φ_k is the discrete time state transition matrix.

The calculation of the discrete time state transition matrix Φ_k is performed by the discretization of the continuous time state transition matrix F_k. First order Euler discretization is used for the process and the discrete time state transition matrix Φ_k is obtained as follows:

$$\Phi_k \approx I_{6\times 6} + F_k \Delta t \tag{4.7}$$

Here $I_{n\times n}$ is $\mathrm{n}\times\mathrm{n}$ identity matrix. The continuous time state transition matrix F_k is basically the Jacobian matrix of the satellite dynamic equation and it is obtained by a linearization process.

$$F_k = \begin{bmatrix} -\left[\hat{\boldsymbol{\omega}}^b_{bi_{k-1|}}\times\right] & I_{3\times 3} \\ 0_{3x3} & J^{-1}\left[\left[\left(J\hat{\boldsymbol{\omega}}^b_{bi_{k-1}} + \boldsymbol{h}_{k-1}\right)\times\right] - \left[\hat{\boldsymbol{\omega}}^b_{bi_{k-1}}\times\right]J\right] \end{bmatrix} \tag{4.8}$$

Where $[a\times]$ defines 3×3 skew symmetric matrix as $\boldsymbol{a}\times\boldsymbol{b} = [\boldsymbol{a}\times]\boldsymbol{b}$ such that,

$$[\boldsymbol{a}\times] = \begin{bmatrix} 0 & -a_3 & a_2 \\ a_3 & 0 & -a_1 \\ -a_2 & a_1 & 0 \end{bmatrix} \tag{4.9}$$

4.4.2 Update (Correction) Phase

The MEKF uses the STR measurements for the updating the propagated states. If the measurements are available, the estimation for the states are improved by the observations. The output quaternion of the star trackers, defines the attitude such that it gives the rotation from inertial frame to the star tracker frame, q_i^{str}. Thus these quaternions have to be transformed in to the satellite body frame for onboard filters. The following equation gives the proper transformation by quaternion product:

$$\tilde{\boldsymbol{q}}_i^b = \boldsymbol{q}_{str}^b \otimes \boldsymbol{q}_i^{str} \tag{4.10}$$

where, q_{str}^{b} is the quaternion which defines the orientation of the related star tracker with respect to the satellite body frame.

Observation Matrix. After transforming the star tracker output to the satellite body frame, the measurement quaternions have exactly the same structure with the state parameter quaternions. On the other hand, to overcome the possible issues such as an ill-conditioned covariance when the attitude is represented with full quaternion vector in the filter, the MEKF uses three-component local attitude error, and updates the global quaternion estimate by quaternion multiplication. In this study, the rotation error vector $\boldsymbol{\delta\vartheta}$ is used as the local state of MEKF and derived by small angle approximation as

$$2\boldsymbol{\delta q}_{1:3} \approx \left[\delta\phi \; \delta\theta \; \delta\psi\right]^{T} \equiv \boldsymbol{\delta\vartheta} \tag{4.11}$$

where the error quaternion is defined as

$$\boldsymbol{\delta q} = \mathbf{q} \otimes \hat{\mathbf{q}}^{-1} = \mathbf{q} \otimes \begin{bmatrix} -\hat{\mathbf{q}}_{1:3} \\ \hat{q}_4 \end{bmatrix} = \begin{bmatrix} \hat{q}_4 \mathbf{q}_{1:3} + q_4 \hat{\mathbf{q}}_{1:3} - \mathbf{q}_{1:3} \times \hat{\mathbf{q}}_{1:3} \\ q_4 \hat{q}_4 - \mathbf{q}_{1:3}{}^{T} \hat{\mathbf{q}}_{1:3} \end{bmatrix} \tag{4.12}$$

As a result, before being used in the filter, the quaternion measurements by the STR must be represented in terms of the rotation error vector $\delta\vartheta$ using the predicted quaternion and provided star tracker measurements:

$$\delta\boldsymbol{\vartheta} = 2\frac{\left(\tilde{\boldsymbol{q}}_i^b \otimes \boldsymbol{q}_{k/k-1}{}^{-1}\right)_{1:3}}{\left(\tilde{\boldsymbol{q}}_i^b \otimes \boldsymbol{q}_{k/k-1}{}^{-1}\right)_4} \tag{4.13}$$

Thus, the observation matrix can be represented by the identity matrix. Since no gyro input is used by the filter, there is no update process for the angular velocities and it could be represented as the zeros in observation matrix. According to that the observation matrix could be given as follows:

$$H_{3\times 6} = \left[I_{3\times 3} \quad 0_{3\times 3}\right] \tag{4.14}$$

Measurement Noise Covariance Matrix. The calculation of the measurement noise covariance matrix R_k is another prerequisite, for the Kalman filter update equations. Star tracker noise is defined in boresight (Z axis) and cross-boresight axes (X and Y

axes). σ_z and σ_{xy} are represented in radian inside the R_k matrix. The resultant R_k which considers the star tracker orientation matrix, C_{STR}^b, could be represented as:

$$R_k = C_{STR}^b \begin{bmatrix} \sin^2\left(\frac{\sigma_{xy}}{2}\right) & 0 & 0 \\ 0 & \sin^2\left(\frac{\sigma_{xy}}{2}\right) & 0 \\ 0 & 0 & \sin^2\left(\frac{\sigma_z}{2}\right) \end{bmatrix} \left(C_{STR}^b\right)^{\mathrm{T}} \tag{4.15}$$

Kalman Gain. Optimal Kalman gain K_k could be calculated by the standard formula:

$$K_k = P_{k|k-1} H_k^{\mathrm{T}} (H_k P_{k|k-1} H_k^{\mathrm{T}} + R_k)^{-1} \tag{4.16}$$

State Update. After every recursive step, the global quaternion is updated using the error quaternion as

$$\hat{\boldsymbol{q}}_k = \delta\hat{\boldsymbol{q}}_k \otimes \hat{\boldsymbol{q}}_{k/k-1} \tag{4.17}$$

whereas the angular velocity vector is updated by

$$\hat{\boldsymbol{\omega}}_k = \hat{\boldsymbol{\omega}}_{k/k-1} + \delta\hat{\boldsymbol{\omega}}_k \tag{4.18}$$

Covariance Update. Finally, the covariance matrix of the states is calculated by the Joseph's rule:

$$P_{k|k} = (I_{6\times6} - K_k H_k) P_{k|k-1} (I_{6\times6} - K_k H_k)^{\mathrm{T}} + K_k R_k K_k^{\mathrm{T}} \tag{4.19}$$

4.5 Gyro-based Multiplicative Extended Kalman Filter- GBMEKF

In GBMEKF, state parameters are the quaternions q_o^b and gyro bias values b. In that filter it is assumed that quaternions are obtained from the star trackers and angular velocities are obtained indirectly from gyros. The bias values of the gyros are estimated as state parameters. It is the most common method used in the literature. The state parameters are given below:

$$\hat{x} = \begin{bmatrix} \hat{q}_o^b \\ \hat{b} \end{bmatrix} \tag{4.20}$$

In this filter, simulated gyro data is used other than using the satellite dynamic equation. The gyro bias model is given in Equation (4.21).

4.5.1 GBMEKF: Propagation phase

4.5.1.1 GBMEKF: Propagation of the state parameters

In GBMEKF, the state parameters of quaternions are propagated through the same kinematic equation given in Equation (4.2). Since the gyro equipment output rates are given in equipment frame, they also need to be transformed into satellite body frame.

4.5.1.1.1 True / Reference Gyro Bias Model

True / reference gyro bias value is simulated by the below equation and a simplified approach is chosen such that it is assumed that the bias is modelled as a random walk process. The details of the bias model is given in [77]. More complex and realistic approaches can be found in literature [93].

$$\dot{\boldsymbol{b}}_g = \eta_{gb} \tag{4.21}$$

$\dot{\boldsymbol{b}}_g$: Modelled Gyro Bias Vector

η_{gb} : Zero mean Gaussian White Noise with the following properties

$$\mathrm{E}\left[\eta_{gbk}\eta_{gbj}^{\mathrm{T}}\right] = \mathrm{I}_{3x3}\left(\frac{\sigma_u^2}{\Delta t}\right)\delta_{kj} \tag{4.22}$$

σ_u : Gyro rate random walk value

4.5.1.1.2 Gyro Noise Model

The Gyro Model used in EKF is given below:

$$\vec{\omega}_{measured} = S \times \vec{\omega}_{true} + \vec{b}_{true} + \vec{n}_r \tag{4.23}$$

$\omega_{measured}$: Simulated noisy gyro measurements

S : Gyro Scale Factor and misalignments matrix (Unity matrix assumed)

$\vec{\omega}_{true}$: Reference / true attitude rates simulated by the satellite dynamic equation given in Equation (4.5).

$\vec{b}_{true}$: Reference / true gyro bias calculated according to Equation (4.21).

$\vec{n}_r$: Rate noise

Rate Noise $\vec{n}_r$ is assumed to be Gaussian white noise with the following characteristics:

$$\begin{aligned} E\left[\vec{n}_r\right] &= \vec{0}_{3x1} \\ E\left[\vec{n}_r(t+\tau)\vec{n}_r{}^T(t)\right] &= \vec{N}_r\delta(\tau) \end{aligned} \tag{4.24}$$

The estimated attitude rates are calculated through following equation:

$$\hat{\vec{\omega}} = \vec{\omega}_{measured} - \hat{\vec{b}} \tag{4.25}$$

In the above equation it is assumed that the states are propagated from gyro measurements and bias estimates. In that filter gyro failures are not taken into consideration.

4.5.1.2 GBMEKF: Propagation of the covariance matrix of the states

The standard propagation equation of the covariance matrix is used as stated in Equation (4.6) . However discrete time state transition matrix Φ_k, and process noise covariance matrix Q_k is obtained as follows:

4.5.1.2.1 Discrete time state transition matrix, Φ_k calculation

Trawny et al. [84], defines the block structure of the Φ_k matrix by considering the notation of Lefferts et al [43] as follows:

$$\Phi(t+\Delta t,t)=\begin{bmatrix}\Theta & \Psi\\ 0_{3X3} & I_{3X3}\end{bmatrix} \tag{4.26}$$

The elements of Φ_k matrix, namely Θ and Ψ, is also driven as follows:

$$\begin{aligned}\Theta &= I_{3x3}-\frac{1}{|\hat{\omega}|}\sin\left(|\hat{\omega}|\Delta t\right)\lfloor\hat{\omega}\times\rfloor+\frac{1}{|\hat{\omega}|^2}\left(1-\cos\left(|\hat{\omega}|\Delta t\right)\right)\lfloor\hat{\omega}\times\rfloor^2\\ \Psi &= -I_{3x3}\Delta t+\frac{1}{|\hat{\omega}|^2}\left(1-\cos\left(|\hat{\omega}|\Delta t\right)\right)\lfloor\hat{\omega}\times\rfloor-\frac{1}{|\hat{\omega}|^3}\left(|\hat{\omega}|\Delta t-\sin\left(|\hat{\omega}|\Delta t\right)\right)\lfloor\hat{\omega}\times\rfloor^2\end{aligned} \tag{4.27}$$

For small values of $|\hat{\omega}|$, L'Hopital's rule could be applied by taking the limit of above expressions and simplified version could be obtained as:

$$\begin{aligned}\lim_{|\hat{\omega}|\to 0}\Theta &= I_{3x3}-\Delta t\lfloor\hat{\omega}\times\rfloor+\frac{\Delta t^2}{2}\lfloor\hat{\omega}\times\rfloor^2\\ \lim_{|\hat{\omega}|\to 0}\Psi &= -I_{3x3}\Delta t+\frac{\Delta t^2}{2}\lfloor\hat{\omega}\times\rfloor-\frac{\Delta t^3}{6}\lfloor\hat{\omega}\times\rfloor^2\end{aligned} \tag{4.28}$$

Trawny et al. [84], defines the error of small ω approximation as $\Delta t^{n+2}|\hat{\omega}|^2$, if the non-approximated term is divided by $|\hat{\omega}|^n$. For example, error for Θ at 100 Hz sampling rate would be in the order of $10^{-6} \cdot |\hat{\omega}_{threshold}|^2$, as $\hat{\omega}_{threshold}$ denotes threshold for the small ω approximation. If the small ω approximation is simply defined as the error between the real ω value and its sinus value, it may give an idea for choosing the threshold value. The error according to this approximation is given in Figure 4-1.

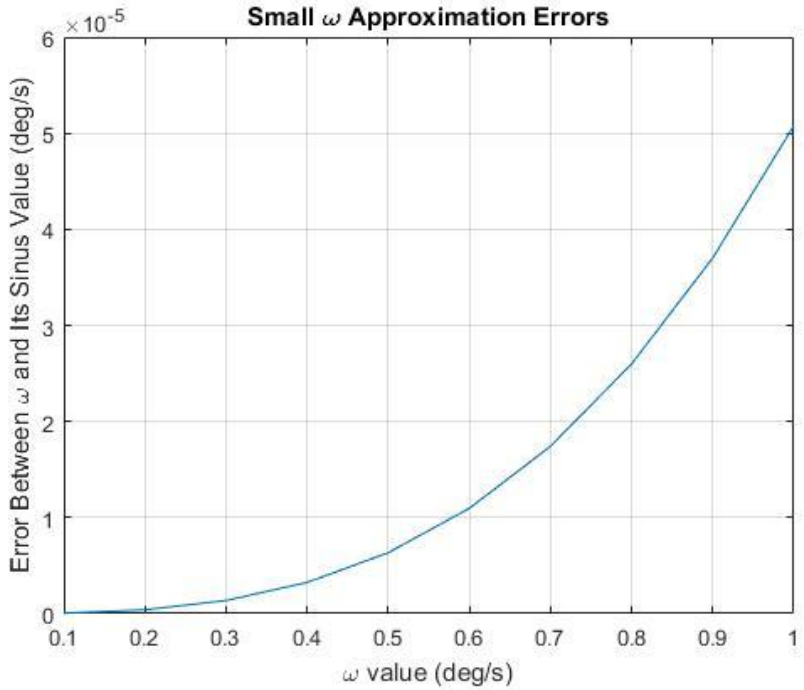

Figure 4-1. Small ω approximation errors

4.5.1.2.2 Discrete noise covariance matrix Q_k calculation

The discrete noise covariance matrix can be obtained as follows in Maybeck [94]:

$$Q_k = \int_{t_k}^{t_{k+1}} \Phi(t_{k+1}, \tau) G_c(\tau) Q_c G_c^T(\tau) \Phi^T(t_{k+1}, \tau) d\tau \tag{4.29}$$

Trawny [84], expand the above equation by assuming white and independent noise and obtains the noise covariance matrix in the following structure:

$$Q_k = \begin{bmatrix} Q_{11} & Q_{12} \\ Q_{12}^{\ T} & Q_{22} \end{bmatrix} \tag{4.30}$$

$$\begin{aligned} Q_{11} &= \sigma_r^{\ 2}\Delta t \cdot I_{3x3} + \sigma_\omega^{\ 2} \cdot \left(I_{3x3}\frac{\Delta t^3}{3} + \frac{\left(\frac{|\hat{\omega}|\Delta t}{3}\right)^3 + 2\sin\left(|\hat{\omega}|\Delta t\right) - 2|\hat{\omega}|\Delta t}{|\hat{\omega}|^5} \cdot \lfloor \hat{\omega}\times \rfloor^2 \right) \\ Q_{12} &= -\sigma_\omega^{\ 2} \cdot \left(I_{3x3}\frac{\Delta t^2}{2} - \frac{|\hat{\omega}|\Delta t - \sin\left(|\hat{\omega}|\Delta t\right)}{|\hat{\omega}|^3} \cdot \lfloor \hat{\omega}\times \rfloor + \frac{\frac{\left(|\hat{\omega}|\Delta t\right)^2}{2} + \cos\left(|\hat{\omega}|\Delta t\right) - 1}{|\hat{\omega}|^4} \cdot \lfloor \hat{\omega}\times \rfloor^2 \right) \\ Q_{22} &= \sigma_\omega^{\ 2}\Delta t \cdot I_{3x3} \end{aligned} \tag{4.31}$$

For small values of $|\hat{\omega}|$, L'Hopital's rule could be applied by taking the limit of above expression again and simplified matrix components could be obtained as:

$$\begin{aligned} \lim_{|\hat{\omega}|\to 0} Q_{11} &= \sigma_r^{\ 2}\Delta t \cdot I_{3x3} + \sigma_\omega^{\ 2}\left(I_{3x3}\frac{\Delta t^3}{3} + \frac{2\Delta t^5}{5!} \cdot \lfloor \hat{\omega}\times \rfloor^2 \right) \\ \lim_{|\hat{\omega}|\to 0} Q_{12} &= -\sigma_\omega^{\ 2} \cdot \left(I_{3x3}\frac{\Delta t^2}{2} - \frac{\Delta t^3}{3!} \cdot \lfloor \hat{\omega}\times \rfloor + \frac{\Delta t^4}{4!} \cdot \lfloor \hat{\omega}\times \rfloor^2 \right) \end{aligned} \tag{4.32}$$

4.5.2 GBMEKF: Update phase

GBMEKF also uses the star tracker measurements for the update phase. The output quaternion of the star trackers should also be transformed into satellite body frame. In GBMEKF, no gyro input is used as a measurement update and thus there is no

update process for the angular velocities and it could be represented as the zeros in observation matrix.

The observation matrix could be given same as the Equation (4.14) . The calculation of the measurement noise covariance matrix R_k is also obtained the same way in GBMEKF. Innovations are also obtained by the same equations and optimal Kalman gain K_k could be calculated by the standard formula given in Equation (4.16).

In terms of the updated / posteriori state estimate equation of the standard formula, states are calculated by the below equation in general:

$$\hat{x}_{k|k} = \hat{x}_{k|k-1} + K_k \tilde{y}_k \tag{4.33}$$

The bias is updated according to the following formula:

$$\hat{b}_{k+1|k+1} = \hat{b}_{k+1|k} + \Delta\hat{b}(+) \tag{4.34}$$

The estimated angular velocity according to updated bias is given as:

$$\hat{\omega}_{k+1|k+1} = \hat{\omega}_{k+1} - \hat{b}_{k+1|k+1} \tag{4.35}$$

And finally, the covariance matrix of the states is also calculated by the Joseph's rule given in Equation (4.19).

CHAPTER 5

INCORPORATING DELAYED STR MEASUREMENTS IN THE MEKF

In this study, we investigate different methods to incorporate delayed STR measurements in the Gokturk-2 satellite attitude filter, which is structured as a Multiplicative Extended Kalman Filter (MEKF). We compare these methods in terms of improvement in accuracy, computational load and their impact on the filter's optimality. We discuss possible extensions to improve the performance, regarding also the main framework of the MEKF with the STR measurements. Methods are first compared using the simulated data for an Earth observation spacecraft in Sun-synchronous orbit. Then, they are also tested with real logged data of Gokturk-2 satellite as from a spacecraft with similar specifications. Due to the absence of gyro measurements, the built MEKF algorithm is a dynamics-based filter that propagates also the spacecraft dynamics and estimates the angular velocities along with the attitude quaternion. Results are compared with those estimated by the real-time attitude and orbit control system- AOCS attitude filter running in-orbit.

This section presents different methods to incorporate the delayed STR measurements in the MEKF. Considering the MEKF structure for the actual spacecraft, for which the methods will be tested with real logged data, sampling time for the filter is set as $\Delta t = 1\text{s}$. The STR measurements are also sampled at every second. All the methods are given considering this filter structure.

5.1 Method-1

In this method, STR measurements are not propagated at all and they are used by the MEKF with delayed values, Figure 5-1. This method is given to see the effects of the STR delays in worst case.

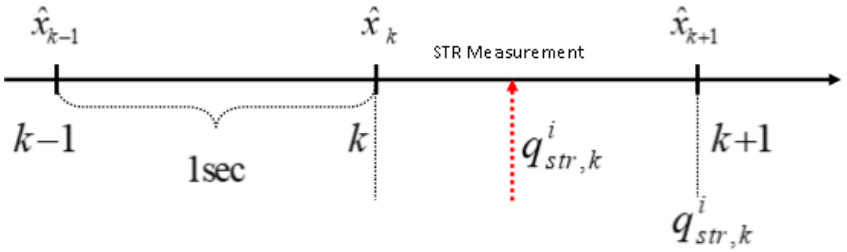

Figure 5-1. Method 1 Time Chart for STR Measurement Propagation

5.2 Method-2

STR measurements are propagated via angular velocity values obtained in previous step without propagation of angular velocities to the star tracker measurement time (e.g. using directly $\hat{\boldsymbol{\omega}}_k$ - Figure 5-2). In method-2, just like the method-3, the STR measurements are propagated to the current step to deal with the delay, however no update is performed in the Kalman filter parameters. When the angular velocity change is negligible, no significant difference occurs between method-3 and 2. Method-2 can be implemented in onboard flight software by considering its simplicity and computational load performance.

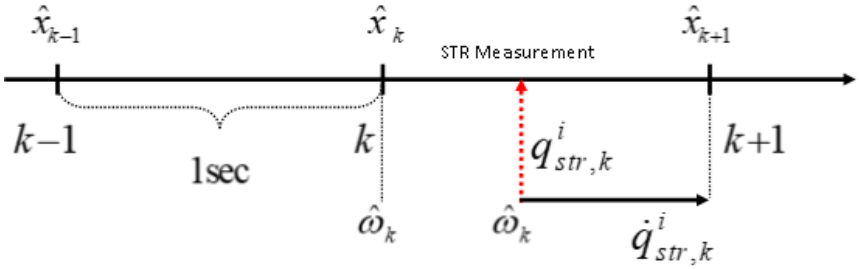

Figure 5-2. Method 2 Time Chart for STR Measurement Propagation

5.3 Method-3

Method-3 is the basic STR measurement propagation method. The time line is given in Figure 5-3. In Method-3, angular velocity $\hat{\boldsymbol{\omega}}_k$, which is estimated in previous step, is propagated to the STR measurement time via satellite's dynamic equation,

Equation (4.5) to get $\hat{\boldsymbol{\omega}}_{s/k}$. Subscript *s* denotes the STR timing. Afterwards, STR measurements is propagated to current time step via kinematic equation using the propagated angular velocity. This option only propagates star tracker measurements to current step to deal with the delay; however, no update is performed in the Kalman filter parameters.

This method is also the one implemented in the onboard attitude filter for the actual Earth observation spacecraft.

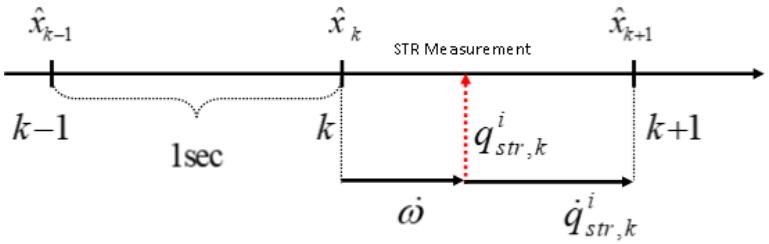

Figure 5-3. Method 3 Time Chart for STR Measurement Propagation

5.4 Method-4

In Method 4, a three-step approach is used as follows:

1. Perform state propagation up to STR measurement time.
2. Perform state update at STR measurement time.
3. Propagate the updated states and the P to the current time.

In this method (Figure 5-4), when the STR measurements are available, states are re-propagated up to the STR time. Update is performed at STR time. Afterwards the states and the covariances are re-calculated. This is similar to filter re-calculation method, which calculates the entire trajectory from the STR measurement up to the current time again. Method 4 offers the best performance theoretically, however requires the states and the covariances to be buffered, which might be

computationally costly if especially the filter time step is higher compared to the sampling frequency of the STR measurements. For example, if Figure 2-2 is recalled, in such case, all the states up to x_{k-3} must be buffered and re-estimated once the STR measurement is available at time step *k*.

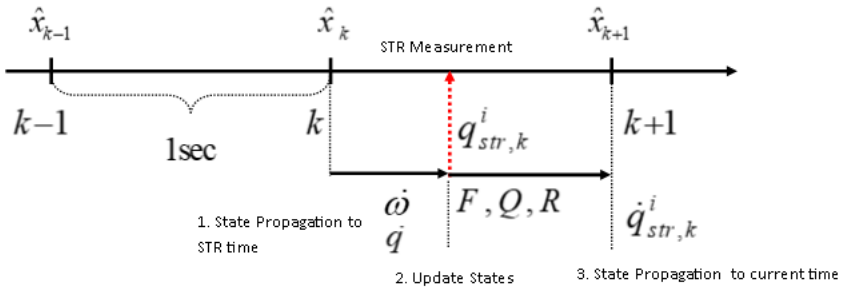

Figure 5-4. Method 4 Time Chart for STR Measurement Propagation

5.5 Method-5

Just like Method 3, in Method 5, angular velocity $\hat{\boldsymbol{\omega}}_k$, estimated in previous step is propagated to STR measurement time via satellite's dynamic equation and STR measurement is propagated to current time step via kinematic equation using the propagated angular velocity. In addition to the measurement propagation, the measurement noise covariance is updated in Method 5 (Figure 5-5) as

$$R_k^* = \left(I_{3\times 3} - \left[\hat{\boldsymbol{\omega}}_{s/k}\times\right]\Delta t\right) R_k \left(I_{3\times 3} - \left[\hat{\boldsymbol{\omega}}_{s/k}\times\right]\Delta t\right)^T + Q_k^* \qquad (5.1)$$

where Q_k^* is 3×3 process noise covariance accounting for the additional uncertainties in STR measurement propagation.

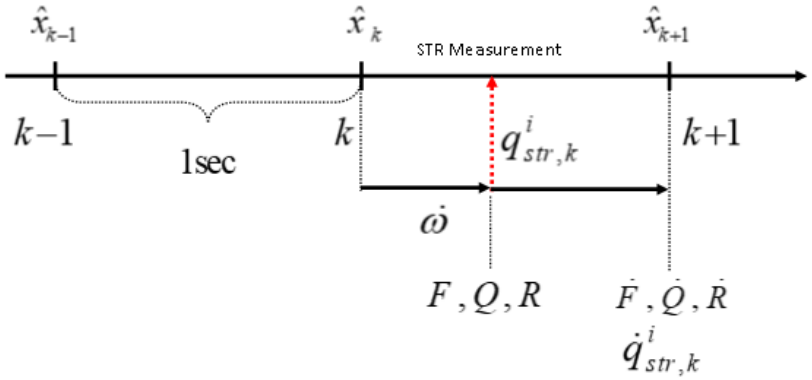

Figure 5-5. Method 5 Time Chart for STR Measurement Propagation

5.6 Evaluation and Comparison of Methods for Incorporating Delayed Star Tracker Measurements

The presented methods are tested for both the simulated and real data and the results are compared. The MEKF algorithm is a dynamics-based filter as discussed previously. The STR measurements are sampled at every second. The delay for the simulated measurements is assumed to be of similar pattern with that of the real logged STR data, which has either $0.3635\,\mathrm{s}$ or $0.4635\,\mathrm{s}$ delay depending on the processing time.

In terms of orbital profile, the spacecraft is on an approximately circular Sun-synchronous orbit with an altitude of 680 km. In agreement with the logged results for the actual spacecraft, the attitude estimation results are given in terms of roll (R), pitch (P) and yaw (Y) angles with respect to the orbit reference frame.

For the simulation cases, the spacecraft maneuver scheme is considered for 4 zones. In zone-1 spacecraft performed 60^0 pitch maneuver for stereo imaging purpose with 1^0 initial errors for each axes. Zone-2 is the steady state zone after the first maneuver.

In zone-3 spacecraft performed its second maneuver to turn back to nadir pointing position. Zone-4 is the steady state zone and indicates the final performance of the estimation results. The “true” reference attitude angle profile is given in Figure 5-6.

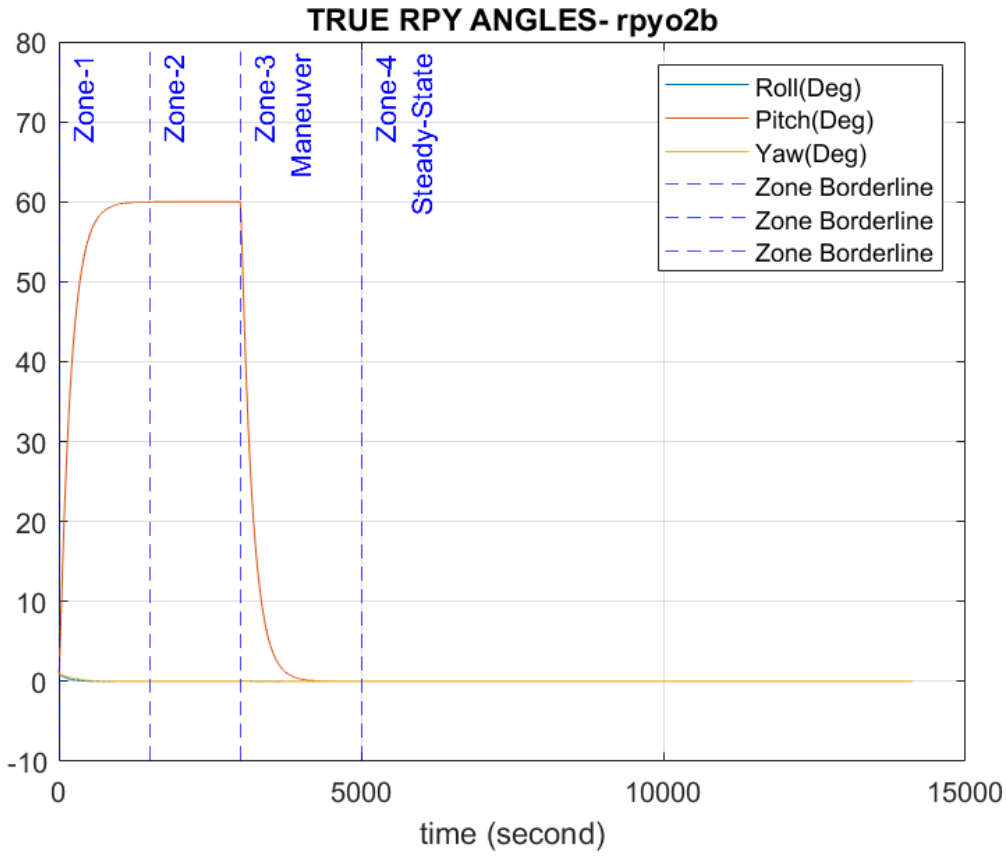

Figure 5-6. Spacecraft Maneuver Scheme for Simulation Cases

As to the filter setting, the process noise covariance is set as

$$Q_k = \mathrm{diag}\left(\begin{bmatrix} 10^{-6} & 10^{-6} & 10^{-6} & 10^{-11} & 10^{-11} & 10^{-11} \end{bmatrix}\right) \tag{5.2}$$

and the measurement noise covariance is set as

$$R_k = \mathrm{diag}\left(\begin{bmatrix} 10^{-8} & 10^{-8} & 10^{-8} \end{bmatrix}\right) \tag{5.3}$$

in both cases, in line with the STR specifications.

5.6.1 Estimation Results for the Simulated Data

Figure 5-7, Figure 5-8 and Figure 5-9 present the attitude estimation errors for the simulated data for Methods 3, 4 and 5, respectively. The 3σ error boundaries for the estimated attitude are also shown on the figures. In terms of accuracy all three

methods perform similar. Nonetheless, 3σ error boundaries show that for Method 3 the filter is not performing optimally as the error exceeds the boundaries occasionally. In contrast for Methods 4 and 5, the attitude estimation errors reside inside the 3σ error boundaries all the time.

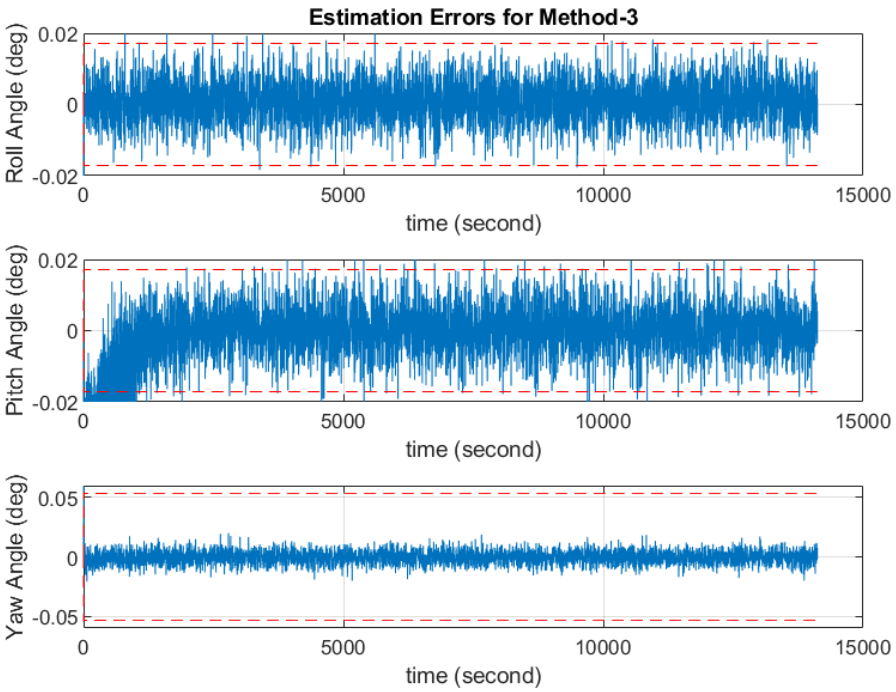

Figure 5-7. Estimation Errors for Simulated Data: Method 3

When the results for Methods 4 and 5 are compared in detail, we see that both are performing very similar in terms of error values and the 3σ error boundaries. It should be noted that Method 4 recalculates all the states throughout the course and Method 5 updates only the last state, but applies also covariance correction. Thus, Method 4, which is considered as the optimal and most accurate method to incorporate the delayed measurements in theory, is computationally more expensive. Monte Carlo simulations are more insightful to better compare the performance of Methods 4 and 5.

As to the other methods, Method 1 and Method 2, as expected Method 1, which is just using the measurements as they are without taking the delay into consideration at all, performs poorer compared to all other methods. Because of the orbital motion of the spacecraft, delay in the measurements is observed as pitch angle error for Method 1, whose level is depending on the angular velocity experienced at that moment. Method 2, just propagates the STR measurements using the latest available angular velocity information. It is computationally more efficient than Method 3 and the results show that there is no significant performance difference between Method 2 and Method 3. Considering this result it may be an ideal Method when the accuracy is not the primary concern and the computational efficiency is more important.

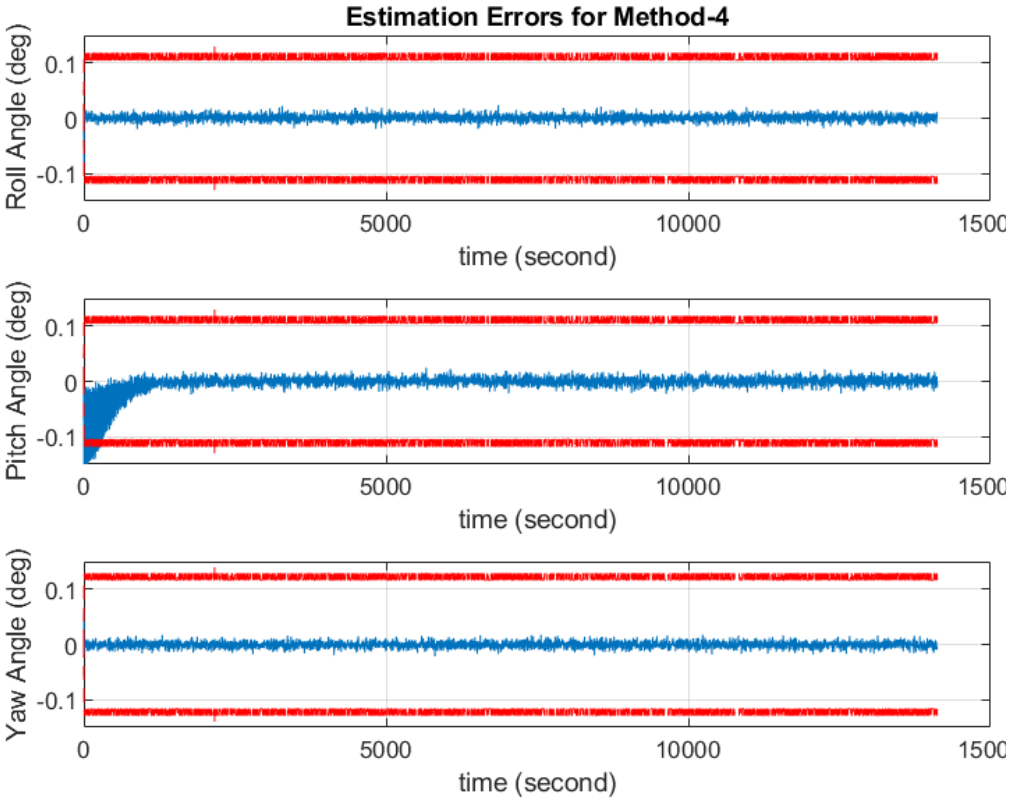

Figure 5-8. Estimation Results for Simulated Data: Method 4

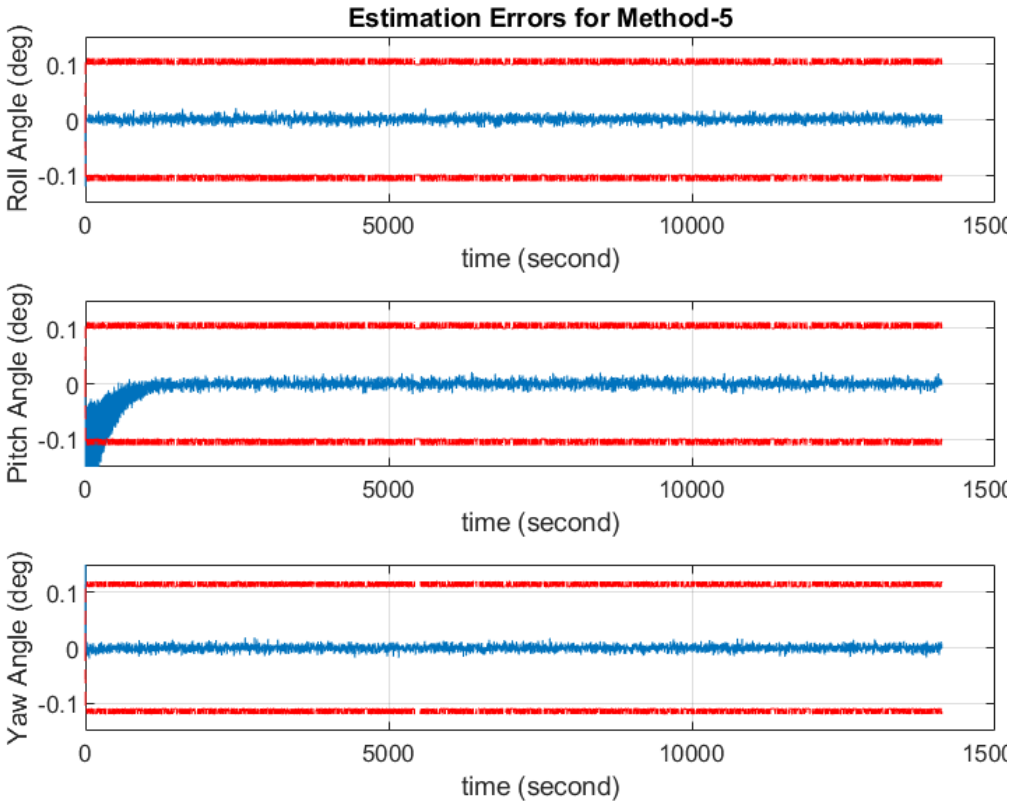

Figure 5-9. Estimation Results for Simulated Data: Method 5

In Table 5-1, Root Mean Square Error- RMSE results of 100 Monte Carlo simulation runs are given for zone-4 in arc seconds. These results proves the consistency of the proposed methods.

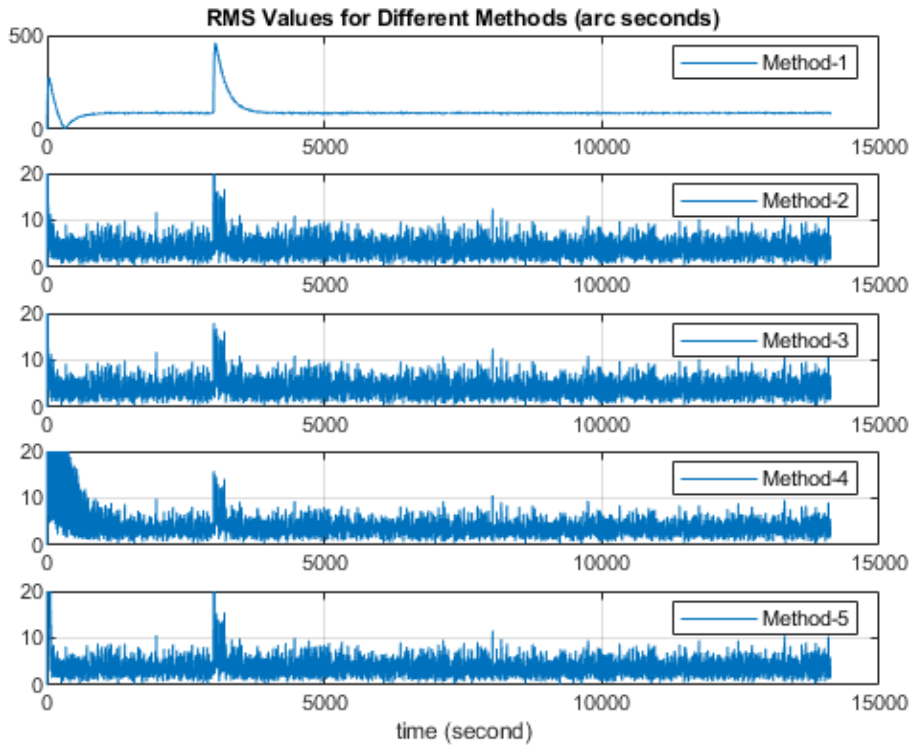

Figure 5-10. Monte Carlo Simulations Results: RMS Values for Different Methods

In terms of Monte Carlo simulations, extra effort has been performed to investigate the reason why Method-4 is not more accurate than Method-5, although it is computationally more expensive but more optimal. The Monte Carlo simulations have been repeated for different process noise covariance matrix values. Moreover, standard deviations of the different methods are compared together with the RMSE values. However the results have not changed. The method-4, only performed better than Method-5 by using extremely high level noise parameters. Since the simulation parameters have been changed drastically, it is concluded that methods could not be compared under these circumstances.

Table 5-1 RMSE Results of 100 Monte Carlo Simulation Runs for Zone-4 (arc seconds)

	Method-1	Method-2	Method-3	Method-4	Method-5
Roll Angle (arc seconds)	0.081	0.081	0.082	0.082	0.081
Pitch Angle (arc seconds)	0.034	0.034	-86.100	0.079	-0.054
Yaw Angle (arc seconds)	0.047	0.047	0.049	0.047	0.046
Resultant (arc seconds)	3.872	3.872	86.160	3.993	3.583
Standard Deviation of Resultant Values (arc seconds)	17.607	17.614	43.953	18.170	16.246

5.6.2 Estimation Results for the True Data

In this section, we first compare the results obtained using the Methods 4 and 5 with the results by the actual filter implemented onboard the spacecraft. Figure 5-11, Figure 5-12 and Figure 5-13 give the comparative estimation results for Method 4. Figure 5-12 give the roll pitch and yaw angles estimated by the onboard computer and with the on ground calculation. Figure 5-13 presents the difference for the estimated attitude. Clearly there is a difference for all three angles at an order of $0.002\,\text{deg}$. When the results for Method 4 are compared with those of the onboard algorithm, the difference is at an order of $2\times10^{-5}\,\text{deg}$. Thus Method 4 produces very close results with those of the onboard algorithm in terms of accuracy. Figure 5-14 and Figure 5-15 gives the similar results for Method-5.

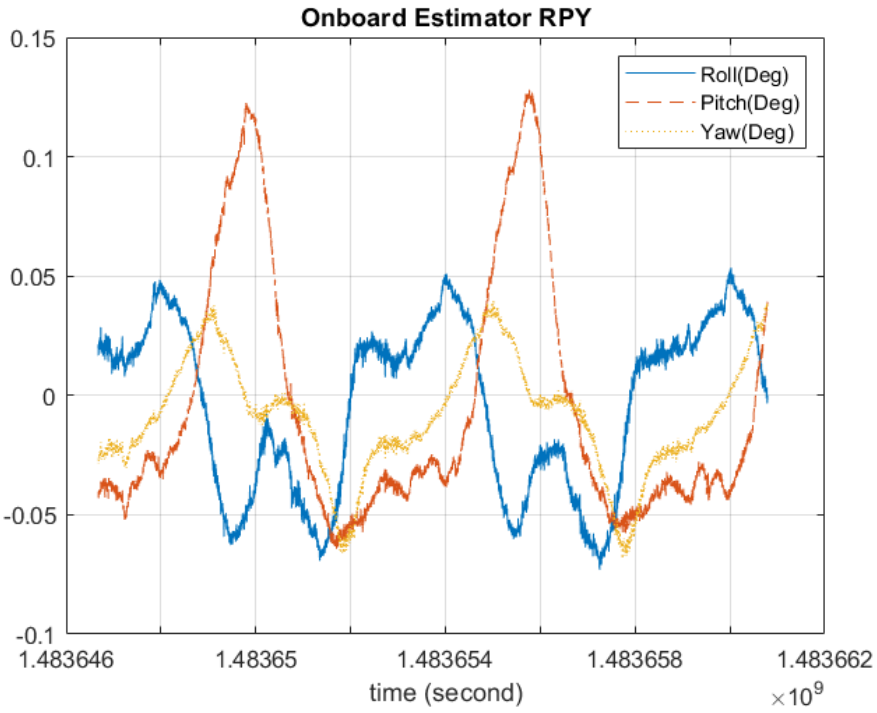

Figure 5-11. Estimation Results for True Data: Onboard Estimator RPY

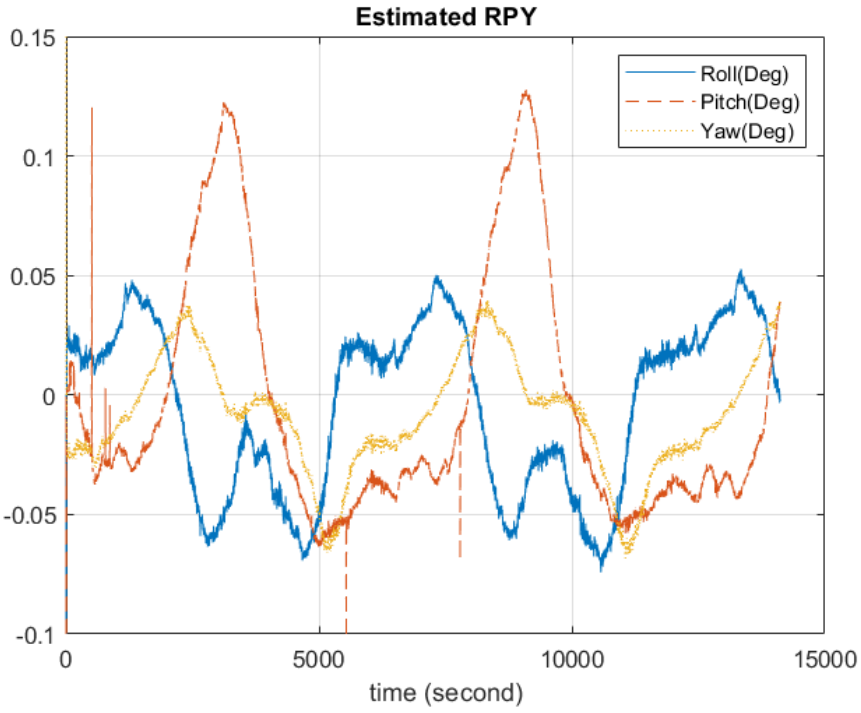

Figure 5-12. Estimation Results for True Data: Method-4 Estimator RPY

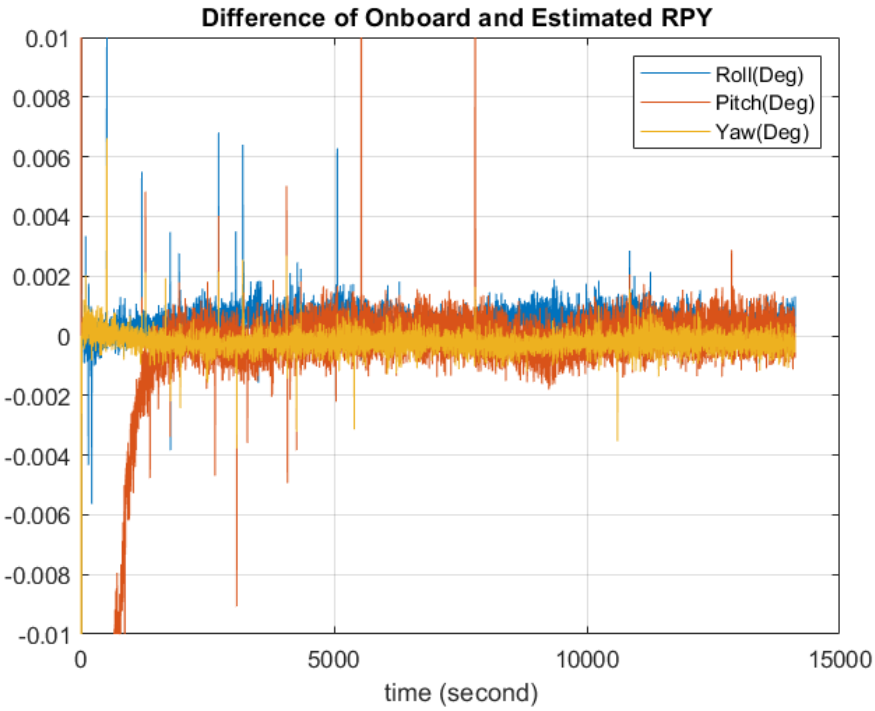

Figure 5-13. Estimation Results for True Data: Method-4 Difference of Onboard and Estimated RPY

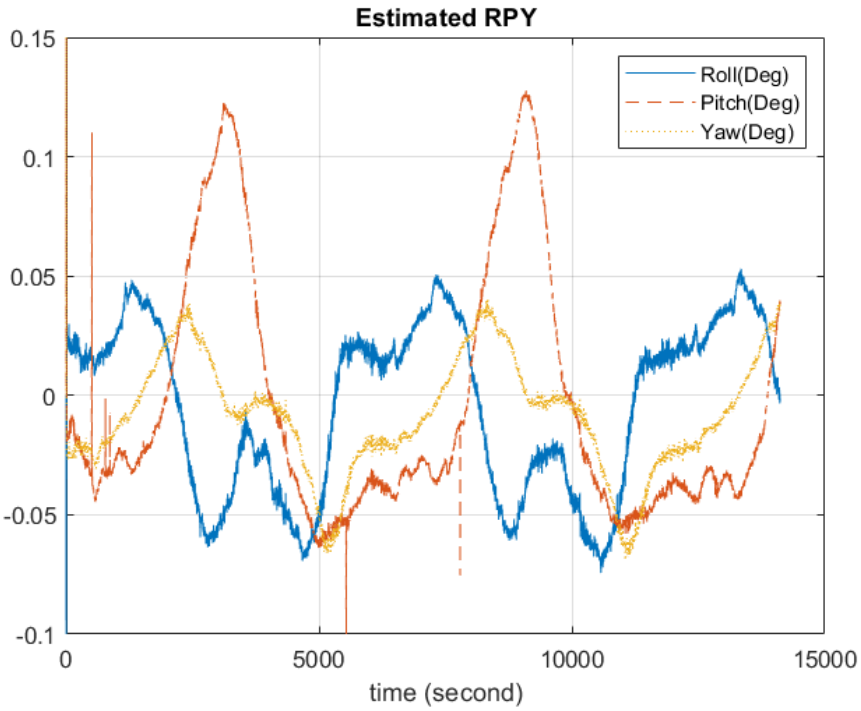

Figure 5-14. Estimation Results for True Data: Method-5 Estimator RPY

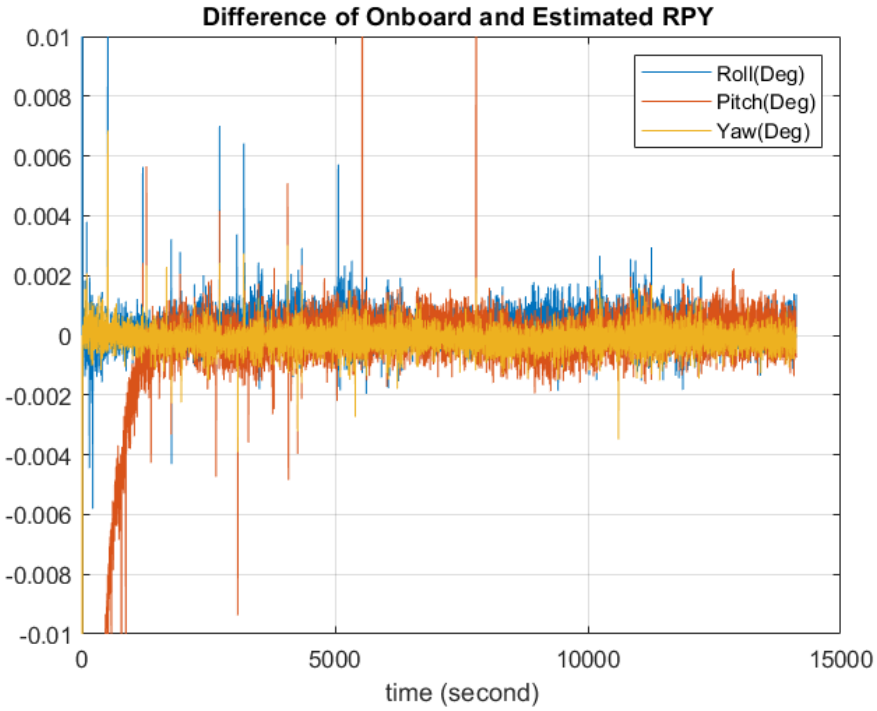

Figure 5-15. Estimation Results for True Data: Method-5 Estimator RPY

5.7 Results and Discussions for Incorporating Delayed STR Measurements in the MEKF

The first enhancement effort of the Gokturk-2 satellite attitude estimation performance is performed by proposing an alternative method to incorporate delayed star tracker measurements in the attitude filter. The study evaluates different methods to incorporate delayed star tracker (STR) measurements in the Gokturk-2 satellite attitude filter, which is structured as a Multiplicative Extended Kalman Filter (MEKF). Five different methods are implemented for both the simulated and real data logged from an actual spacecraft for an Earth observation mission, and compared in terms of accuracy. Similar results are obtained using both the simulation data and real data. This shows that the results have consistency. Simulation results give flexibility for better evaluation of different methods since the actual orientation of the spacecraft is known.

As it stated before, Method 1 is given to demonstrate the worst condition. Method 2, is just propagating the STR measurements using the latest available angular velocity information. It is computationally more efficient than Method 3 and the results show that there is no significant performance difference between Method 2 and Method 3.

The Method 4, which re-calculates all the states from the measurement timing to the actual time, theoretically has to offer best performance. Method 5, in contrast, propagates the measurements and applies covariance correction. The results show that the performance of Method 5 is comparable with that of Method 4. Moreover, since all the filter parameters are re-calculated in Method 4, Method 5 is computationally more efficient than the Method 4. The proposed method-5 can be implemented to be used in onboard computer for the real operations.

CHAPTER 6

PERFORMANCE EVALUATION OF GOKTURK-2 SATELLITE AOCS VIA GYRO BASED MEKF

In Gokturk-2 satellite, AOCS architecture is inherited from RASAT satellite. Since these type of basic platforms have low resolution cameras, the early versions of the AOCS are based on coarse attitude hardware such as magnetometers and sun sensors. When the platform enlarges with the higher resolution image needs, more accurate sensors such as star trackers and gyros are necessary. In most platforms MEMS gyro units are used for low cost solutions and when the system is more complex fiber optic or laser gyros are used in common. Likewise, the star trackers provides attitude angles directly and they have to be the critical choice for accurate attitude estimations. In Gokturk-2 platform, star tracker units are easily integrated to the system architecture as they are only involved in the update phase of the Kalman Filtering algorithm. However MEMS gyro units are not preferred and the satellite dynamic equation is used instead of using the gyro data into the propagation phase.

In this chapter, it is claimed that the total performance of the satellite attitude estimation can be evaluated by using the MEMS gyro units even if they offer poorer performance with respect to the accurate star trackers. For this purpose, a test has been conducted in Gokturk-2 satellite. The second redundant star tracker unit and the gyros are enabled and their data is stored and downloaded. However, they are not used in closed loop of the attitude software for not disturbing the ongoing operations. The star tracker's data and the gyro data is fused in an onground gyro based MEKF and the results show that the total estimation performance can be enhanced via proposed methods.

6.1 Gyro Noise Analysis

The bias instability value of the Gyro Unit used in Gokturk-2 satellite is defined as 20 ^{0}/h which corresponds to 5.6 x 10^{-3} ^{0}/s or 9.7 x 10^{-5} rad/s. These values indicates that if the states are propagated via gyro unit only, it adds 20 degree error for each hour. This indicates that this gyro is not "good" enough for precise attitude estimation purposes. For example, IMECE satellite has fiber optic gyro unit which provides better performance. The bias instability term is used by the manufacturer and the value is given as 0.05 ^{0}/h which corresponds to 1.38 x 10^{-5} ^{0}/s or 2.42 x 10^{-7} rad/s.

In terms of Gyro Noise Analysis, the Allen Variance Graphics are plotted by Matlab and given in Figure 6-1. In this graphic, the results are similar with the same graphics obtained from the test bench results given in Figure 3-10, Figure 3-11, and Figure 3-12. However the differences occurred because the onboard data is collected for only a limited period of time and the flight conditions differ from the onground test conditions.

The angular random walk values can be obtained from these figures. However, for the process noise covariance matrix values, the standard deviation of the bias values offer more reliable results.

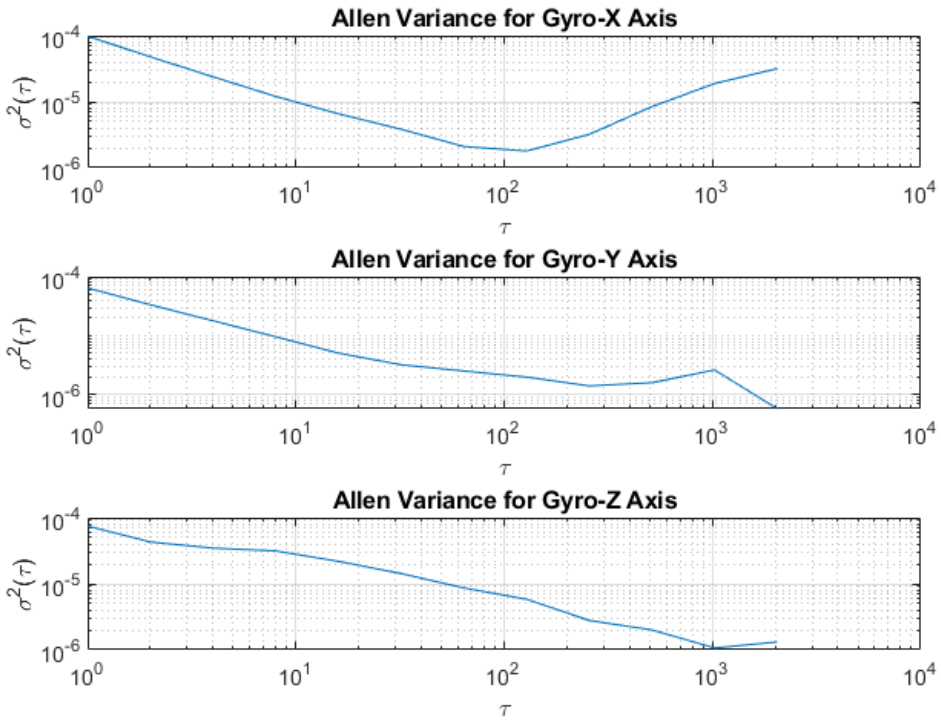

Figure 6-1. Allen Variance Graphics of The Gyro Unit obtained from Onboard Data

The satellite dynamic equation which is given in Equation (4.5), indicates the necessary ambiguity level of the process noise. The approximate values of the external disturbance torques for a LEO satellite is given below [95]:

- Gravity gradient [1 x 10^{-5} Nm]
- Solar radiation pressure [1 x 10^{-6} Nm]
- Magnetic torques [1 x 10^{-5} Nm]
- Air drag [1 x 10^{-7} Nm]

The maximum deviation of the parameters can be assumed as 3 x 10^{-5} rad/s level. When we compare this value with the Gokturk-2 Gyro bias value of 8.7 x 10^{-3} rad/s, in addition to above disturbance torques, actuator misalignments, reaction wheel

speed estimation errors and inertia errors will increase the total amount of the disturbances. In the simulations, the gyro data is used with the star tracker data and the bias values are estimated throughout the Kalman Filter update process. Thus, these results show that, gyro-based filter could be used in Gokturk-2 satellite, instead of dynamic based results and we could expect more accurate estimation results.

6.2 Performance Evaluation of Gokturk-2 Satellite AOCS via Gyro Based MEKF: Results and Discussions

The gyro-based MEKF is implemented and the filter is run with the real onboard Gokturk-2 data. The results indicate that the similar performances with dynamics-based filter have been assured via gyro-based filter despite the relatively poor performance of the gyro unit. The comparison of the star tracker measurements has already been performed in previous section via dynamics-based MEKF by using simulated data. In this chapter, gyro-based filter has been implemented with the real-onboard Gokturk-2 data of both star tracker and the gyro unit.

Onboard Estimator's attitude angles are given in Figure 6-2. In this figure, it is clearly seen that satellite is performing a small attitude maneuver for imaging purpose. In Figure 6-3, the similar results are obtained for method-5 via onground estimator. The difference between onboard and estimated attitude angles are given in Figure 6-4. The results indicates that the filter converges smoothly.

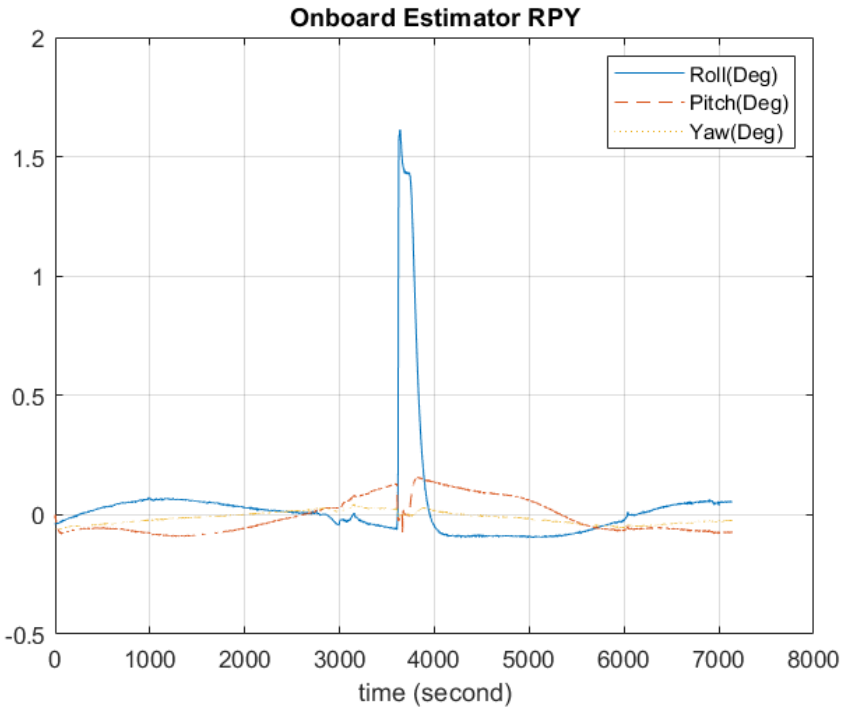

Figure 6-2. Estimation Results for Attitude Angles: Method 5- Onboard Estimator RPY

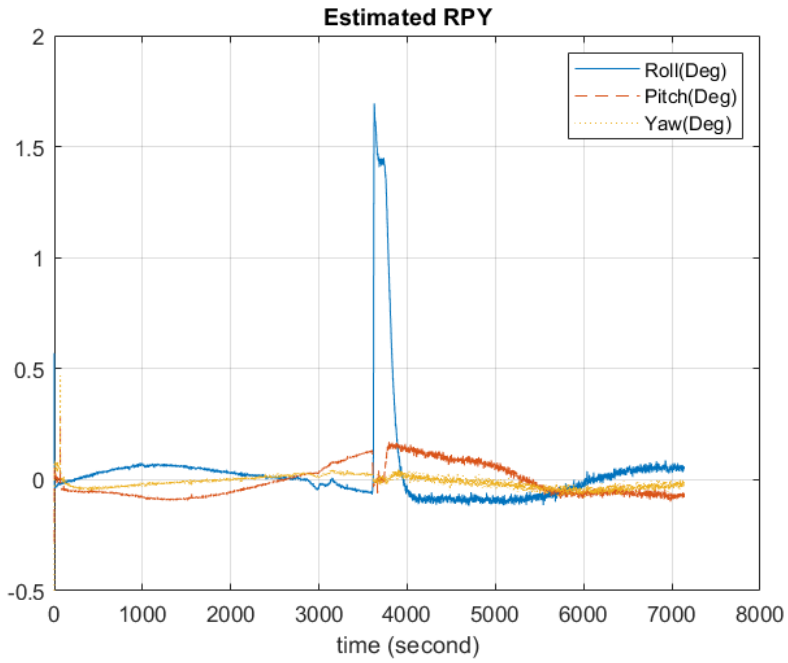

Figure 6-3. Estimation Results for Attitude Angles: Method 5- Estimated RPY

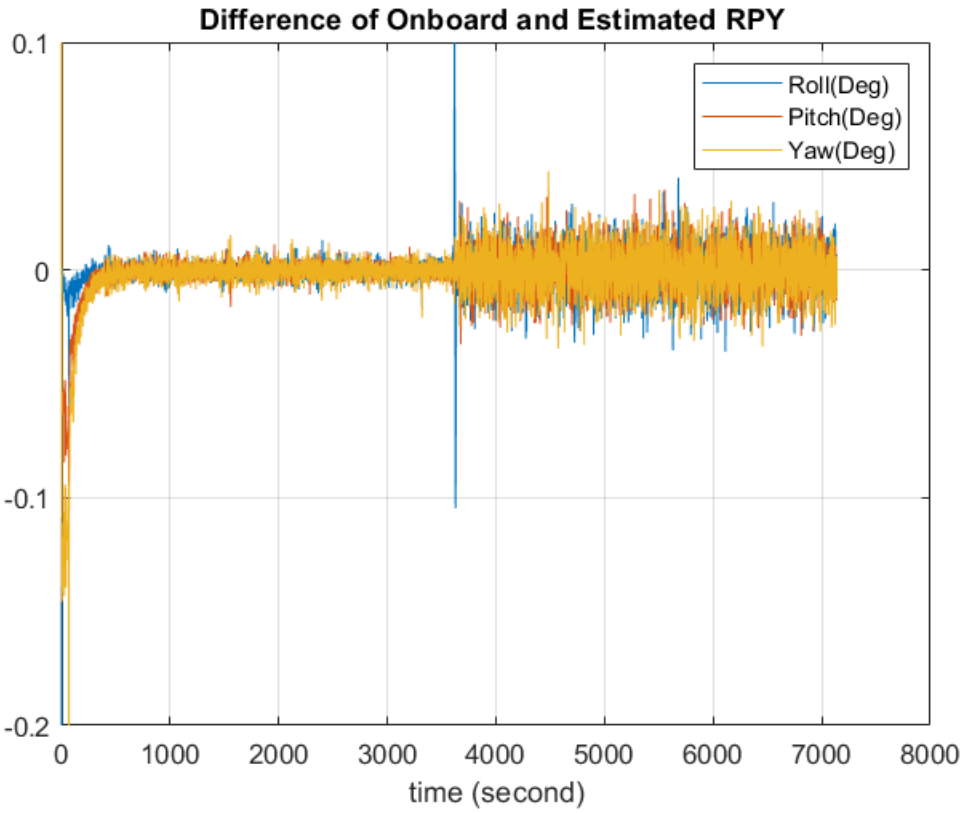

Figure 6-4. Estimation Results for Attitude Angles: Method 5- Difference of Onboard and Estimated RPY

Onboard filter estimation results for attitude rates which are obtained indirectly from bias values via Method 5 defined with respect to orbital frame is given in Figure 6-5. The same results could also be obtained in inertial frame and it is given in Figure 6-6. In Figure 6-7, onground estimation results for attitude rates which are obtained indirectly from bias values via Method 5 is given in inertial frame.

The results show that the estimation performance of dynamics-based filter is very similar with the gyro-based MEKF which uses MEMS gyro data.

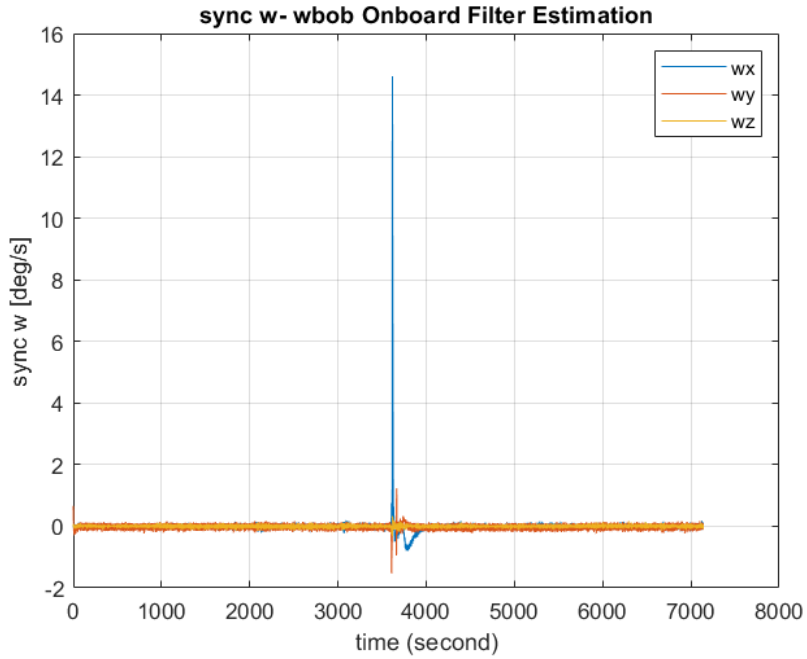

Figure 6-5. Estimation Results for Attitude Rates (Obtained indirectly from bias values): Method 5- Onboard Filter Estimation- w_{bob}

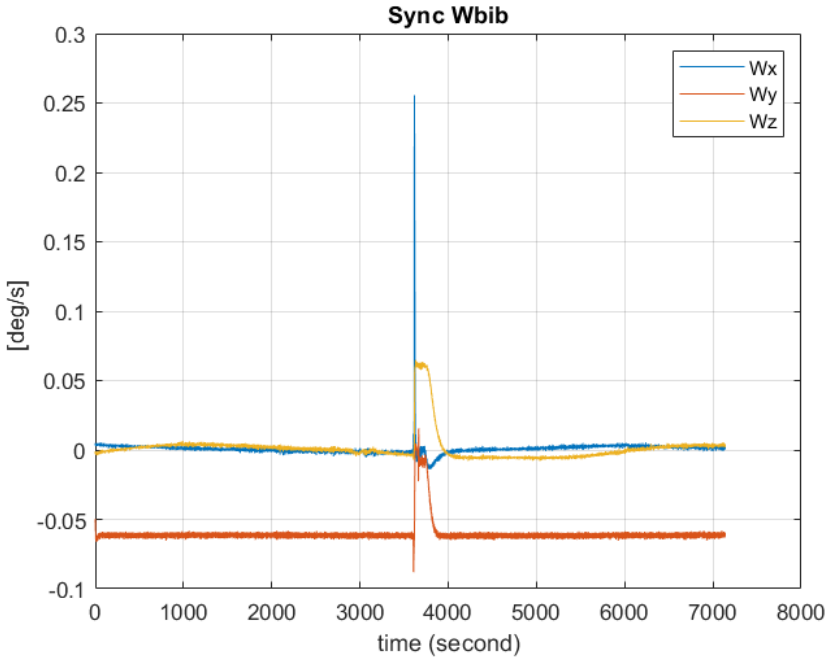

Figure 6-6. Estimation Results for Attitude Rates (Obtained indirectly from bias values): Method 5- Onboard Filter Estimation- Sync w_{bib}

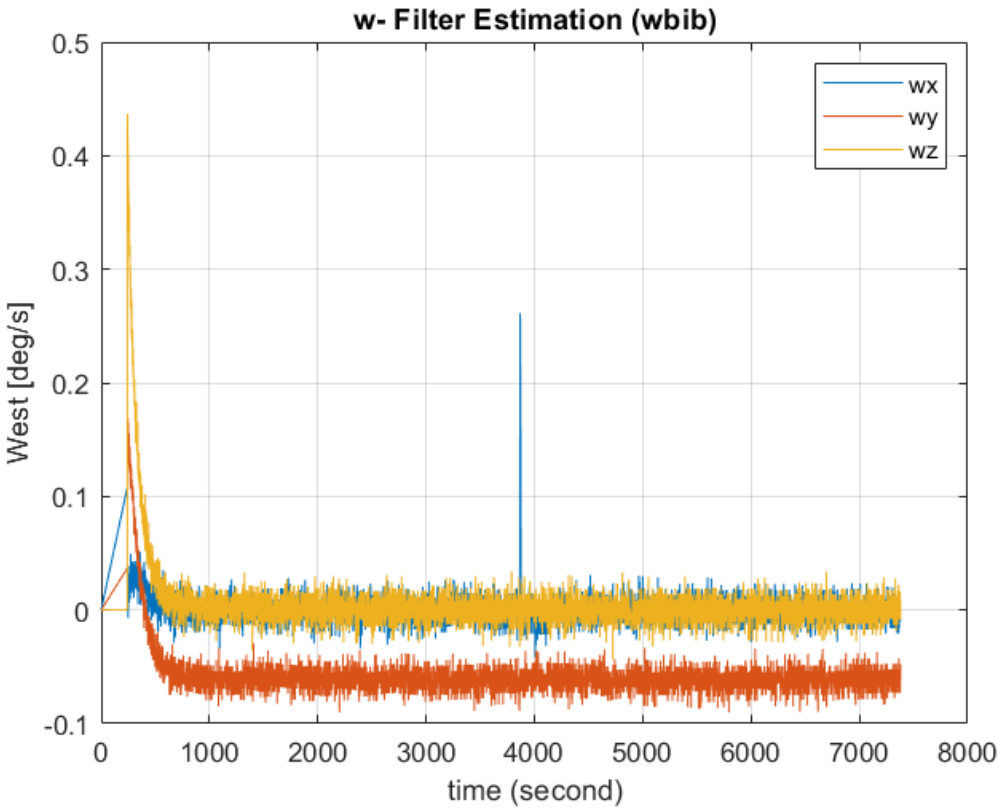

Figure 6-7. Estimation Results for Attitude Rates (Obtained indirectly from bias values): Method 5- Filter Estimation- w_{bib}

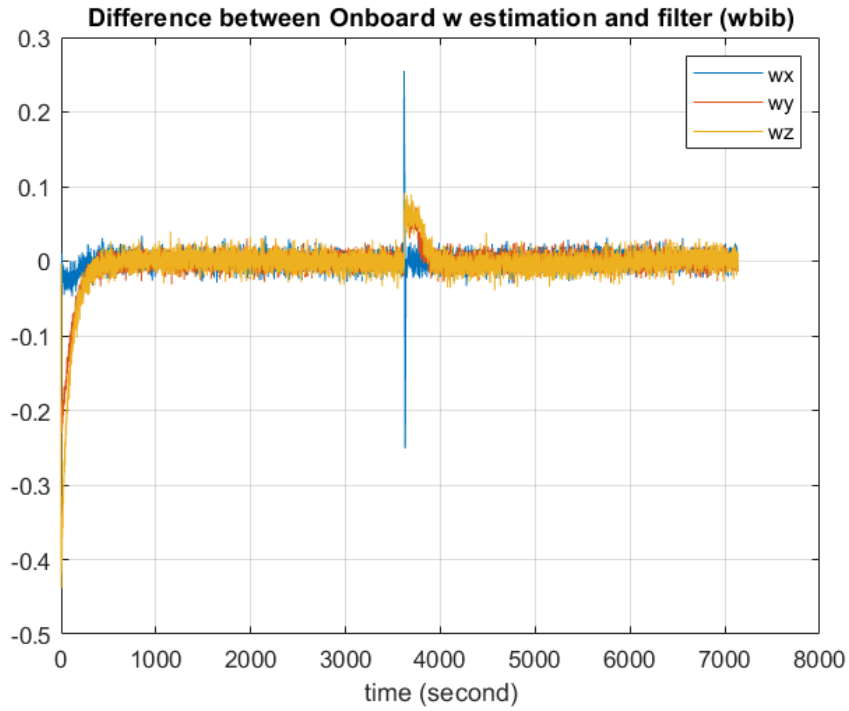

Figure 6-8. Estimation Results for Attitude Rates (Obtained indirectly from bias values): Difference Between Onboard Filter Estimation and Filter Estimation

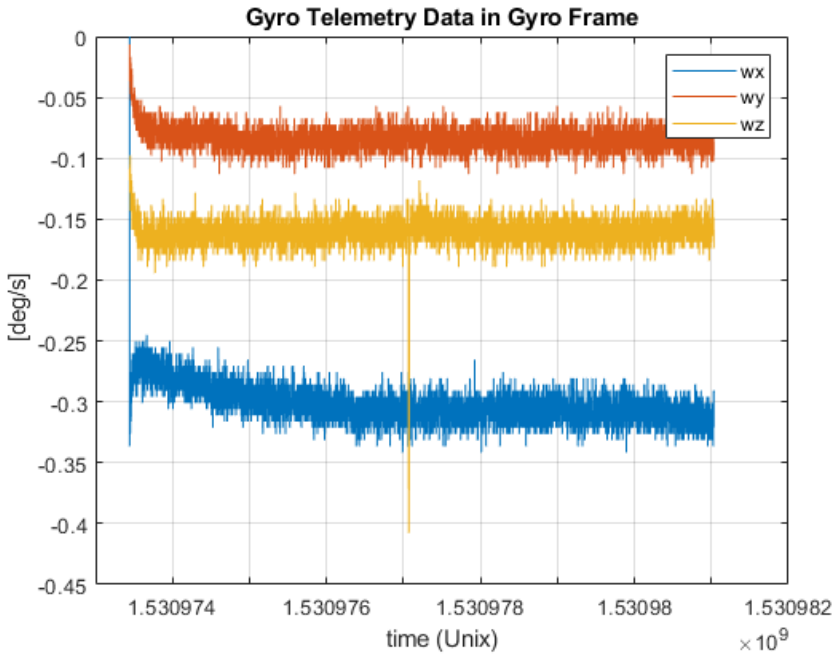

Figure 6-9. Attitude Rates obtained from the Gyro Data in Gyro Frame

The data which is taken in 07.07.2018 from Gokturk-2 satellite is logged in 1 second time interval during the test. The gyro data in gyro and body frames are given in Figure 6-9 and Figure 6-10. The estimated bias values via Method-5 is finally presented in Figure 6-11. This results indicate that the gyro biases show stable fashion during the estimation.

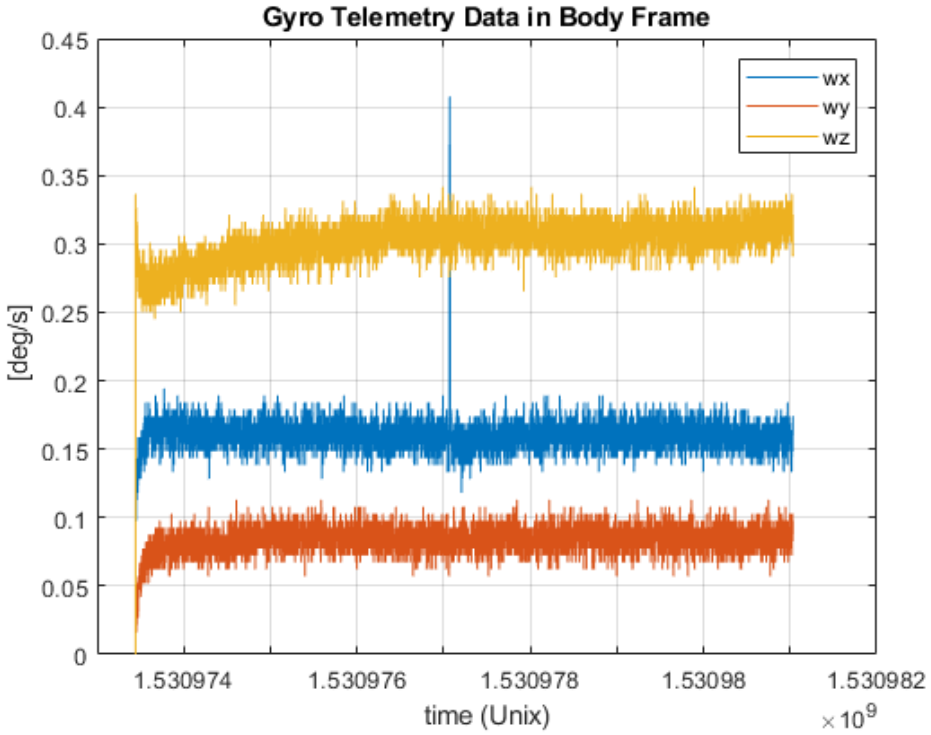

Figure 6-10. Attitude Rates obtained from the Gyro Data in Body Frame

The similar results have been obtained via different star tracker propagation methods as method-1, 2, 4 and 5. Since the motivation is to compare the attitude estimation performance of the gyro-based and dynamics-based filters, the comparison of the different methods is not considered.

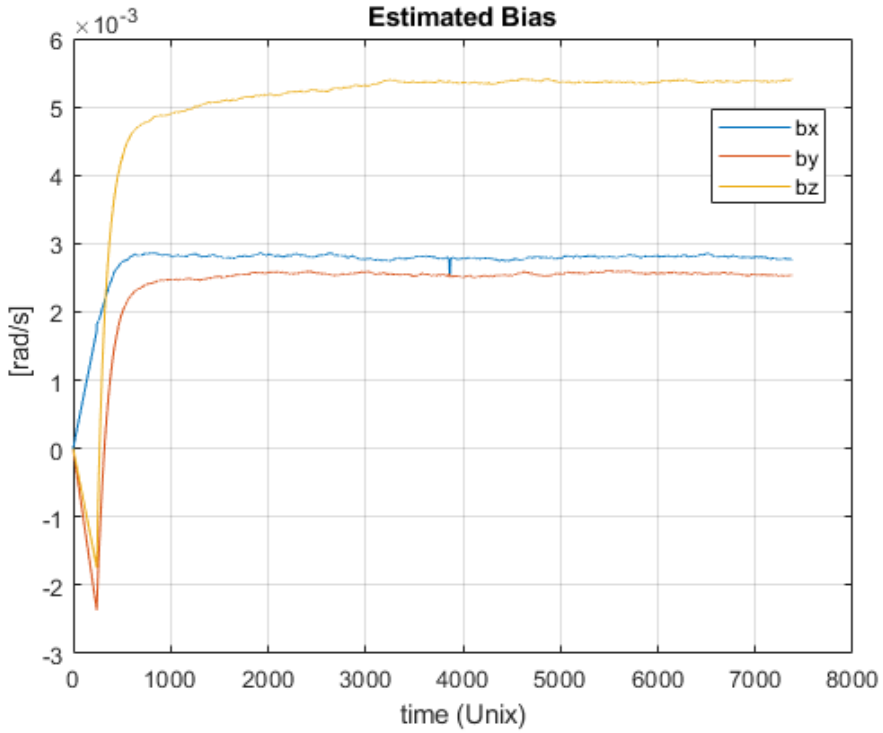

Figure 6-11. Gyro Biases Estimated via Gyro-based MEKF: Method 5

In terms of comparing the results with previous works, Winkler et. al., [49], used gyro stellar multiplicative error Kalman Filter via similar standard filter tuning. However, an alternative approach has been applied such that the influence of the time-correlated star tracker noises and time-variant gyro and STR misalignment are considered. Moreover, Ghezal et. al. [96], the performance of gyro based Kalman filter is increased via dynamic filtering for low cost missions. Since a low performance Gyro is used in Gokturk-2 satellite, same approach could be considered.

Yıldırım et. al. [90], compared both gyro-based and dynamical model based multiplicative extended Kalman filter with each other and proposed fault detection, isolation and recovery scheme. An alternative methods could also be used for this study as a future work.

Springman et. al. [52], used coarse Sun sensors and gyro units for the AOCS and by using on orbit calibration methods and it is claimed that it maximizes the

performance. In this study, pre-flight and on-orbit calibration method could increase the attitude estimation accuracy and low performance gyro units could be used for this type of missions. Gyro bias values could be estimated according to this approach.

CHAPTER 7

CONCLUSIONS AND RECOMMENDATIONS

Gokturk-2 satellite is a milestone in Turkish Space Industry. The attitude and orbit control subsystem onboard software of Gokturk-2 satellite is developed by TUBITAK UZAY Space Technologies Research Institute. The heritage gained from this project led the new generation sub-meter resolution IMECE satellite. In terms of the lessons learned from Gokturk-2 satellite, the new systems are improved and native payloads such as star tracker, sun sensor, reaction wheel, magnetometer, and magnetorquer have been developed and will gain heritage after the launch. During the nominal operations of Gokturk-2 satellite, performance enhancement efforts have been made, however some of the implementations could not be performed.

The main objective of this thesis is to provide enhancements to the AOCS performance of the satellite. The proposed improvements are categorized in two main headlines. The first effort is incorporating delayed star tracker measurements in the multiplicative extended Kalman filter. The results indicate that the proposed method could increase the attitude estimation performance. The compared methods will be implemented to the new generation satellites. In terms of the contribution of the thesis, the comparison of the propagation methods are not common and this study could enrich the literature.

However, in terms of the weak side of the study, theoretically most optimal method, method-4 results slow performance because of the unpredicted noise. As a future study, this ambiguity could be searched in terms of coding errors. Moreover, the propagation methods could be implemented in the onboard software and their behavior could be examined for different dynamic conditions. For example during stereo imaging the effects of using different star tracker propagation methods could make a difference.

The second effort is to show that the gyro-based MEKF has similar performance with the dynamics-based MEKF and could be used operationally. However the reason of why the gyro data is not used in closed loop, is obviously the poor gyro performance. In terms of the contribution of the thesis, the comparison of dynamics-based and gyro-based filter performances could be examined for the given maneuver schemes. The difference between the Allen Variance graphics could practically be considered for real missions.

In conclusion, the attitude enhancement methods proposed in this study could be implemented for onboard software and could be applied to the other satellites. The incorporating star tracker measurement delays in MEKF provides original contributions to the literature. For example next generation IMECE satellite AOCS design could be performed via proposed enhancements. Moreover, gyro-based filter results shows that it could perform better than the dynamic based filter.

For future work, longer data can be collected from the satellite and more realistic Allen Variance graphics which are closer to the onground results could be achieved. Again, the gyro choice considerations, contribute to the literature in that sense.

REFERENCES

[1] A. Bradford, L. M. Gomes, S. M. Sweeting, G. Yuksel, C. Ozkaptan, and U. Orlu, "BILSAT-1: A low-cost, agile, earth observation microsatellite for Turkey," *Acta Astronaut.*, vol. 53, no. 4–10, pp. 761–769, Aug. 2003, doi: 10.1016/S0094-5765(03)00125-5.

[2] L. Gomes *et al.*, "BILSAT: Advancing Smallsat Capabilities," Aug. 2003, Accessed: Dec. 27, 2022. [Online]. Available: https://digitalcommons.usu.edu/smallsat/2003/All2003/42.

[3] G. Yüksel, A. Okan, and U. M. Leloğlu, "First LEO satellite built in Turkey: RASAT," in *Proceedings of the 3rd International Conference on Recent Advances in Space Technologies, RAST 2007*, 2007, pp. 78–82, doi: 10.1109/RAST.2007.4284098.

[4] Ö. Kahraman *et al.*, "Uzaktan algılamada RASAT: Türkiye'de üretilen ilk yer gözlem uydusu (RASAT in remote sensing: First earth observation satellite built in Turkey)," 2012.

[5] M. Teke *et al.*, "GEOPORTAL: Tübitak Uzay satellite data processing and sharing system," in *2015 7th International Conference on Recent Advances in Space Technologies (RAST)*, 2015, pp. 233–238, doi: 10.1109/RAST.2015.7208347.

[6] M. Teke, "Satellite image processing workflow for RASAT and Göktürk-2," *J. Aeronaut. Sp. Technol.*, vol. 9, no. 1, pp. 1–13, 2016, [Online]. Available: http://www.rast.org.tr/JAST/index.php/JAST/article/view/38.

[7] E. Cinar and O. Turhan, "Command and data handling subsystem of Göktürk-2 flight model," in *Proceedings of 7th International Conference on Recent Advances in Space Technologies-RAST2015*, 2015, pp. 379–384, doi: 10.1109/RAST.2015.7208373.

[8] H. Ozkaya, E. Akkus, F. E. Karagoz, and B. G. Ozdemir, "Power subsystem

of Göktürk-2 flight model," in *2013 6th International Conference on Recent Advances in Space Technologies (RAST)*, Jun. 2013, pp. 699–704, doi: 10.1109/RAST.2013.6581300.

[9] G. Gurgenburan and E. Cinar, "Göktürk-2: Two years of operation," in *Proceedings of 7th International Conference on Recent Advances in Space Technologies-RAST2015*, Jun. 2015, pp. 405–409, doi: 10.1109/RAST.2015.7208378.

[10] R. Küpcü, M. Teke, and A. Çabuk, "RASAT ve Göktürk-2 görüntülerinin ortorektifikasyon başarımına referans ve sayısal yükseklik modeli seçiminin etkisi (Comparison of effect of reference and DEM selection to orthorectification performance for RASAT and Göktürk-2 images- Turkish)," in *5. UZAKTAN ALGILAMA-CBS SEMPOZYUMU (UZAL-CBS 2014), 14-17 Ekim 2014, İstanbul*, 2014, pp. 14–17, Accessed: Sep. 16, 2018. [Online]. Available: http://uzalcbs.org/wp-content/uploads/2016/11/2014_028.pdf.

[11] K. Kalkan, B. G. Filiz, O. Ozer, and M. Teke, "Vegetation discrimination analysis from Göktürk-2 imagery," in *2015 7th International Conference on Recent Advances in Space Technologies (RAST)*, Jun. 2015, pp. 329–332, doi: 10.1109/RAST.2015.7208364.

[12] H. Topan, A. Cam, M. Oruç, and M. Teke, "Göktürk-2 görüntülerinin geometrik ve radyometrik açıdan değerlendirilmesi," in *6. UZAKTAN ALGILAMA-CBS SEMPOZYUMU (UZAL-CBS 2016)*, 2016, pp. 804–809, Accessed: Sep. 17, 2018. [Online]. Available: http://geomatik.beun.edu.tr/topan/files/2012/06/UZAL_CBS_2016_Topan_Gokturk.pdf.

[13] U. Sakarya *et al.*, "Absolute radiometric calibration of the Göktürk-2 satellite sensor using Tuz Gölü (Landnet Site) from NDVI perspective," *ISPRS - Int. Arch. Photogramm. Remote Sens. Spat. Inf. Sci.*, vol. XLI-B1, pp. 373–377, 2016, doi: 10.5194/isprs-archives-XLI-B1-373-2016.

[14] M. Teke and Y. Yardimci, "Crop classification with Göktürk-2 time series

imagery," in *2016 24th Signal Processing and Communication Application Conference (SIU)*, May 2016, pp. 1553–1556, doi: 10.1109/SIU.2016.7496049.

[15] M. Ozendi, H. Topan, A. Cam, and Ç. Bayık, "PAN Sharpening quality investigation of Turkish in-operation remote sensing satellites: Applications wih RASAT and Göktürk-2 images," *ISPRS - Int. Arch. Photogramm. Remote Sens. Spat. Inf. Sci.*, vol. XLII-2/W1, pp. 131–135, Oct. 2016, doi: 10.5194/isprs-archives-XLII-2-W1-131-2016.

[16] M. Özendi, H. Topan, A. Cam, and Ç. Bayik, "RASAT ve Göktürk-2 görüntülerinden PAN-keskinleştirilmiş görüntü üretimi ve kalite değerlendirmesi," in *6. UZAKTAN ALGILAMA-CBS SEMPOZYUMU (UZAL-CBS 2016)*, 2016, pp. 447–453, Accessed: Sep. 16, 2018. [Online]. Available: http://geomatik.beun.edu.tr/topan/files/2012/06/UZAL_CBS_2016_Ozendi.pdf.

[17] A. O. Ok, "Automated matching of Göktürk-2 stereoscopic images," in *2016 24th Signal Processing and Communication Application Conference (SIU)*, May 2016, pp. 2229–2232, doi: 10.1109/SIU.2016.7496218.

[18] I. Gurcan, M. Teke, and U. M. Leloglu, "Land use/land cover classification for Göktürk-2 satellite," in *2016 24th Signal Processing and Communication Application Conference (SIU)*, May 2016, pp. 2097–2100, doi: 10.1109/SIU.2016.7496185.

[19] M. Efendioglu, M. Teke, H. Topan, S. E. Imre, and A. Cam, "Position accuracy assessment of Göktürk-2 satellite images by using Rational Function Model," in *2016 24th Signal Processing and Communication Application Conference (SIU)*, May 2016, pp. 2137–2140, doi: 10.1109/SIU.2016.7496195.

[20] E. Bugday and K. Menemencioglu, "Determining unofficial forest roads by using Göktürk-2 satellite images," in *1st International Symposium of Forest*

Engineering and Technologies (FETEC 2016), 2016, pp. 164–169.

[21] C. M. Bağdatlı, A. Özdarıcı Ok, A. Ö. OK, O. Erdoğan, S. Albut, and H. İ. Oğuz, "Görüntü sınıflandırması yoluyla Göktürk-2 görüntüsünden tarımsal desenin belirlenmesi: Nevşehir-Sarhıdır köyü Kızılırmak sahil bandı tarım arazileri pilot uygulaması," in *6. UZAKTAN ALGILAMA-CBS SEMPOZYUMU (UZAL-CBS 2016)*, 2016, pp. 194–201.

[22] S. Bulut, A. Günlü, and S. Keleş, "Estimation of some stand parameters using Göktürk-2 satellite image," in *1st International Symposium of Forest Engineering and Technologies (FETEC 2016)*, 2016, no. June, pp. 118–124.

[23] A. Ö. Ok, "Göktürk-2 stereoskopik görüntülerinden sayısal yüzey modeli üretimi," *Afyon Kocatepe Üniversitesi Fen ve Mühendislik Bilim. Derg.*, no. Special Issue, pp. 18–26, 2017, Accessed: Sep. 16, 2018. [Online]. Available: https://dosyalar.nevsehir.edu.tr/9b98167f682fd0d1a9f09106706266e8/n17_aook_tufuab2017.pdf.

[24] Ö. Mutluoğlu and M. Güven, "Accuracy investigation of DEM based on Göktürk-2 stereo images," *Selcuk Univ. J. Eng. ,Science Technol.*, vol. 5, pp. 220–227, 2017, doi: 10.15317/Scitech.2017.83.

[25] S. Kocaman, S. Ural, G. Karakas, and S. Bakici, "3D Processing of Gokturk-2 Imagery," 2017.

[26] S. Kahraman and A. Ertürk, "A comprehensive review of pansharpening algorithms for Göktürk-2 satellite images," *ISPRS Ann. Photogramm. Remote Sens. Spat. Inf. Sci.*, vol. IV-4/W4, pp. 263–270, 2017, doi: 10.5194/isprs-annals-IV-4-W4-263-2017.

[27] R. Göğerçin and A. Günlü, "Çankırı Karatekin Üniversitesi Orman Fakültesi Araştırma Ormanında Göktürk-2 uydu görüntüsü kullanılarak bazı meşcere parametrelerinin tahmin edilmesi," *Anatol. J. For. Res.*, vol. 3, no. 1, pp. 1–13, 2017.

[28] B. Bayram *et al.*, "The Efficiency of random forest method for shoreline

extraction from LANDSAT-8 and Göktürk-2 imageries," *ISPRS Ann. Photogramm. Remote Sens. Spat. Inf. Sci.*, vol. IV-4/W4, pp. 141–145, 2017, doi: 10.5194/isprs-annals-IV-4-W4-141-2017.

[29] E. Batur and D. Maktav, "Transformation of surface reflectance of Göktürk-2 images using image-based methods," in *2017 8th International Conference on Recent Advances in Space Technologies (RAST)*, Jun. 2017, pp. 155–159, doi: 10.1109/RAST.2017.8003012.

[30] O. B. Bakioğlu, H. Topan, M. Özendi, and A. Cam, "Pansharpening of RASAT and Göktürk-2 images via high pass filter," *Int. Arch. Photogramm. Remote Sens. Spat. Inf. Sci.*, vol. XLII-4/W6, pp. 27–29, 2017, doi: 10.5194/isprs-archives-XLII-4-W6-27-2017.

[31] H. Başak and M. Yıldırım Ağca, "Göktürk-2 uydu görüntüsünün otomatik detay çıkarımında kullanılabilirliğinin araştırılması 'Eskişehir ili örneği,'" 2017.

[32] G. Yesilyurt and A. Erturk, "Path opening based road extraction for Göktürk-2 images," in *2018 26th Signal Processing and Communications Applications Conference (SIU)*, May 2018, pp. 1–4, doi: 10.1109/SIU.2018.8404823.

[33] D. U. Ufuk, I. S. Acikgoz, M. Teke, and A. M. Ozbayoglu, "Satellite image band registration with Dynamic Time Warping and Discrete Wavelet Transform," in *2018 26th Signal Processing and Communications Applications Conference (SIU)*, May 2018, pp. 1–4, doi: 10.1109/SIU.2018.8404249.

[34] M. Kaynarca, N. Demir, M. Kaynarca, and N. Demir, "Detection of urban buildings by using multispectral Gokturk-2 and Sentinel 1A synthetic aperture radar images," *Proceedings*, vol. 2, no. 7, p. 360, Mar. 2018, doi: 10.3390/ecrs-2-05173.

[35] A. Cam and H. Topan, "RASAT ve Göktürk-2 görüntülerinin gerçek yer örnekleme aralığının belirlenmesi," *Karaelmas Fen ve Mühendislik Derg.*, vol. 8, no. 1, pp. 292–298, Jun. 2018, doi: 10.7212/ZKUFBD.V8I1.1057.

[36] M. Teke, C. Demirkesen, O. Haliloğlu, and E. İmre, “Göktürk-2 uydusunun bağıl ve mutlak çapraz radyometrik kalibrasyonu (Relative and absolute cross radiometric calibration of Göktürk-2 satellite),” *Harit. Derg.*, vol. Ocak, no. 155, pp. 32–52, 2016, Accessed: Sep. 17, 2018. [Online]. Available: https://www.harita.gov.tr/images/dergi/makaleler/89ae0fe22c47d37.pdf.

[37] V. O. Atak, M. Erdoğan, and A. Yilmaz, “Göktürk-2 uydu görüntü testleri (Gokturk-2 satellite imagery tests) (Turkish),” *Harit. Derg.*, vol. Ocak, no. 153, 2015, Accessed: Sep. 16, 2018. [Online]. Available: https://www.harita.gov.tr/images/dergi/makaleler/283062995206f8c.pdf.

[38] F. Gulmammadov, C. Yavuzyilmaz, O. Kahraman, M. Akbas, and Y. Acar, “Commissioning of attitude and orbit determination and control system of RASAT satellite,” 2013.

[39] C. Yavuzyilmaz *et al.*, “Rasat ADCS flight software testing with dynamic attitude simulator environment,” 2011, doi: 10.1109/RAST.2011.5966987.

[40] C. S. Tufekci, N. Ertongur, C. Yavuzyilmaz, F. Gulmammadov, O. Kahraman, and Y. Subasi, “Attitude performance requirements and budgeting for RASAT satellite,” 2011, doi: 10.1109/RAST.2011.5966986.

[41] E. Imre *et al.*, “Orbital dynamics system of TUBITAK UZAY for earth orbiting spacecraft,” in *Proceedings of 9th International Conference on Recent Advances in Space Technologies, RAST 2019*, Jun. 2019, pp. 313–320, doi: 10.1109/RAST.2019.8767450.

[42] R. E. Kalman, “A New approach to linear filtering and prediction problems,” *Trans. ASME, Ser. D, J. Basic Eng. 82*, vol. 82, no. 1, pp. 35–45, 1960, doi: 10.1115/1.3662552.

[43] E. J. Lefferts, F. L. Markley, and M. D. Shuster, “Kalman filtering for spacecraft attitude estimation,” *J. Guid. Control. Dyn.*, vol. 5, no. 5, pp. 417–429, Sep. 1982, doi: 10.2514/3.56190.

[44] S. J. Julier, J. K. Uhlmann, and H. F. Durrant-Whyte, “A new approach for

filtering nonlinear systems," in *Proceedings of 1995 American Control Conference - ACC'95*, 1995, vol. 3, pp. 1628–1632, doi: 10.1109/ACC.1995.529783.

[45] S. J. Julier and J. K. Uhlmann, "Unscented Filtering and Nonlinear Estimation," *Proc. IEEE*, vol. 92, no. 3, pp. 401–422, Mar. 2004, doi: 10.1109/JPROC.2003.823141.

[46] J. L. Crassidis and F. L. Markley, "Unscented Filtering for Spacecraft Attitude Estimation," *J. Guid. Control. Dyn.*, vol. 26, no. 4, pp. 536–542, 2003, doi: 10.2514/2.5102.

[47] J. L. Crassidis, F. L. Markley, and Y. Cheng, "Survey of Nonlinear Attitude Estimation Methods," *J. Guid. Control. Dyn.*, vol. 30, no. 1, pp. 12–28, 2007, doi: 10.2514/1.22452.

[48] Q. M. Lam and J. L. Crassidis, "Precision Attitude Determination Using a Multiple Model Adaptive Estimation Scheme," in *2007 IEEE Aerospace Conference*, 2007, pp. 1–20, doi: 10.1109/AERO.2007.352657.

[49] S. Winkler, G. Wiedermann, and W. Gockel, "High-Accuracy on-board attitude estimation for the GMES Sentinel-2 satellite: Concept, design, and first results," in *AIAA Guidance, Navigation and Control Conference and Exhibit*, American Institute of Aeronautics and Astronautics, 2008.

[50] M. Yang *et al.*, "Space Flight Validation of Design and Engineering of the ZDPS-1A Pico-satellite," *Chinese J. Aeronaut.*, vol. 25, no. 5, pp. 725–738, Oct. 2012, doi: 10.1016/S1000-9361(11)60439-1.

[51] Y. Nakajima, N. Murakami, T. Ohtani, Y. Nakamura, K. Hirako, and K. Inoue, "SDS-4 Attitude Control System: In-Flight Results of Three Axis Attitude Control for Small Satellites," *IFAC Proc. Vol.*, vol. 46, no. 19, pp. 283–288, Jan. 2013, doi: 10.3182/20130902-5-DE-2040.00077.

[52] J. C. Springmann and J. W. Cutler, "Flight results of a low-cost attitude determination system," *Acta Astronaut.*, vol. 99, no. 1, pp. 201–214, Jun.

2014, doi: 10.1016/J.ACTAASTRO.2014.02.026.

[53] A. Slavinskis *et al.*, “Flight Results of ESTCube-1 Attitude Determination System,” *J. Aerosp. Eng.*, vol. 29, no. 1, Jan. 2016, doi: 10.1061/(ASCE)AS.1943-5525.0000504.

[54] S. Nakasuka, K. Miyata, Y. Tsuruda, Y. Aoyanagi, and T. Matsumoto, “Discussions on attitude determination and control system for micro/nano/pico-satellites considering survivability based on Hodoyoshi-3 and 4 experiences,” *Acta Astronaut.*, vol. 145, pp. 515–527, Apr. 2018, doi: 10.1016/J.ACTAASTRO.2018.02.006.

[55] O. J. Kim *et al.*, “In-Orbit Results and Attitude Analysis of the SNUGLITE Cube-Satellite,” *Appl. Sci. 2020, Vol. 10, Page 2507*, vol. 10, no. 7, p. 2507, Apr. 2020, doi: 10.3390/APP10072507.

[56] M. R. Mughal *et al.*, “Aalto-1, multi-payload CubeSat: In-orbit results and lessons learned,” *Acta Astronaut.*, vol. 187, pp. 557–568, Oct. 2021, doi: 10.1016/J.ACTAASTRO.2020.11.044.

[57] H. Heidt, J. Puig-Suari, A. S. Moore, S. Nakasuka, and R. J. Twiggs, “CubeSat: A new Generation of Picosatellite for Education and Industry Low-Cost Space Experimentation,” in *14th Annual USU Conference on Small Satellites*, 2000, pp. 1–19.

[58] Y. Yang and Z. Zhou, “Spacecraft dynamics should be considered in Kalman filter attitude estimation,” *Adv. Astronaut. Sci.*, vol. 158, pp. 83–94, 2016.

[59] M. Marin and H. Bang, “Design and simulation of a high-speed star tracker for direct optical feedback control in ADCS,” *Sensors (Switzerland)*, vol. 20, no. 8, 2020, doi: 10.3390/s20082388.

[60] J. Ouaknine, L. Blarre, L. Oddos-Marcel, J. Montel, and J.-M. Julio, “Reduction of low frequency error for SED36 and APS based HYDRA star trackers,” in *International Conference on Space Optics — ICSO 2006*, Nov. 2017, vol. 10567, no. June 2006, p. 52, doi: 10.1117/12.2308086.

[61] A. Gopalakrishnan, N. S. Kaisare, and S. Narasimhan, “Incorporating delayed and infrequent measurements in Extended Kalman Filter based nonlinear state estimation,” *J. Process Control*, vol. 21, no. 1, pp. 119–129, Jan. 2011, doi: 10.1016/J.JPROCONT.2010.10.013.

[62] L. Khosravian, O. Trumpf, and O. Mahony, “State estimation for nonlinear systems with delayed output measurements,” *Proc. IEEE Conf. Decis. Control*, vol. 54rd IEEE, no. Cdc, pp. 6330–6335, 2015, doi: 10.1109/CDC.2015.7403216.

[63] A. Khosravian, J. Trumpf, R. Mahony, and T. Hamel, “Recursive attitude estimation in the presence of multi-rate and multi-delay vector measurements,” *Proc. Am. Control Conf.*, vol. 2015-July, pp. 3199–3205, Jul. 2015, doi: 10.1109/ACC.2015.7171825.

[64] J. A. Isaza, H. A. Botero, and H. Alvarez, “State Estimation Using Non-uniform and Delayed Information: A Review,” *Int. J. Autom. Comput.*, vol. 15, no. 2, pp. 125–141, Apr. 2018, doi: 10.1007/s11633-017-1106-7.

[65] R. Dubois, S. Bertrand, and A. Eudes, “Performance evaluation of a moving horizon estimator for multi-rate sensor fusion with time-delayed measurements,” *2018 22nd Int. Conf. Syst. Theory, Control Comput. ICSTCC 2018 - Proc.*, pp. 664–669, Nov. 2018, doi: 10.1109/ICSTCC.2018.8540711.

[66] E. H. Guechi, K. Belharet, and S. Blažič, “Tracking Control for Wheeled Mobile Robot Based on Delayed Sensor Measurements,” *Sensors 2019, Vol. 19, Page 5177*, vol. 19, no. 23, p. 5177, Nov. 2019, doi: 10.3390/S19235177.

[67] E. A. Hogan and B. A. Woo, “Treatment of measurement variance for star tracker-based attitude estimation,” *Adv. Astronaut. Sci. Astrodyn.*, vol. 162, 2017.

[68] S. Gaisser, U. Mohr, J. Keim, D. Triloff, and S. Klinkner, “Improvements in attitude determination and control of the small satellite flying laptop,” in *Proceedings of the 33rd Annual AIAA / USU Conference on Small Satellites, Technical Session 3: Year in Review 1, SSC19-III-06*, 2019, pp. 1–8, [Online].

Available: https://digitalcommons.usu.edu/smallsat/2019/all2019/275/.

[69] A. Comellini, D. Casu, E. Zenou, V. Dubanchet, and C. Espinosa, "Incorporating delayed and multirate measurements in navigation filter for autonomous space rendezvous," *J. Guid. Control. Dyn.*, vol. 43, no. 6, pp. 1164–1172, 2020, doi: 10.2514/1.G005034.

[70] T. D. Larsen, N. A. Andersen, O. Ravn, and N. K. Poulsen, "Incorporation of time delayed measurements in a discrete-time Kalman filter," in *Proceedings of the IEEE Conference on Decision and Control*, 1998, vol. 4, pp. 3972–3977, doi: 10.1109/cdc.1998.761918.

[71] R. Rummel and T. Peters, "Reference Systems in Satellite Geodesy," 2001.

[72] D. A. Vallado and W. D. McClain, *Fundamentals of astrodynamics and applications*, 4th Editio. Kluwer Academic Publishers, 2013.

[73] G. Seeber, *Satellite Geodesy*, 2nd Editio. 2003.

[74] M. İpek, "Satellite Orbit Estimation Using Kalman Filters, Master Thesis," Middle East Technical University, 2017.

[75] P. Gerard and B. Luzum, "IERS Conventions (2010), IERS Technical Note No. 36," Frankfurt am Main, 2010.

[76] G. H. Kaplan, "The IAU Resolutions on Astronomical Reference Systems, Time Scales, and Earth Rotation Models," Feb. 2006, doi: 10.48550/arxiv.astro-ph/0602086.

[77] H. E. Soken and C. Hajiyev, *Fault Tolerant Attitude Estimation for Small Satellites*. 2020.

[78] F. L. Markley and J. L. Crassidis, *Fundamentals of spacecraft attitude determination and control*. Springer New York, 2014.

[79] M. D. Shuster, "Survey of attitude representations," *J. Astronaut. Sci.*, vol. 41, no. 4, pp. 439–517, 1993.

[80] J. Wertz, *Spacecraft Attitude Determination and Control*, vol. 73. Dordrecht:

Springer Netherlands, 1978.

[81] T. Bak, “Spacecraft Attitude Determination: A Magnetometer Approach,” Aalborg University, Denmark, Ph.D. Thesis, 1999.

[82] Ö. Kahraman, “Control allocation against actuator failures in overactuated small satellites,” Middle East Technical University, 2007.

[83] W. R. Hamilton, *Elements of Quaternions*. Cambridge University Press, 2010.

[84] N. Trawny and S. I. Roumeliotis, “Indirect Kalman filter for 3D attitude estimation, Multiple Autonomous Robotic Systems Laboratory Technical Report Number 2005-002 , Rev . 51,” 2005.

[85] A. Colmon, L. Oddos-Marcel, and B. Gelin, “Star trackers roadmap, and how lessons learnt help to design future Sodern star trackers,” *11th ESA Workshop on Avionics, Data, Control and Software Systems*, 2017. https://indico.esa.int/event/182/contributions/1504/.

[86] M. J. M. Meerman, M. N. Unwin, S. Gleason, S. Jason, M. N. Sweeting, and A. da Silva Curiel, “A nanosatellite to demonstrate GPS oceanography reflectometry,” *Sp. Technol.*, vol. 23, no. 4, pp. 235–247, 2003.

[87] A. Carrel and P. Alderton, “MEMS in Space – A New Technology Advancing from Flight Experiment to Proven COTS Product,” in *Proceedings of the 23rd Annual AIAA / USU Conference on Small Satellites, Advanced Technologies, SCC09-XI-11*, Aug. 2009, pp. 1–7, Accessed: Dec. 23, 2022. [Online]. Available: https://digitalcommons.usu.edu/smallsat/2009/all2009/75.

[88] J. L. Crassidis, F. L. Markley, and Y. Cheng, “Survey of nonlinear attitude estimation methods,” *J. Guid. Control. Dyn.*, vol. 30, no. 1, pp. 12–28, 2007, doi: 10.2514/1.22452.

[89] K. Reif, S. Günther, E. Yaz, and R. Unbehauen, “Stochastic stability of the discrete-time extended Kalman filter,” *IEEE Trans. Automat. Contr.*, 1999, doi: 10.1109/9.754809.

[90] C. Yıldırım and H. E. Soken, “Bayes Ağı ile Küçük Uyduların Yönelim

Kestirim ve Kontrol Algoritmalarının Hata Tespitinin Yapılması, Ayıklanması ve Düzeltilmesi," in *8. Ulusal Havacılık ve Uzay Konferansı, İZMİR, UHUK-2022-044*, 2022, pp. 1–11.

[91] A. M. Fosbury, "Steady-state accuracy solutions of more spacecraft attitude estimators," in *AIAA Guidance, Navigation, and Control Conference 2011, AIAA 2011-6433*, 2011, pp. 1–19, doi: 10.2514/6.2011-6433.

[92] J. R. Wertz, "Attitude prediction," in *Spacecraft Attitude Determination and Control*, J. R. Wertz, Ed. Dordrecht: Springer Netherlands, 1978, pp. 558–587.

[93] M. Pigg *et al.*, "Development of Generic AOCS Unit Simulation Models," in *SESP 2012: Simulation and EGSE facilities for Space Programmes*, 2012, no. September 2012, pp. 1–8.

[94] P. S. Maybeck, *Stochastic models, estimation, and control*, vol. 1. 1979.

[95] M. Tolstoj, "Analysis of Disturbance Torques On Satellites in Low-Earth Orbit Based Upon GRACE," RWTH Aachen, 2017.

[96] M. Ghezal, B. Polle, C. Rabejac, and J. Montel, "Gyro Stellar Attitude Determination," in *Guidance, Navigation and Control Systems*, 2006, vol. 606, p. 22.1.

[97] M. K. Özgören, "Advance Dynamics Lecture Notes, METU Mechanical Engineering Department." 2007.

[98] M. K. Özgören, *Robot Manipülatörlerin Dinamiği ve Kontrolü*. Makina Teorisi Derneği Yayınları Ders Notları Serisi No:2, 2016.

APPENDICES

A. Explicit form of the left handed representation of the direction cosine matrix

$$
\begin{aligned}
&A(\boldsymbol{q}) = (q_4^2 - \boldsymbol{q}^2) I_{3x3} + 2\boldsymbol{q}\boldsymbol{q}^T - 2q_4 Q \\
&= \begin{bmatrix} q_4^2 - q_1^2 - q_2^2 - q_3^2 & 0 & 0 \\ 0 & q_4^2 - q_1^2 - q_2^2 - q_3^2 & 0 \\ 0 & 0 & q_4^2 - q_1^2 - q_2^2 - q_3^2 \end{bmatrix} \\
&+ 2 \begin{bmatrix} q_1 \\ q_2 \\ q_3 \end{bmatrix} \begin{bmatrix} q_1 & q_2 & q_3 \end{bmatrix} \\
&-2q_4 \begin{bmatrix} 0 & -q_3 & q_2 \\ q_3 & 0 & -q_1 \\ -q_2 & q_1 & 0 \end{bmatrix} \\
&= \begin{bmatrix} q_4^2 - q_1^2 - q_2^2 - q_3^2 & 0 & 0 \\ 0 & q_4^2 - q_1^2 - q_2^2 - q_3^2 & 0 \\ 0 & 0 & q_4^2 - q_1^2 - q_2^2 - q_3^2 \end{bmatrix} \\
&+ \begin{bmatrix} 2q_1^2 & 2q_1q_2 & 2q_1q_3 \\ 2q_2q_1 & 2q_2^2 & 2q_2q_3 \\ 2q_3q_1 & 2q_3q_2 & 2q_3^2 \end{bmatrix} + \begin{bmatrix} 0 & 2q_4q_3 & -2q_4q_2 \\ -2q_4q_3 & 0 & 2q_4q_1 \\ 2q_4q_2 & -2q_4q_1 & 0 \end{bmatrix} \\
&= \begin{bmatrix} q_1^2 - q_2^2 - q_3^2 + q_4^2 & 2q_1q_2 + 2q_4q_3 & 2q_1q_3 - 2q_4q_2 \\ 2q_2q_1 - 2q_4q_3 & -q_1^2 + q_2^2 - q_3^2 + q_4^2 & 2q_2q_3 + 2q_4q_1 \\ 2q_3q_1 + 2q_4q_2 & 2q_3q_2 - 2q_4q_1 & -q_1^2 - q_2^2 + q_3^2 + q_4^2 \end{bmatrix}
\end{aligned}
\tag{8.1}
$$

B. Explicit form of the right handed representation of the direction cosine matrix

$$
\begin{aligned}
&A(\boldsymbol{q}) = (q_4^2 - \boldsymbol{q}^2) I_{3x3} + 2\boldsymbol{q}\boldsymbol{q}^T + 2q_4 Q \\
&= \begin{bmatrix} q_4^2 - q_1^2 - q_2^2 - q_3^2 & 0 & 0 \\ 0 & q_4^2 - q_1^2 - q_2^2 - q_3^2 & 0 \\ 0 & 0 & q_4^2 - q_1^2 - q_2^2 - q_3^2 \end{bmatrix} \\
&+ 2\begin{bmatrix} q_1 \\ q_2 \\ q_3 \end{bmatrix} \begin{bmatrix} q_1 & q_2 & q_3 \end{bmatrix} \\
&+ 2q_4 \begin{bmatrix} 0 & -q_3 & q_2 \\ q_3 & 0 & -q_1 \\ -q_2 & q_1 & 0 \end{bmatrix} \\
&= \begin{bmatrix} q_4^2 - q_1^2 - q_2^2 - q_3^2 & 0 & 0 \\ 0 & q_4^2 - q_1^2 - q_2^2 - q_3^2 & 0 \\ 0 & 0 & q_4^2 - q_1^2 - q_2^2 - q_3^2 \end{bmatrix} \\
&+ \begin{bmatrix} 2q_1^2 & 2q_1q_2 & 2q_1q_3 \\ 2q_2q_1 & 2q_2^2 & 2q_2q_3 \\ 2q_3q_1 & 2q_3q_2 & 2q_3^2 \end{bmatrix} + \begin{bmatrix} 0 & -2q_4q_3 & 2q_4q_2 \\ 2q_4q_3 & 0 & -2q_4q_1 \\ -2q_4q_2 & 2q_4q_1 & 0 \end{bmatrix} \\
&= \begin{bmatrix} q_1^2 - q_2^2 - q_3^2 + q_4^2 & 2q_1q_2 - 2q_4q_3 & 2q_1q_3 + 2q_4q_2 \\ 2q_2q_1 + 2q_4q_3 & -q_1^2 + q_2^2 - q_3^2 + q_4^2 & 2q_2q_3 - 2q_4q_1 \\ 2q_3q_1 - 2q_4q_2 & 2q_3q_2 + 2q_4q_1 & -q_1^2 - q_2^2 + q_3^2 + q_4^2 \end{bmatrix}
\end{aligned}
\tag{8.2}
$$

C. Possible cases for the left handed notation of quaternion to direction cosine matrix transformation

Case 1:

$$
\begin{aligned}
q_1 &= \pm\frac{1}{2}\left(1+A_{11}-A_{22}-A_{33}\right)^{1/2} = \pm\frac{1}{2}\left(1+2A_{11}-trace(A)\right)^{1/2} \\
q_2 &= \frac{1}{4q_1}\left(A_{12}+A_{21}\right) = \left(2q_1q_2+2q_3q_4+2q_1q_2-2q_3q_4\right)/4q_1 = q_2 \\
q_3 &= \frac{1}{4q_1}\left(A_{13}+A_{31}\right) = \left(2q_1q_3+2q_2q_4+2q_1q_3-2q_2q_4\right)/4q_1 = q_3 \\
q_4 &= \frac{1}{4q_1}\left(A_{23}-A_{32}\right) = \left(2q_2q_3+2q_4q_1-2q_3q_2+2q_4q_1\right)/4q_1 = q_4
\end{aligned}
\tag{8.3}
$$

Case 2:

$$
\begin{aligned}
q_2 &= \pm\frac{1}{2}\left(1-A_{11}+A_{22}-A_{33}\right)^{1/2} = \pm\frac{1}{2}\left(1+2A_{22}-trace(A)\right)^{1/2} \\
q_1 &= \frac{1}{4q_2}\left(A_{12}+A_{21}\right) = \left(2q_1q_2+2q_3q_4+2q_1q_2-2q_3q_4\right)/4q_2 = q_1 \\
q_3 &= \frac{1}{4q_2}\left(A_{23}+A_{32}\right) = \left(2q_2q_3+2q_4q_1+2q_3q_2-2q_4q_1\right)/4q_2 = q_3 \\
q_4 &= \frac{1}{4q_2}\left(A_{31}-A_{13}\right) = \left(2q_3q_1+2q_4q_2-2q_1q_3+2q_4q_2\right)/4q_2 = q_4
\end{aligned}
\tag{8.4}
$$

Case 3:

$$
\begin{aligned}
q_3 &= \pm\frac{1}{2}\left(1-A_{11}-A_{22}+A_{33}\right)^{1/2} = \pm\frac{1}{2}\left(1+2A_{33}-trace(A)\right)^{1/2} \\
q_1 &= \frac{1}{4q_3}\left(A_{13}+A_{31}\right) = \left(2q_1q_3-2q_4q_2+2q_3q_1+2q_4q_2\right)/4q_3 = q_1 \\
q_2 &= \frac{1}{4q_3}\left(A_{23}+A_{32}\right) = \left(2q_2q_3+2q_4q_1+2q_3q_2-2q_4q_1\right)/4q_3 = q_2 \\
q_4 &= \frac{1}{4q_3}\left(A_{12}-A_{21}\right) = \left(2q_1q_2+2q_4q_3-2q_2q_1+2q_4q_3\right)/4q_3 = q_4
\end{aligned}
\tag{8.5}
$$

Case 4:

$$
\begin{aligned}
q_4 &= \pm\frac{1}{2}\left(1 + A_{11} + A_{22} + A_{33}\right)^{1/2} = \pm\frac{1}{2}\left(1 + trace(A)\right)^{1/2} \\
q_1 &= \frac{1}{4q_4}\left(A_{23} - A_{32}\right) = \left(2q_2q_3 + 2q_4q_1 - 2q_3q_2 + 2q_4q_1\right)/\,4q_4 = q_1 \\
q_2 &= \frac{1}{4q_4}\left(A_{31} - A_{13}\right) = \left(2q_3q_1 + 2q_4q_2 - 2q_1q_3 + 2q_4q_2\right)/\,4q_4 = q_2 \\
q_3 &= \frac{1}{4q_4}\left(A_{12} - A_{21}\right) = \left(2q_1q_2 + 2q_4q_3 - 2q_2q_1 + 2q_4q_3\right)/\,4q_4 = q_3
\end{aligned}
\tag{8.6}
$$

D. Possible Cases for the Right Handed Notation of Quaternion to Direction Cosine matrix transformation

Case 1:

$$
\begin{aligned}
q_1 &= \pm\frac{1}{2}\left(1+A_{11}-A_{22}-A_{33}\right)^{1/2} = \pm\frac{1}{2}\left(1+2A_{11}-trace(A)\right)^{1/2} \\
q_2 &= \frac{1}{4q_1}\left(A_{12}+A_{21}\right) = \left(2q_1q_2-2q_3q_4+2q_1q_2+2q_3q_4\right)/4q_1 = q_2 \\
q_3 &= \frac{1}{4q_1}\left(A_{13}+A_{31}\right) = \left(2q_1q_3+2q_2q_4+2q_1q_3-2q_2q_4\right)/4q_1 = q_3 \\
q_4 &= \frac{1}{4q_1}\left(A_{32}-A_{23}\right) = \left(2q_2q_3+2q_1q_4-2q_2q_3+2q_1q_4\right)/4q_1 = q_4
\end{aligned}
\tag{8.7}
$$

Case 2:

$$
\begin{aligned}
q_2 &= \pm\frac{1}{2}\left(1-A_{11}+A_{22}-A_{33}\right)^{1/2} = \pm\frac{1}{2}\left(1+2A_{22}-trace(A)\right)^{1/2} \\
q_1 &= \frac{1}{4q_2}\left(A_{12}+A_{21}\right) = \left(2q_1q_2-2q_3q_4+2q_1q_2+2q_3q_4\right)/4q_2 = q_1 \\
q_3 &= \frac{1}{4q_2}\left(A_{23}+A_{32}\right) = \left(2q_2q_3-2q_1q_4+2q_2q_3+2q_1q_4\right)/4q_2 = q_3 \\
q_4 &= \frac{1}{4q_2}\left(A_{13}-A_{31}\right) = \left(2q_1q_3+2q_2q_4-2q_1q_3+2q_2q_4\right)/4q_2 = q_4
\end{aligned}
\tag{8.8}
$$

Case 3:

$$
\begin{aligned}
q_3 &= \pm\frac{1}{2}\left(1-A_{11}-A_{22}+A_{33}\right)^{1/2} = \pm\frac{1}{2}\left(1+2A_{33}-trace(A)\right)^{1/2} \\
q_1 &= \frac{1}{4q_3}\left(A_{13}+A_{31}\right) = \left(2q_1q_3+2q_2q_4+2q_1q_3-2q_2q_4\right)/4q_3 = q_1 \\
q_2 &= \frac{1}{4q_3}\left(A_{23}+A_{32}\right) = \left(2q_2q_3-2q_1q_4+2q_2q_3+2q_1q_4\right)/4q_3 = q_2 \\
q_4 &= \frac{1}{4q_3}\left(A_{21}-A_{12}\right) = \left(2q_1q_2+2q_3q_4-2q_1q_2+2q_3q_4\right)/4q_3 = q_4
\end{aligned}
\tag{8.9}
$$

Case 4:

$$
\begin{aligned}
q_4 &= \pm\frac{1}{2}\left(1 + A_{11} + A_{22} + A_{33}\right)^{1/2} = \pm\frac{1}{2}\left(1 + trace(A)\right)^{1/2} \\
q_1 &= \frac{1}{4q_4}\left(A_{32} - A_{23}\right) = \left(2q_2q_3 + 2q_1q_4 - 2q_2q_3 + 2q_1q_4\right)/\,4q_4 = q_1 \\
q_2 &= \frac{1}{4q_4}\left(A_{13} - A_{31}\right) = \left(2q_1q_3 + 2q_2q_4 - 2q_1q_3 + 2q_2q_4\right)/\,4q_4 = q_2 \\
q_3 &= \frac{1}{4q_4}\left(A_{21} - A_{12}\right) = \left(2q_1q_2 + 2q_3q_4 - 2q_1q_2 + 2q_3q_4\right)/\,4q_4 = q_3
\end{aligned}
\tag{8.10}
$$

E. Spacecraft Dynamics: Derivation of Satellite's Dynamic Equation via Dyadic Tensor

The derivation of a generic satellite's dynamic equation could be performed by the basic principles of the dynamics as follows [97]. In this derivation dyadic and tensor notation is used and the detailed information about this notation can be found in [98]. The notation used in this section is different that the notation used in the whole thesis. The fundamental equation for the attitude dynamics relates the time derivative of the angular momentum to the external torques. For a constant moment of inertia, this relation is given as Euler's equations of motion;

$$\sum \vec{M}_2 = \frac{dA}{dt} \vec{H}_2 \tag{8.11}$$

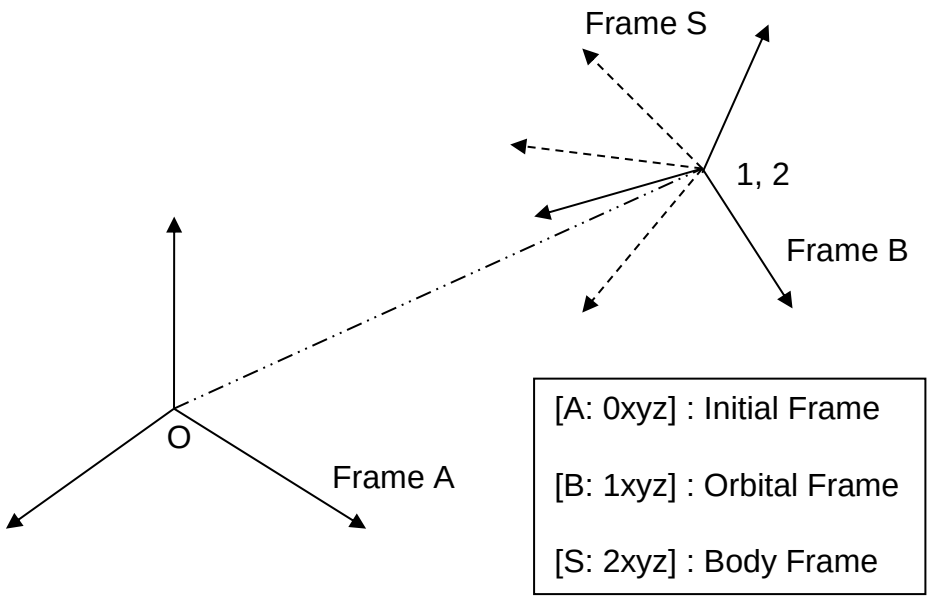

Figure 7-1 Reference Frames for the derivation of spacecraft dynamic equation

For the frames represented by Figure 7-1, the variables in Equation (8.28) are;

$\sum \vec{M}_2$: Net moment vector acting about frame 2

$\frac{dA}{dt}$: Derivation with respect to time in frame A

$\vec{H}_2$: Net angular momentum vector acting about frame 2

Using the following notation, Equation (8.28) can be expanded as the following arrangements;

$\vec{H}_{s/2}$: Angular momentum vector without wheels acting about frame 2

$\vec{H}_{\omega/2}$: Angular momentum vector of wheels only acting about frame 2

$\vec{\vec{I}}_{s/2}$: Inertia dyadic of satellite with respect to frame 2 (without wheels)

$\vec{\vec{I}}_{\omega/2}$: Inertia dyadic of wheels with respect to frame 2 (without wheels)

$\vec{\omega}_s$: Angular velocity vector of satellite

$\vec{\omega}_\omega$: Angular velocity vector of wheels

$\vec{\omega}_{\omega/s}$: Angular velocity vector of wheels with respect to satellite

$\vec{\vec{I}}_{s\omega/2}$: Satellite plus wheels inertia dyadic

$$\vec{H}_2 = \vec{H}_{s/2} + \vec{H}_{\omega/2} \tag{8.12}$$

$$\vec{H}_{s/2} = \vec{\vec{I}}_{s/2} \cdot \vec{\omega}_s \tag{8.13}$$

$$\vec{H}_{\omega/2} = \vec{\vec{I}}_{\omega/2} \cdot \vec{\omega}_\omega \tag{8.14}$$

$$\vec{H}_2 = \vec{\vec{I}}_{s/2} \cdot \vec{\omega}_s + \vec{\vec{I}}_{\omega/2} \cdot \vec{\omega}_\omega \tag{8.15}$$

$$\vec{\omega}_\omega = \vec{\omega}_{\omega/s} + \vec{\omega}_s \tag{8.16}$$

$$\frac{ds}{dt}\vec{H}_2 = \frac{ds}{dt}\vec{H}_2 + \vec{\omega}_s \times \vec{H}_2 \tag{8.17}$$

$$\frac{dA}{dt}\vec{H}_2 = \frac{ds}{dt}\left[\ddot{I}_{s/2}\cdot\vec{\omega}_s + \ddot{I}_{\omega/2}\cdot\vec{\omega}_{\omega/s} + \ddot{I}_{\omega/2}\cdot\vec{\omega}_s\right] + \vec{\omega}_s \times \left[\ddot{I}_{s/2}\cdot\vec{\omega}_s + \ddot{I}_{\omega/2}\cdot\vec{\omega}_{\omega/s} + \ddot{I}_{\omega/2}\cdot\vec{\omega}_s\right] \tag{8.18}$$

$$\frac{dA}{dt}\vec{H}_2 = \frac{ds}{dt}\left[\ddot{I}_{s/2}\cdot\vec{\omega}_s\right] + \frac{ds}{dt}\left[\ddot{I}_{\omega/2}\left(\vec{\omega}_{\omega/s} + \vec{\omega}_s\right)\right] + \vec{\omega}_s \times \left[\ddot{I}_{s\omega/2}\cdot\vec{\omega}_s + \ddot{I}_{\omega/2}\cdot\vec{\omega}_{\omega/s}\right] \tag{8.19}$$

If we consider the left side of the Equation (8.19):

$$\sum \vec{M}_2 = \vec{M}_2\left(\text{Thruster}\right) + \vec{M}_2\left(\text{Gravity Gradient}\right) + \vec{M}_2\left(\text{Disturbance}\right) \tag{8.20}$$

Let's assume a fourth frame which is fixed in satellite body frame as the wheel frame:

$$\left[w:\ 3xyz\right]:\ \textit{wheel frame} \tag{8.21}$$

Express wheel angular velocity vector with respect to satellite in wheel frame;

$$\left[\vec{\omega}_{\omega/s}\right]_w = \bar{\omega}_{\omega/s}^{(w)} \tag{8.22}$$

Since we know the conversion matrix which maps wheel frame to satellite frame we can write;

$$\left[\vec{\omega}_{\omega/s}\right]_s = \hat{C}^{(s,\omega)}\cdot\bar{\omega}_{\omega/s}^{(w)} \tag{8.23}$$

Express wheel inertia dyadic with respect to Frame 2 in Wheel Frame;

$$\left[\ddot{I}_{w/2}\right]^{(s)} = \bar{I}_{w/2}^{(w)} \tag{8.24}$$

And then we can expand the Equation (8.24) as follows:

$$\left[\ddot{I}_{w/2}\right]^{(s)} = \left[\hat{C}^{(s,\omega)}\right]\bar{I}_{w/2}^{(w)}\left[\hat{C}^{(s,\omega)}\right]^T \tag{8.25}$$

By rearranging Equation (8.19):

$$\frac{dA}{dt}\vec{H}_2 = \frac{ds}{dt}\left[\ddot{I}_{s/2}\cdot\vec{\omega}_s\right] + \frac{ds}{dt}\left[\vec{h}_{w-\text{Relative}} + \ddot{I}_{\omega/2}\cdot\vec{\omega}_s\right] + \vec{\omega}_s \times \left[\ddot{I}_{s\omega/2}\cdot\vec{\omega} + \vec{h}_{w-\text{Relative}}\right] \tag{8.26}$$

Where,

$\vec{h}_{w-\text{Relative}} = \ddot{I}_{w/2}\cdot\vec{\omega}_{\omega/s}$ (Relative angular momentum vector of wheel assembly)

$$\frac{dA}{dt}\vec{H}_2 = \frac{ds}{dt}\left[\left(\ddot{I}_{s/2} + \ddot{I}_{\omega/2}\right)\cdot\vec{\omega}_s\right] + \vec{\omega}_s \times \left[\ddot{I}_{s\omega/2}\cdot\vec{\omega}_s + \vec{h}_{w-Relative}\right] + \frac{ds}{dt}\left[\vec{h}_{w-Relative}\right] \quad (8.27)$$

In S frame;

$$\left[\frac{dA}{dt}\vec{H}_2\right]_s = \frac{d}{dt}\left[\bar{I}_{s\omega/2}^{(s)}\cdot\bar{\omega}_s^{(s)}\right] + \tilde{\omega}_s^{(s)}\left[\bar{I}_{s\omega/2}\cdot\vec{\omega}_s\right] + \tilde{\omega}_s^{(s)}\left[\vec{h}_{w-Relative}^{(s)}\right] + \frac{d}{dt}\vec{h}_{w-Relative}^{(s)} \quad (8.28)$$

Considering left hand side of Equation (8.28) and recalling Equations (8.28) and (8.28) thus we can rewrite;

$$\bar{M}_2^{(s)} = \bar{I}_{s\omega/2}^{(s)}\cdot\frac{d}{dt}\bar{\omega}_s^{(s)} + \tilde{\omega}_s^{(s)}\left\{\bar{I}_{s\omega/2}\cdot\bar{\omega}_s^{(s)}\right\} + \tilde{\omega}_s^{(s)}\cdot\vec{h}_{w-Relative}^{(s)} + \frac{d}{dt}\vec{h}_{w-Relative}^{(s)} \quad (8.29)$$

$$\frac{d}{dt}\bar{\omega}_s^{(s)} = \bar{I}_{s\omega/2}^{(s)-1}\cdot\bar{M}_2^{(s)} - \bar{I}_{s\omega/2}^{(2)-1}\cdot\tilde{\omega}_s^{(s)}\cdot\left\{\bar{I}_{s\omega/2}\cdot\bar{\omega}_s^{(s)}\right\}\cdot\bar{I}_{s\omega/2}^{(s)-1}\cdot\tilde{\omega}_s^{(s)} \cdot\bar{h}_{w-Relative}^{(s)}\cdot\bar{I}_{s\omega/2}^{(s)-1}\frac{d}{dt}\bar{h}_{w-Relative}^{(s)} \quad (8.30)$$

In order to write in a more "neat" form lets make the following definitions;

$\bar{\omega}_s^{(s)} \equiv \bar{\omega}_s$ Angular Velocity of Satellite expressed in Body Frame

$\bar{I}_{s\omega/2}^{(s)} \equiv \bar{I}_s$ Moment of inertia matrix of satellite (including wheels) with respect to center of mass expressed in body frame

$\bar{M}_2^{(s)} \equiv \bar{T}$ All external torques acting about center of mass expressed in body frame

$\tilde{w}_s^{(s)} \equiv \tilde{w}_s$ Cross Product Matrix of $\bar{\omega}_s$

$\bar{h}_{\omega-Relative}^{(s)} \equiv \bar{h}_{\omega-Relative}$ Relative angular momentum of wheel assembly with respect to satellite expressed in satellite frame

Thus Equation (8.30) simplifies to;

$$\dot{\bar{\omega}} = \bar{I}_s^{-1}\cdot\bar{T} - \bar{I}_s^{-1}\tilde{\omega}_s\left\{\bar{I}_s\cdot\bar{\omega}_s\right\} - \bar{I}_s^{-1}\tilde{\omega}_s\bar{h}_{\omega-Relative} - \bar{I}_s^{-1}\dot{\bar{h}}_{\omega-Relative} \quad (8.31)$$

Alternatively dynamic equations of motion can be generalized as;

$$\dot{\bar{\omega}} = \bar{I}_s^{-1}\left\{\bar{T} - \dot{\bar{h}}_{\omega-\text{Relative}}\right\} - \bar{I}_s^{-1}\tilde{\omega}_s\left\{\bar{I}_s \cdot \bar{\omega}_s\right\} - \bar{I}_s^{-1}\tilde{\omega}_s\bar{h}_{\omega-\text{Relative}} \tag{8.32}$$

The more common form can be written as follows:

$$\begin{aligned}\dot{\bar{\omega}} &= \bar{I}_s^{-1}\left[\bar{T} - \dot{\bar{h}}_{\omega-\text{Relative}} - \tilde{\omega}_s\left\{\bar{I}_s \cdot \bar{\omega}_s\right\} - \tilde{\omega}_s\bar{h}_{\omega-\text{Relative}}\right] \\ \dot{\bar{\omega}} &= \bar{I}_s^{-1}\left[\bar{T} - \dot{\bar{h}}_{\omega-\text{Relative}} - \left\{\tilde{\omega}_s \times \left(\bar{I}_s \cdot \bar{\omega}_s + \bar{h}_{\omega-\text{Relative}}\right)\right\}\right]\end{aligned} \tag{8.33}$$

In this study derivation of the satellite dynamics equation is given by the above notation, however in terms of Kalman Filtering equations following notation is used such that: $\dot{\bar{\omega}}$ is given as $\frac{d\boldsymbol{\omega}_{bi}^{b}}{dt}$ and defined as derivative of $\boldsymbol{\omega}_{bi}^{b}$, which is defining the body rates with respect to the inertial frame and expressed in body frame. In terms of Inertia J value is preferred instead of I. $\bar{T}$ is given as $\boldsymbol{T}^{b}$ and defined as the total disturbance torque acting on the satellite. $\bar{h}_{\omega-\text{Relative}}$ is given as $\boldsymbol{h}_{wheel}^{b}$ and defined as the reaction wheel's angular momentum vector represented in satellite body frame. The used form is given in Equation (4.5).

CURRICULUM VITAE

Surname, Name: Kahraman, Özgür

EDUCATION

Degree	Institution	Year of Graduation
MS	METU Aerospace Engineering	2007
BS	ITU Astronautical Engineering	2004
High School	İAL İzmir Atatürk High School, İzmir	1998

FOREIGN LANGUAGES

Advanced English

SHORT BIOGRAPHY

Ozgur Kahraman started his career at TUBITAK UZAY- Space Technologies Research Institute in 2004 and currently working as Attitude and Orbit Control Systems Group Lead. Ozgur Kahraman is responsible for the technical coordination of all subsystems as a lead system engineer in IMECE Satellite Project since 2016.

RESEARCH INTEREST

Attitude Estimation and Control Systems of Small Satellites, Dynamic Systems Modeling, Kalman Filtering, Nonlinear Systems and Analysis, Calibration Processes, Hardware / Software in the loop tests of the satellites, Simulators and AOCS test benches.

Satellite System Engineering, Space Geodesy.

PROJECTS

- IMECE Satellite Project- Technical Leader / Lead System Engineer (2016-2023)
- IMECE Star Tracker Development Project- Team Lead (2013-2023)

- TURKSAT 6A Satellite Project- AOCS Team Lead (2014-2016)
- GOKTURK 2 Satellite Project- AOCS Engineer / Team Lead (2007-2012)
- RASAT Satellite Project- AOCS Engineer / Team Lead (2004-2011)
- BILSAT 1 Satellite Project – AOCS Engineer / Satellite Operator (2004-2006)

RESEARCH AND APPLIED ENGINEERING EXPERIENCE

IMECE Technical Leader / Lead System Engineer – Satellite system design and analysis activities, technical coordination of all subsystems, requirement management, interface management, validation and verification activities, planning and conducting satellite AIT process.

IMECE Star Tracker Development Project- Team Leader – Management of the technical work packages, coordination of star tracker equipment development, supporting all subsystems for native subcontractors. (The design, development and qualification of engineering models have been completed; the flight models are being manufactured as of 2021).

TURKSAT 6A AOCS Team Leader- Management and the design of the AOCS subsystem, connection with all subcontractors, AOCS software structural design and software team lead,

GOKTURK 2 AOCS Team Leader – Management and the design of the AOCS subsystem, connection with all subcontractors, AOCS software structural design and software team lead, AOCS AIT activities, commissioning activities of the satellite.

AOCS Software Engineer – Analysis of AOCS software algorithms for BILSAT 1 project, update and implementation of RASAT AOCS software, GOKTURK 2 ADCS software structural design and implementation.

Satellite Dynamic Modeling in Matlab Simulink Environment - Modeling of satellite dynamics, modeling of sensors and actuators such as magnetometers, sun sensors,

reaction wheels, magnetorquers and star trackers in Matlab Simulink environment for RASAT satellite project.

Responsible for procurement of ADCS components by tender process - Preparing the technical specification, administrative specification and Contract documents of procurement processes related with AOCS components, in RASAT project.

Satellite Operator - Responsible for BILSAT-1 satellite operations in TUBITAK ground station. Operational planning, Mission analysis, Orbital test planning.

PUBLICATIONS

Ö. Kahraman et al., "IMECE Satellite Attitude and Orbit Control Subsystem - AOCS Overview," 2023 10th International Conference on Recent Advances in Air and Space Technologies (RAST), Istanbul, Turkiye, 2023, pp. 1-4, doi: 10.1109/RAST57548.2023.10197994.

Ö. Kahraman, M. Sungur and A. S. Kutay, "IMECE Satellite Systems Engineering Activities," 2023 10th International Conference on Recent Advances in Air and Space Technologies (RAST), Istanbul, Turkiye, 2023, pp. 1-4, doi: 10.1109/RAST57548.2023.10197977

Kahraman, O, and Soken, H.E., "Incorporating Delayed Star Tracker Measurements in Gokturk-2 Satellite Attitude Filter," *Adv. Sp. Res.*, Mar. 2023, doi: 10.1016/J.ASR.2023.03.005.

Kahraman, O, and Soken, H.E., "Attitude Orbit Control Subsystem Overview of Gokturk-2 Satellite," 28th International Symposium on Space Flight Dynamics, Beijing, China / Online 29 August – 2 September 2022.

Kahraman, O, and Soken, H.E., "Incorporating Delayed Star Tracker Measurements in Attitude Filter," AAS 2021-680. AIAA / AAS Astrodynamics Specialist Conference Big Sky Virtual. August 2021.

Mustafa Akbas, Yusuf Acar, Farid Gulmammadov, Cagatay Yavuzyilmaz and Ozgur Kahraman. "*Commissioning of Attitude and Orbit Determination and Control System of RASAT Satellite*," AIAA 2013-5174. AIAA Guidance, Navigation, and Control (GNC) Conference. August 2013.

F. Gulmammadov, Ç. Yavuzyilmaz, and Ö. Kahraman, "*The lessons learned from the commissioning and operation phases of RASAT: an AODCS perspective*," in UN/Japan Nano-Satellite Symposium, 2012.

Ö. Kahraman et al., "*Uzaktan algılamada RASAT: Türkiye'de üretilen ilk yer gözlem uydusu (RASAT in remote sensing: First earth observation satellite built in Turkey*)," IV. Uzak. Algılama ve Coğrafi Bilgi Sist. Sempozyumu (UZAL-CBS 2012), Zonguldak,Turkey, 2012.

C. S. Tüfekci, N. Ertongur, Ç. Yavuzyılmaz, F. Gulmammadov, O. Kahraman and Y. Subaşi, "*Attitude performance requirements and budgeting for RASAT satellite*," Proceedings of 5th International Conference on Recent Advances in Space Technologies - RAST2011, 2011, pp. 968-973, doi: 10.1109/RAST.2011.5966986.

Ç. Yavuzyılmaz et al., "*Rasat ADCS flight software testing with Dynamic Attitude Simulator Environment*," Proceedings of 5th International Conference on Recent Advances in Space Technologies - RAST2011, 2011, pp. 974-977, doi: 10.1109/RAST.2011.5966987.

F. Gulmammadov, O. Kahraman, C. Yavuzyilmaz, C. S. Tufekci, and Y. Subasi, "*Magnetorquers only attitude maintaining using dynamic attitude simulator environment,*" in AIAA Modeling and Simulation Technologies Conference, Toronto, Ontario, Canada, 2010.

Kahraman, O., and Tekinalp. O., "*Satellite Attitude Control Using Dissimilar Redundant Actuators*," Proceedings of the 19th AIAA/AAS Space Flight Mechanics Meeting, AAS 09-252, pp. 2303-2315, Savannah, GA, Feb. 9-12, 2009.